Development and Characterization of Gastro-Intestinal Simulator (GIS)

by

Nicholas Job

A dissertation submitted in partial fulfillment
of the requirements for the degree of
Doctor of Philosophy
(Pharmaceutical Sciences)
in the University of Michigan
2020

Doctoral Committee:

Professor Gordon L. Amidon, Co-Chair
Professor Gregory E. Amidon, Co-Chair
Professor David Smith
Professor Robert Ziff

Nicholas M. Job
njob@umich.edu
ORCID iD: 0000-0002-0823-3955

© Nicholas M. Job 2020

Acknowledgments

This work would not be possible without my family and I would like to dedicate it to them all. To my wife, Allyson, your patience, care, love, and positivity helped carry me through the past five and a half years. You cheered me on from the start of the application process all the way onto today. You trusted in me enough to follow me across the country away from our families and start our own out here. Words can't begin to describe everything you've done for me and how thankful I am, always and forever. To my parents, you've been amazing supporters of this, making frequent twelve hour drives out to see us and to help us with whatever you could. To Al's parents, Pat & Mark and Jim & Katie, thank you for being supportive of Al and I moving out here and showing your support. It means so much to have not just one set of parents cheering me on, but three. To PJ, the best dog on the planet: Whenever, I was having a bad time with work or needed cheering up, you were always there trying to squeeze your enormous head into my lap. A day doesn't go by without wishing I could be as happy as you are, and you do your best to try to make me that happy.

To my graduate school friends, Lindsay, Nick, Pat, Phil, Morgan, Emily, Katie, Jason, and Brian: thanks for all of the fun times in and out of lab. Thanks for all of the dumb inside jokes; the late nights at bar trivia; the endless, bizarre conversations, discussions, and arguments; and for the "athletic" endeavors in intramural sports and playing hockey down at the Cube. We developed a great network of mutual support that made this herculean task bearable for us all. Thank you to all of the older students who came before me who gave great wisdom, without being jaded; and the younger students who will follow who gave great enthusiasm to help me stay motivated on the toughest days. To the rest of my friends that I've made in the past five years, you've helped me learn the difficulties in trying something new and just dive-in; you've helped me look at things in new ways and maintaining constant rotation and creativity.

To my lab-mates, undergrads, graduate students and postdocs, alike: thank you for your unique points of view and willingness to always listen and contribute. To Pat and Niloufar: I spoke above about mutual support, but the support that I received from you will, in my eyes, always outweigh anything I've done for you both. Listening to absurd

ideas I've had and bringing them back to reality and having the patience to help me finally grasp countless concepts was extremely important to helping me succeed. I couldn't have done this without you. To Troy, Meagan and Sarah: your growth as researchers in your time in the lab was great to see and I know you will succeed at whatever you want to do. Thank you for your patience, your senses of humor and being able to make me say "Wow". Randy and Pam: Your drive to help get GIS-2 off the ground was outstanding. You both found a way to make me laugh through the low points of development and helped keep me on task. To my entire committee, thank you for your patience it allowing me to find my way to the end of the progress and for sticking with me throughout. I definitely never made it easy for you all, but you all did an amazing job making me into the research I am today. I cannot begin to describe how thankful I am for your commitment to me and my growth.

Table of Contents

List of Figures

List of Tables

List of Appendices

Abstract

For oral drug formulations, the efficacy of a formulation in an individual is dependent on many physiological processes and variables. For most immediate release drug products, the formulation must disintegrate and dissolve, undissolved mass must empty from the stomach into the upper gastrointestinal (GI) tract, and remaining undissolved drug must dissolve and be absorbed across the intestinal wall to reach systemic circulation. Despite understanding the relevant processes, conventional in vitro methods only capture a part of these processes by performing dissolution at one pH without any other processes acting on the formulation. In this work, a dissolution device is developed that simulates the relevant in vivo processes that can affect drug dissolution. This device is called the Gastro-Intestinal Simulator or (GIS) and is designed to simulate in vivo conditions in a way that maintains ease of use. Compared to other multi-vessel dissolution devices, the GIS can be run multiple times in a day by just one analyst. The device has been designed with customizability in mind, with the ability for vessel geometry to be easily selected, a variety of gastric emptying rates applied, and a titration function to maintain pH in the chamber representing the upper intestine (e.g. duodenum) when using biorelevant media. Applications of the device were evaluated with two sets of experiments: determination of in vitro – in vivo correlations (IVIVC), and formulation screening tests to determine sensitivity to formulation variables and results compared to conventional testing procedures. IVIVCs are a valuable tool in quantifying drug release into systemic circulation but require physiologically relevant dissolution data. The dissolution data generated for two ibuprofen formulations in the GIS did not produce a successful IVIVC. Although the results of this work failed to meet strict FDA requirements for an IVIVC, the results showed promise and provide a framework for future correlative dissolution. The GIS

system has the capability for further optimization to better represent the conditions of the human intestine, which could allow for improved correlations including biorelevant media selection, gastric emptying, and introduction of an absorption compartment. For formulation optimization, a similar framework as other industrial process optimizations can be applied. However, multiple process and formulation variables increases the challenge of developing an understanding of these effects and therefore benefits from an appropriate experimental design. This empirical approach requires a statistical design of experiments and a Plackett-Burman design was selected as a screening approach designed to limit the number of experiments to determine the main effects of interest. The GIS results showed the most statistically significant factors compared to compendial disintegration and dissolution methods. In both applications, the GIS, when configured to simulate the relevant conditions of the human intestine showed significant promise for assessing formulations and mechanisms that lead to improved in vivo drug dissolution.

Chapter 1.

Introduction

The reduction of drug costs must occur without removing necessary regulatory controls to prevent patient harm. This does not prevent novel technologies from being created to reduce expensive testing for drug products that may eventually fail during pre-clinical or clinical testing. Attrition levels have been consistently high, ranging from 10-21% of all drug products that enter Phase I clinical human testing will reach the market [1]. With pharmaceutical research and development (R&D) costs projected to grow to almost $160 billion USD by 2020 [2] and the desire to outpace patent expiration, there is little luxury for industrial scientists to research processes fundamental to producing optimal drug formulations. The idea of studying the fundamental processes of oral formulations is not one denounced by the pharmaceutical industry. By understanding these processes, improved predictions can be created to reduce adverse effects on patients, thereby improving safety, and enhance efficacy of the drug molecule in vivo. In order to provide added value to R&D, a cost efficient, robust in vitro test or set of tests is necessary to properly predict differences between formulations for a specific drug product.

A greater understanding of underlying mechanisms have been an ongoing area of research for the past half century. The biopharmaceutical classification system (BCS) was created to categorize molecules by two of their key physical chemical properties: solubility and permeability [3,4]. The system provided a binary methodology to guide product viability and necessary formulation excipients to ensure proper dissolution and absorption kinetics. The BCS was the basis for the creation of the biowaivers system by

the FDA [4] to assist generic companies in rapidly generating generic products. Further iteration of the original BCS has been used to differentiate between molecule species that have similar physical properties, but differing ionization behaviors, (i.e. weak acid or weak base). By others, the BCS has been modified into a three-region coordinate system based on fraction of dose absorbed, with each region delineated by its expected or measured fraction absorbed. [5] The BCS has been recently expanded to provide further guidance for in vitro/in vivo correlative (IVIVC) dissolution. This expansion provides subclassifications within the BCS II class (and BCS class IV, as necessary): subclass IIa, b & c for weak acids, weak bases, and neutral, or unionizable, drugs, respectively. [6] In order to provide a robust, simple solution to current need for consistent IVIVC methodology, there are two necessary arms of research that must be performed. First, adequately estimating the hydrodynamics of the in vivo gastrointestinal tract mechanically in vitro is necessary to approximate dissolution kinetics under certain circumstances. Second, the BCS, and the refinements from the original system, can be wielded alongside research into biorelevant dissolution media to provide a systematic means to determine drug formulation viability in the pre-formulation and formulation stages. In addition, the studies previously performed on weakly basic drugs in bicarbonate buffer will be expanded upon to improve the equivalent phosphate buffer relationship.

1.1. Theory of Mass Transfer, Dissolution and the Gastrointestinal Tract

1.1.1. Solubility and the Boundary Layer Theorm

Molecules must be dissolved into solution in order for transport across the gastrointestinal membrane, which is almost always needed to cause the desired effect of the drug. Solubility, or the extent of dissolution, is the maximum concentration of a drug that can be dissolved into a specific medium. Generally in pharmaceutical sciences, solubility is the term used for kinetic solubility, or the concentration at which

a precipitate first appears. This tends to overestimate as compared to the thermodynamic solubility, but kinetic solubility is a more simple determination can provide a generally adequate estimation. For most mass transfer situations, Fick's laws of diffusion, named after its creator Adolf Fick in 1855, are the typical starting point. Fick's first and second laws of diffusion are show below, respectively:

$$J = -D\frac{\delta C}{\delta x} \tag{1.1}$$

$$\frac{\delta C}{\delta t} = -D\frac{\delta^2 C}{\delta^2 x} \tag{1.2}$$

where J molar flux, in units of moles per area-time, D is the diffusion coefficient in area per time, C is concentration in moles, and x is the unit of length over which diffusion is occurring. Fick's first law, equation 1.1, has been simplified from the typical chemical engineering form where temperature dependence for density, viscosity and species specific diffusion coefficients can appear at extreme temperatures, and any presumed reaction rate is minimal or unrelated to dissolution. Fick's second law, in equation 1.2, has also been simplified and is shown in the rectangular coordinate form. This was simplification can be justified by the assumption that generally there will be little to no variation in the angular directions of theta and phi, that is the angle between the x-axis and the y-z-plane and the angle between the z-axis and the x-y plane, respectively. Fick's law has some disadvantages as it can cause an oversimplification of the system, but due to the nature of the differential equations, the boundary conditions can increase in complexity to match the system. For most oral drug products, dissolution rate is not solely based on the physicochemical properties of the drug molecule. Disintegration of particles assists in increasing the rate of in vivo and in vitro dissolution. This occurs due to the increase in surface area. This increase in dissolution rate related to an increase in surface area is shown in the Noyes-Whitney equation for dissolution rate [7,9,10], shown below in equation 1.3:

$$\frac{\delta m}{\delta t} = k_{diss}(C_s - C_0) = Ak_{mass}(C_s - C_0) = Ak_{mass}\Delta C \tag{1.3}$$

where k_{diss} is the dissolution rate coefficient in volume per time, k_{mass} is the mass transfer coefficient in distance per time, A is the total surface area of the system, C_s is the kinetic solubility at the solid surface in mass per volume and C_0 is the bulk drug concentration in mass per volume. By increasing the total number of particles, thereby increasing the effective surface area, the dissolution rate increases. In order to model the rate of change of the concentration, the Noyes-Whitney equation can be rearranged into the form shown below in equation 1.4:

$$\frac{\delta C_0}{\delta t} = \frac{AD}{h}(C_s - C_0) \tag{1.4}$$

where D is the effective diffusion coefficient and h is the thickness of the boundary layer in units of distance. The boundary layer is an important parameter for determining rate and extent of dissolution. The boundary layer describes a thin layer of unmixed fluid at the surface of a solid. See Figure 1.1 for a schematic of the boundary layer: The

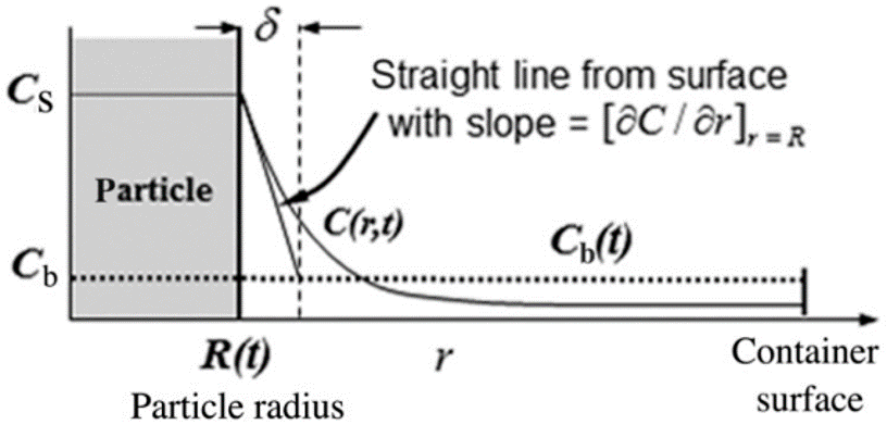

Figure 1.1: Concentration field gradient with respect to the particle surface with diffusion into the boundary layer.

boundary layer, thickness δ, is shown in Figure 1.1, for a particle with a radius of R(t), and a bulk solution concentration of C_b. The figure also shows the expected concentration gradient with respect to r, the distance from the center of the particle. As time increases and the particle begins to dissolve, the boundary layer begins to shrink.

The boundary layer will shrink until the concentration in the boundary is equal to the maximum solubility. Generally, the boundary layer for highly kinetic fluids, like gases, is assumed to be smaller than the particle radius. This assumption is not applicable for aqueous systems like pharmaceutical dissolution and typically a boundary layer on the same order of magnitude as the particle radius is used. [8, 22] This is likely not perfectly applicable to regions of the GI like the mucosa, because of the high viscosity of the mucosa increasing the boundary layer thickness, but diffusion into the mucosa can likely be encompassed into the absorption component of IVIVC dissolution. Understanding the boundary layer provides insight into two phenomena surround stagnant film diffusion from solids: particle confinement and particle size effect. Particle confinement is a nonideal circumstance for dissolution where there is not sufficient time, volume or inter-particle spacing for dissolution to occur completely. Though this circumstance departs for an ideal system, it allows for an understanding of undissolved drug: as a single particle approaches the drug molecules solubility limit locally, the dissolution rate will slow, causing saturation to occur without fully dissolving the drug in the system. It has been observed that duodenal volumes are typically much lower than the typical dissolution volume (50 mL vs 900 mL), so the particle confinement effect is a crucial part of modeling the GI. The other phenomenon related to boundary layer is regarding the effect of particle size on dissolution. Pharmaceutical science models, like Noyes-Whitney, do not account for particle size as a part of the equation, though one could argue that a decrease in particle size does increase dissolution rate by increasing the area to volume ratio. Uniform particle size is highly improbable, but a rational estimation may be used for boundary layer calculations, with the desire for an approximately normal distribution and any particles larger or smaller than the used for boundary layer calculations will approximately cancel each other out. There is some disagreement on whether the thickness of the boundary layer is constant, has an effective maximum or has an empirical relationship with particle size that is a strong approximation over certain ranges. For the sake of simplicity, a constant boundary layer may be applicable when there is a very small range of particle sizes in the system, but tends to be not as accurate at estimating boundary layer size across larger ranges. The Hintz-Johnson model is an empirical model that claims there is a maximum

boundary layer size once a critical particle size radius is reached. However, Wang et al., claim the assigning of a maximum boundary layer is not supported by the laws of conservation of energy and are merely an empirical adjustment factor to create a better fit to observed dissolution data [8]. One simple means for approximating the boundary layer thickness is by using the Sherwood number (Sh). The use of the Sherwood number is commonly used in the engineering field to describe mass transport systems, but its use in the pharmaceutical sciences realm is relatively recent [10]. The Sherwood number is a dimensionless number, as described in equation 1.5, below:

$$Sh = \frac{K}{\frac{D}{L}} = \frac{MassTransferRate}{DiffusionRate} \tag{1.5}$$

where K is the mass transfer coefficient and D is the mass diffusivity, in units of area over time and L is the characteristic length. For the typical drug dissolution system, the characteristic length is equal to the particle diameter. By comparing the Noyes-Whitney equation to the mass transfer equation from fluid dynamics, the following equations can be surmised to determine boundary layer thickness:

$$\frac{AD}{h}(C_s - C_0) = \frac{AD(Sh)}{L}(C_s - C_0) \tag{1.6}$$

$$\frac{1}{h} = \frac{(Sh)}{L} \tag{1.7}$$

Generally, the Sherwood number is applied for a local point on the drug particle as conditions may cause mass transfer to differ from point to point. To approximate the average Sherwood number for a drug particle, the Ranz-Marshall equation can be applied, using the Reynolds number (Re) and the Schmitt number (Sc) [10]. The Reynolds number is a dimensionless number that describes the type of flow that's occurring, whether it is turbulent or laminar. The Schmitt number describes the ratio of the viscous sheer diffusion compared to the mass diffusion rate. The Ranz-Marshall equation, the Reynolds and Schmitt Numbers equations are shown below in equation

1.8-1.10:

$$Sh_{particle} = 2 + 0.6Re^{\frac{1}{2}}Sc^{\frac{1}{3}} \tag{1.8}$$

$$Re = \frac{Ud}{\nu} \tag{1.9}$$

$$Sc = \frac{\nu}{D} \tag{1.10}$$

Where υ is the kinematic viscosity of the media, d is the particle diameter, U is the particle velocity and D is the diffusivity. The first term of the Sherwood number is present to allow mass transfer that occurs when the system has no flow, or Re = 0; the second term is the convective diffusion, dominated by the Reynolds and Schmitt numbers. Inserting a form of equation 1.8 without the dimensionless numbers into a rearranged form of equation 1.7 allows for the boundary layer thickness to be determined given a known experiment, as shown below in equation 1.11:

$$h = \frac{d}{0.6\frac{Ud}{\nu}^{\frac{1}{2}}\frac{\nu}{D}^{\frac{1}{3}}} \tag{1.11}$$

All values in equation 1.11 can be empirically determined or estimated within an acceptable range for a given experiment. For pharmaceutical sciences, this equation does not provide a large advantage over the Noyes-Whitney equation due to most experiments being performed with similarly sized particles in an aqueous media, however for the sake of comparison the Ranz-Marshall equation is useful. Though the USP provides guidance for at least 7 apparatuses for dissolution, the most frequently used is Apparatus 2: paddle dissolution at 37°C. This system, though simple has some disadvantages in terms of hydrodynamics. First, in order to provide a homogenous solution for sampling, the mixing speed (in RPM) must be set high enough to attempt to prevent stagnate particles from depositing on the bottom of the dissolution vessel. This high rotational speed causes increased shear effects on particles and other solids, potentially increase the dissolution rate of the solids. Second, despite the high mixing speed, two types of particles are present: floating particles, caught in the eddys of the mixing, and stationary particles, typically occurring early in the experiment when a

tablet has not completely disintegrated; and each particle type must be accounted for mathematically. The difficulty with tablets on the bottom of the vessel is their hydrodynamics require computational fluid dynamics (CFD) calculations in order to determine the flow pattern and the linear velocities present around the outside of the tablet.

1.1.2. Computational Fluid Dynamics

According to Lomax, Pulliam and Zinng, the goal of computational fluid dynamics (CFD) is using modeling of known geometry to gain an understanding of fluid flow in and around the experimental area [12]. This includes the phenomena of "dissipation, diffusion, convection, shock waves, slip surfaces, boundary layers and turbulence" [12]. Typically, CFD has more applications to aerodynamics than pharmaceutical sciences, but with regards to the latter, CFD has been used in many dissolution studies to determine hydrodynamics of many vessels. [11, 13] As in most modeling areas, the selection of criteria, such as the geometry and flow conditions for CFD is crucial to the accuracy. In addition, selecting which governing equations, Navier-Stokes versus Euler equations, for instance, and the boundary conditions for the system; the method of gridding the volume of flow and the numbering system, such as a finite-volume system, are also crucial. There are commercial software packages, like Fluent by Ansys Inc., that are typically used to analyze fluid dynamics. These software packages are capable of solving coupled non-linear partial differential equations for the necessary parameters: for dissolution studies, this is typically only momentum, since the system is assumed to be isothermal with mass transport not considered to determine bulk fluid dynamics.

1.2. Bicarbonate Buffer Systems and buffer selection

1.2.1. Comparisons between in vivo and in vitro buffer systems

When it pertains to in vivo predictive dissolution studies, it remains to be determined the extent of complexity needed to get desired results. A review by Mudie, et al.

encompasses various studies on the upper GI to determine concentrations of bile salts, ions, lipids and enzymes that play a role in dissolution and absorption in vivo, along with summarizing pH, viscosity, surface tension, osmolality and buffering capacity. [14] The importance of these parameters cannot be understated. Surface tension affects wetting of the drug product, decreased wetting leads to a decreased disintegration, thereby decreasing the dissolution rate. Viscosity is highly involved in the boundary layer, which was previously discussed in great detail. Osmolality is a measure of ionic concentration, or ionic strength, based upon cellular osmotic pressure and ion content. One study by Kararli, Kirchkoff and Truelove showed that increasing ionic strength in vitro caused increased dissolution rate for enteric coated formulations.$_{23}$ Some parameters, are easily generated, such as pH, viscosity or buffering capacity, can be easily generated in a manner that simulates in vivo conditions. For instance, buffering capacity of the GI, regardless of fed or fasted state, is much lower than that of 50 mM phosphate buffer. Another deviation from typical in vitro analysis is the stomach pH under a fasted state, though typically simulated using 0.1 N hydrochloric acid, with a pH around 1.0, the mean pH of the stomach in a fasted state is 2.9 ± 1.97.[14] Not only is that a large variance from the mean, but it is a much higher pH than that typically used in vivo.

1.2.2. Bicarbonate Buffer and equivalent phosphate buffer

Typically, simple quality control dissolution studies are performed in 50mM phosphate buffers at a pH between 6.5 and 7. However, this does not adequately resemble the buffer behavior in vivo. The buffer system of the gastrointestinal tract is a bicarbonate buffer system, created by carbonic anhydrase enzymes in the pancreas and excreted into the small intestine. The role of bicarbonate is the prevent damage to the mucosa of the intestine from secreted acids from the stomach and surrounding region. The neutralization of acids by bicarbonate creates carbonic acid as a product. Figure 1.2, below, shows the general scheme of bicarbonate excretion and uptake into the duodenum. Figure 1.2 shows that there are three pathways for bicarbonate secretion into the duodenum: uptake from the blood into the intestinal epithelial cells and

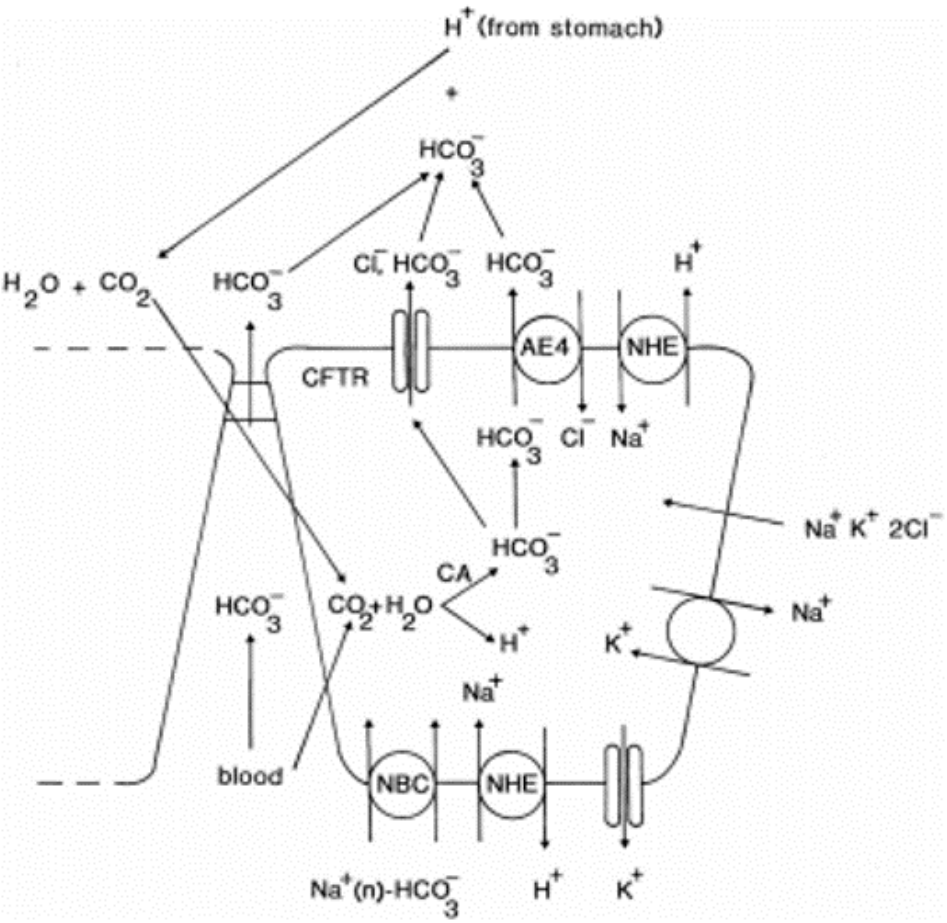

Figure 1.2: Schematic of duodenal transporters for the bicarbonate secretion and uptake system.

subsequent secretion via the cystic fibrosis transmembrane conductance receptor (CFTR) and anion exchange receptor 4 (AE4), intracellular carbonic anhydrase converting water and carbon dioxide into bicarbonate which utilize the same secretion mechanisms, and transcellular diffusion through the mucosa. Fasted human intestinal fluid has been shown to have limited buffer capacity, near the order of magnitude of 10 mM per unit of pH, with presumably a large degree of the buffering capacity being supplied by the bicarbonate buffer [14]. Compared to common dissolution buffers, like fasted and fed state simulated intestinal and stomach fluid (FaSSIF and FeSSIF,

respectively), the buffering capacity of human intestinal fluid is five times lower. This is one major reason why 50 mM phosphate buffer, though sufficient for quality control dissolution studies where consistency is more important than correlation to in vivo conditions, is not an adequate buffer under most circumstances where in vivo correlation is necessary. However, matching buffering capacities between two buffer systems is not the sole governing parameter, since buffering capacity controls both bulk pH and surface pH. Krieg, et al, showed that the physiochemical properties of the drug molecule also play a role in the buffer selection, specifically in determining the pH at the surface of the dissolving drug. This difference in buffering reactions are shown below: where reaction 1 governs the bulk buffer system and the pKa of bicarbonate

$$CO_2\,(aq) + H_2O \rightleftharpoons H_2CO_3 \rightleftharpoons H^+ + HCO_3^-$$

$$CO_2\,(aq) + H_2O \leftarrow H_2CO_3 \rightleftharpoons H^+ + HCO_3^-$$

(6.04) approximates the reaction kinetics [16]. In the boundary layer, the carbonic acid to water and carbon dioxide reaction is unidirectional, as the reaction rate to generate carbonic acid is unable to compensate for the reaction of carbonic acid in the boundary layer and the pKa is 3.55. For the in vitro bicarbonate buffer system typically used in the Amidon lab, carbon dioxide gas is sparged into an isotonic solution and then adjusted to the desired pH using sodium hydroxide, typically a pH between 6.5 and 7.0. For this system, carbon dioxide gas is continuously sparged even after the system has reached equilibrium. This system therefore has a third reaction, which governs the buffer system, the dissolution of gas into solution. Since experiments do not commence until the system has reached an equilibrated dissolved carbon dioxide content and pH, this equilibrium should not affect bulk buffering capacity and pH over a short time period, but over time the dissolved gas should drive the reaction in the bulk back towards the initial equilibrium conditions. For this system, the surface pH should act similar to the in vivo bicarbonate system. Despite the in vivo relevance, the in vitro carbon dioxide sparged bicarbonate buffer is complicated and requires extra equipment compared to a conventional apparatus 2 USP dissolution device. These additional

components may alter homogeneity of the solution, cause delayed drug dissolution due to solid particles adhering to the additional surfaces or alternative hydrodynamics caused by the sparging of carbon dioxide and air. In addition, the preparation of bicarbonate buffer can be tedious due to the precision required in selecting gas flow rate to ensure proper buffer strength and pH. For this reason, it's desirable to attempt to find an equivalent phosphate buffer to give similar dissolution kinetics. Figure 1.3 shows equivalent phosphate buffers for 15mM isotonic bicarbonate at pH values of 6.0, 6.5 and 7.0. The predicted equivalent phosphate buffer concentration is plotted on the y-axis in

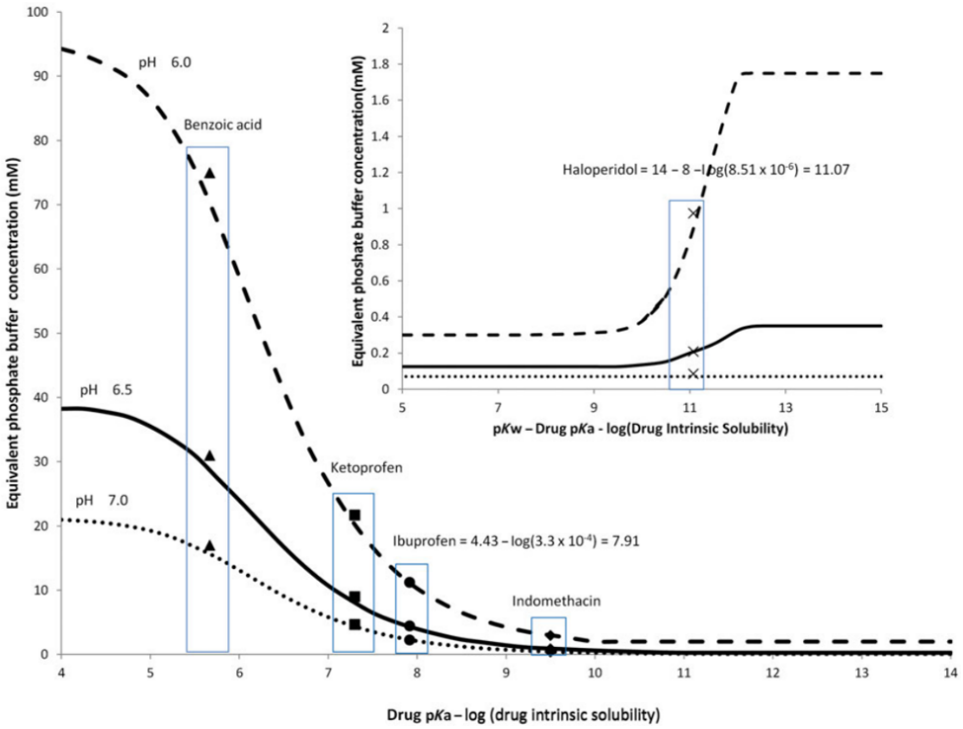

Figure 1.3: Equivalent phosphate buffers to 15 mM isotonic bicarbonate buffer at pH 6.0, 6.5 and 7.0. Weak acids are on the main axes, weak bases are on the inlay.

units of mM of phosphate, and the x-axis is the drug pKa subtracted by the log of the intrinsic solubility for weak acids; and for weak bases the x-axis is 14 (or pKw) subtracted by the drug pKa and the log of the intrinsic drug solubility. For each curve, the Hintz and Johnson approximation for the boundary layer was used (30 μm). The relationship between the intrinsic solubility and the pKa, or pKw minus pKa and

intrinisic solubility are both appear in the equation for the irreversible (Reaction 2 on page 10) reaction, and are multiplied together. If both parameters are altered in equal but opposite directions, there is no net change in the equation and the surface pH is assumed to be the same. In this case the same equivalent phosphate can be used for both drugs. Figure 1.3 also shows the direct role bulk pH has on the system. The more acidic a bulk pH, the greater the phosphate concentration that is need, and generally for weak acids at pH 6.0 the equivalent phosphate buffer will exceed the concentration of the bicarbonate buffer, and in some extreme cases, even surpass the ubiquitous 50 mM phosphate buffer. This further cements the need for biologically relevant buffer concentrations, which can be easily produced without the need for gas sparging.

1.3. Gastrointestinal Simulator, Artificial Stomach Duodenum, and Other in vivo predictive dissolution methodologies

As previously discussed, USP-type dissolution apparatuses, do not properly simulate the gastro-intestinal physiology in a manner that can provide predictive dissolution in most cases. Due to the void left behind by the USP, several in vivo predictive methodologies have been created, including: biphasic dissolution, the gastro intestinal simulator (GIS), the artificial stomach duodenum (ASD), and the TNO GI Tract Model (TIM). In addition, to the unique apparatuses and methodologies associated with these technologies, they also may take advantage of biorelevant dissolution media, as discussed in the previous subsection. Biphasic dissolution attempts to model the absorption component of dissolution, in order to more accurately predict in vivo performance, specifically for compounds where permeability predominates: BCS class II and IV compounds. As seen in figure 1.4, the biphasic system has a double paddle, similar in shape to a USP apparatus 2 paddle, with an aqueous media on the bottom (dark grey) and a lower density organic phase, typically octanol, on top (light grey). Since the interface between the organic and aqueous phases can be easily disrupted, a predissolved solution of drug is added to the buffer system in the bottom layer. The

drug concentration is monitored in the both phases until equilibrium is achieved. These experiments allow for drug absorption to be simulated while using an appropriate volume of biorelevant media. The GIS is an attempt to create improved IVIVC by

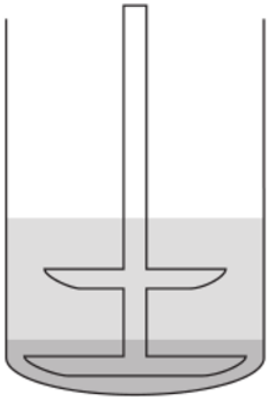

Figure 1.4: Biphasic dissolution schematic

approximating the in vivo conditions in a laboratory bench top setting. The term has become interchangeable with ASD, as both are similarly set up [18-20]. Figure 1.5, below shows an example schematic of a GIS device. In Figure 1.5, three chambers are show to represent the first three GI sections: the stomach (orange), the duodenum (cyan) and the jejunum (blue). The ASD, such as the one used by Polster and Sperry, lacks the final jejuna compartment [20]. For the stomach and the duodenum, there are also secretion reservoirs which provide dissolution media at a constant rate throughout the course of the experiment. Each vessel has computer controlled volume and fluid transfer rates to precisely represent the in vivo conditions. Each vessel utilizes biorelevant dissolution mediums to create a bulk and local pH that is biorelevant. For this system, the stomach has an acidic condition and the duodenum and jejunum are closer to neutral pH. For BCS subclass compounds like BCS IIa and IIb, this may lead to different observed dissolution behavior than that observed in a conventional dissolution experiment. In a publication by Matsui, et al., two drugs, one a BCS I drug and one BCS IIb (weak base), fluconazole and dipyridamole respectively, were compared in a GIS system using varied gastric pHs, in an attempt to show potential drug-drug interaction between these drugs and acid-reducing drugs Each panel shows two comparative experiments, one with a

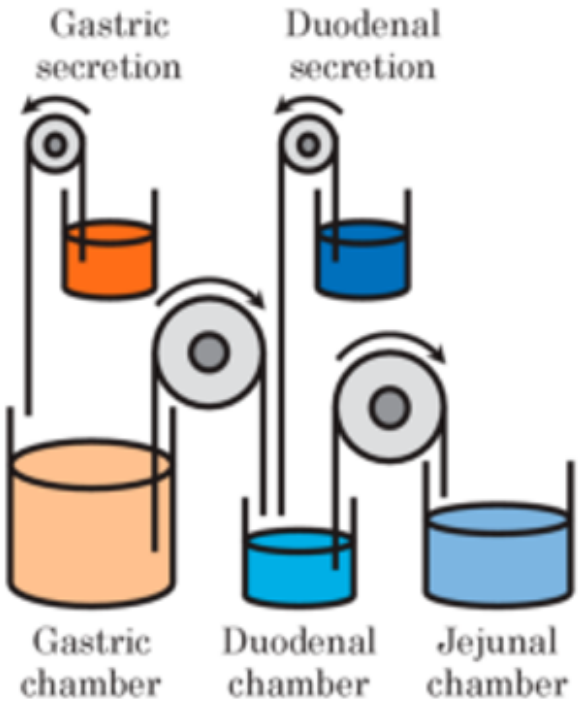

Figure 1.5: Gastrointestinal Simulator (GIS) schematic

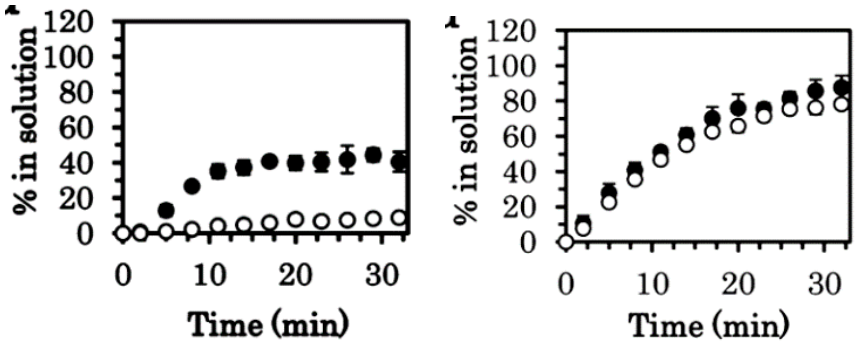

Figure 1.6: Dipyridamole (a BCS IIb compound) (left) and fluconazole (BCS I) (right) GIS dissolution; concentration in intestinal regions

gastric pH of 2.0 (closed circles) and one at pH 6.0 (open circles). This study shows that the extent of dissolution for fluconazole is not affected by gastric pH. However, for dipyridamole, the concentration in the intestinal region is altered by changing gastric

pH. This study shows the value added by IVIVC dissolution, not only for differentiating between drugs, but also the importance of pH on dissolution [18]. The final dissolution apparatus to be discussed is TIM. TIM was designed to simulate the luminal conditions of the gastrointestinal tract in a multicompartment model. TIM is typically used for food products but has been applied to pharmaceuticals. In figure 1.7, below is a schematic for TIM. Compartments of note in Figure 1.7 are A–the gastric compartment;

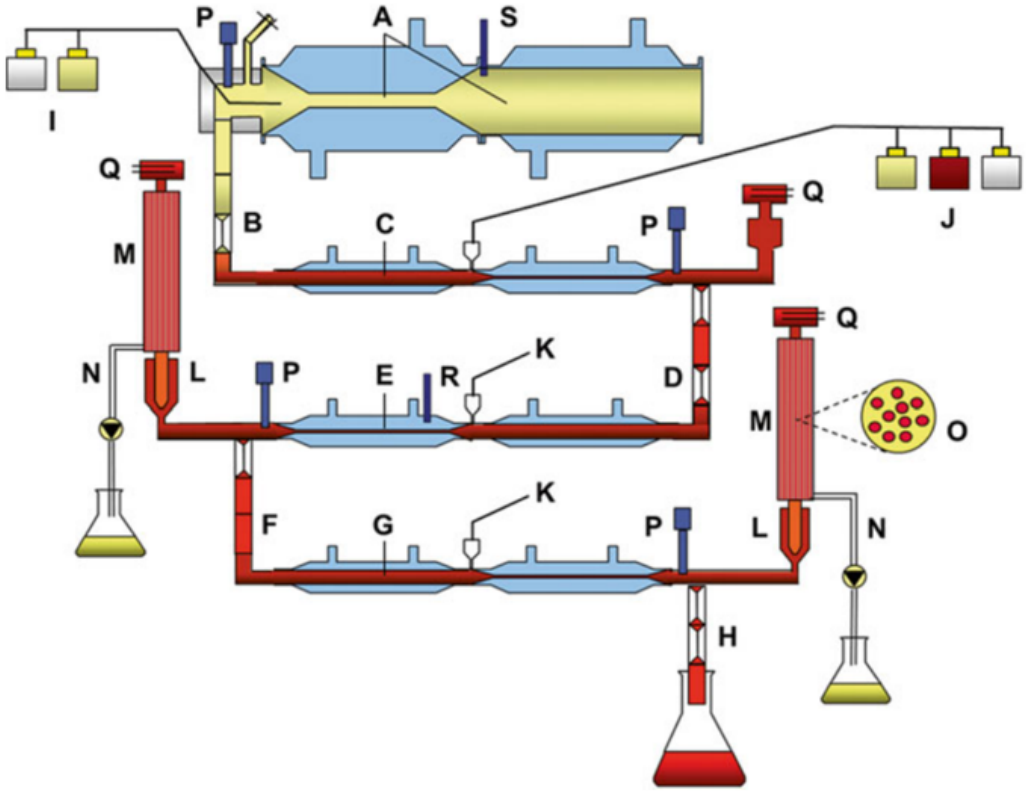

Figure 1.7: Schematic of the TIM system

C–the duodenal compartment; E–the jejunal compartment, G– the ileal compartment; and N & O– the absorption components, consisting of a hollow fiber for absorption and the associated collection of the simulated bioavailable fraction. In comparison to the GIS/ASD and the biphasic system, TIM takes a lot of the addition components, like secretion vessels and peristaltic fluid flow, and iterates on them to attempt to . It utilizes

tubular flow to attempt to simulate in vivo hydrodynamics. In addition, each the jejunum and ileum compartments have hollow fiber membranes to provide an absorptive component.

1.4. References

1. Hay, Michael, et al. ”Clinical development success rates for investigational drugs.” Nature biotechnology 32.1 (2014): 40-51.

2. Pharma, Evaluate. ”World Preview 2018.” Dostupno na: http://www. evaluategroup. com/Public/EvaluatePharma-World-Preview-2018-Embracing-the-Patent-Cliff. aspx [30.6. 2013.] (2011).

3. Amidon, Gordon L., et al. ”A theoretical basis for a biopharmaceutic drug classification: the correlation of in vitro drug product dissolution and in vivo bioavailability.” Pharmaceutical research 12.3 (1995): 413-420.

4. Food and Drug Administration. Guidance for Industry: Waiver of in vivo bioavailability and bioequivalence studies for immediate-release solid oral dosage forms based on a Biopharmaceutics Classification System. Food and Drug Administation; Rockville, MD: 2000. Retrieved fromwww.fda.gov/cder/guidance/index.htm.

5. Macheras, Panos, and Vangelis Karalis. ”A non-binary biopharmaceutical classification of drugs: The ABΓ system.” International journal of pharmaceutics 464.1 (2014): 85-90.

6. Tsume, Yasuhiro, et al. ”The Biopharmaceutics Classification System: subclasses for in vivo predictive dissolution (IPD) methodology and IVIVC.”European Journal of Pharmaceutical Sciences 57 (2014): 152-163.

7. Sugano, Kiyohiko. ”Aqueous boundary layers related to oral absorption of a drug: from dissolution of a drug to carrier mediated transport and intestinal wall metabolism.” Molecular pharmaceutics 7.5 (2010): 1362-1373.

8. Wang, Yanxing, et al. ”Analysis of Diffusion-Controlled Dissolution from Polydisperse Collections of Drug Particles with an Assessed Mathematical Model.” Journal of pharmaceutical sciences 104.9 (2015): 2998-3017.

9. Noyes, Arthur A., and Willis R. Whitney. ”The rate of solution of solid substances in their own solutions.” Journal of the American Chemical Society 19.12 (1897): 930-934.

10. Deen, William M. Analysis of Transport Phenomena. New York: Oxford UP, 2012. Print.

11. Wang, Bing, and Piero M. Armenante. ”Experimental and computational determination of the hydrodynamics of mini vessel dissolution testing systems.” International Journal of Pharmaceutics 510.1 (2016): 336-349.

12. Lomax, Harvard, T. H. Pulliam, and D. W. Zingg. Fundamentals of Computational Fluid Dynamics. Berlin: Springer, 2001. Print.

13. Kakhi, Maziar. ”Mathematical modeling of the fluid dynamics in the flow-through cell.” International journal of pharmaceutics 376.1 (2009): 22-40.

14. Mudie, Deanna M., Gordon L. Amidon, and Gregory E. Amidon. ”Physiological parameters for oral delivery and in vitro testing.” Molecular pharmaceutics 7.5 (2010): 1388-1405.

15. Allen, Adrian, and Gunnar Flemström. ”Gastroduodenal mucus bicarbonate barrier: protection against acid and pepsin.” American Journal of Physiology-Cell Physiology 288.1 (2005): C1-C19.

16. Krieg, Brian J., et al. ”In Vivo Predictive Dissolution: Comparing the Effect of Bicarbonate and Phosphate Buffer on the Dissolution of Weak Acids and Weak Bases.” Journal of pharmaceutical sciences 104.9 (2015): 2894-2904.

17. Mudie, Deanna M., et al. ”Mechanistic analysis of solute transport in an in vitro physiological two-phase dissolution apparatus.” Biopharmaceutics & drug disposition 33.7 (2012): 378-402.

18. Matsui, Kazuki, et al. ”In Vitro Dissolution of Fluconazole and Dipyridamole in Gastrointestinal Simulator (GIS), Predicting in Vivo Dissolution and Drug–Drug

Interaction Caused by Acid-Reducing Agents." Molecular pharmaceutics 12.7 (2015): 2418-2428.

19. Polster, Christopher S., et al. "Use of Artificial Stomach– Duodenum Model for Investigation of Dosing Fluid Effect on Clinical Trial Variability." Molecular pharmaceutics 7.5 (2010): 1533-1538.

20. Carino, Stephen R., David C. Sperry, and Michael Hawley. "Relative bioavailability estimation of carbamazepine crystal forms using an artificial stomach-duodenum model." Journal of pharmaceutical sciences 95.1 (2006): 116-125.

21. Minekus, Mans. "The TNO gastro-intestinal model (TIM)." The Impact of Food Bioactives on Health. Springer International Publishing, 2015. 37-46.

22. Lindfors, Lennart, et al. "Hydrodynamic effects on drug dissolution and deaggregation in the small intestine—a study with felodipine as a model drug." Journal of pharmaceutical sciences 104.9 (2015): 2969-2976.

23. Kararli, T. T., Kirchhoff, C. F., & Truelove, J. E. (1995). Ionic strength dependence of dissolution for Eudragit S-100 coated pellets. Pharmaceutical research, 12(11), 1813-1816.

Chapter 2.

Evaluation of Amorphous Solid Dispersion Dissolution in Biorelevant Dissolution Media

2.1. Introduction

Drug molecules with low aqueous solubility and high permeability rates, classified as BCS Class II molecules, can be further separated by their behavior with respect to pH into three subclasses: acid (a), bases (b), and neutral (c).[1,2] As the extent of ionization increases across a pH range, the aqueous solubility increases. The active pharmaceutical ingredient, Compound A, used in this study is a BCS Class IIb drug with low aqueous solubility (<1ug/mL), high permeability (logP >3, cLogP 4.11) and pKa of 3.93. It is non-ionized at neutral pH (approximately 6.5). Hydroxypropyl methylcellulose acetate succinate (HPMCAS) is a weak acid polymer exhibiting pH dependent solubility and dissolution with a pKa of approximately 5 and very low intrinsic aqueous solubility at low pH. For certain compounds, formulation techniques are used to increase the solubility of the compound, in order to increase bioavailability. The solubility enhancement of amorphous forms compared to the crystalline form can be on the range of 2-fold to over 100-fold.[3-6] This enhancement is affected by the difference between energy states of the crystalline and amorphous forms and the

changes in free energy due to water sorption.[3,6] However, amorphous compounds are unstable and begin to crystalize over time, losing the solubility enhancement the amorphous form provides. Thus, crystallization inhibition may be necessary to utilize the solubility enhancement of amorphous forms. Crystallization can be inhibited with the formulation of an amorphous solid dispersion. An amorphous solid dispersion is a mix of a polymer and drug, both in amorphous state. The drug must be soluble in the polymer of interest for the polymer to impart stability against crystallization.[7] Hydrogen bonding between polymer and drug has also been shown to play a role in crystallization inhibition.[8] By preventing crystallization, solid dispersions allow for the drug to reach supersaturation, a concentration well above the intrinsic solubility of the crystalline form. The ratio between drug and polymer can be tuned so that drug dissolution and drug solution stability can be optimized. At high polymer levels, drug dissolution rates can be increased to the point of being congruent with the dissolution rate of the polymer and therefore controlled by the dissolution of polymer.[9] Promoting supersaturation and extending the supersaturation are desirable properties of amorphous solid dispersions.7 HPMCAS has been shown to provide the enhancement to various drugs.[10,11] It remains a significant challenge to identify in vitro dissolution test conditions that are predictive of in vivo performance. Mudie, et al. reviewed the physiology of the human gastrointestinal tract to identify parameters relevant to the development of biorelevant dissolution methodologies including concentrations of bile salts, ions, lipids, and enzymes that play a role in dissolution and absorption in vivo, along with pH, viscosity, surface tension, osmolality, buffer type and buffer capacity.[12] While a wide range of luminal osmolalities has been reported in the literature[12] and is dependent upon fasted or fed states and location of sampling, a range of approximately 150-300 mOsm/kg would appear reasonable and corresponds to approximately isotonic conditions and can therefore be considered physiologically realistic (e.g. 150 mM NaCl).[13-15] Typically, conventional dissolution studies are performed in high buffer media, such as 50mM phosphate buffer, at a pH between 6.5 and 7.0 to ensure robust analysis with minimal pH changes during dissolution testing. However, in vitro systems for evaluating formulation differences may be expected to better correlate with in vivo performance by using buffer concentrations and species reflective of the intestine.

Bicarbonate is the physiologic buffer of the intestinal tract and is created in vivo by secretion of bicarbonate ions. These bicarbonate ions are generated by the presence of carbon dioxide with carbonic anhydrase enzymes in the pancreas and small intestine. However, in vitro use of low buffer capacity bicarbonate buffer systems is more difficult to use for routine dissolution analysis. Bicarbonate dissolution systems typically sparge carbon dioxide or a carbon dioxide: air mixture into solution to maintain the dissolved carbon dioxide concentration, creating a complex dissolution media and the presence of dissolved gas. Furthermore, bicarbonate buffer has unique properties that result in a more complex mass transport and dissolution process.[16] As a result of this complexity, a buffer with similar behavior to bicarbonate buffer is extremely desirable. A method for determining equivalent phosphate buffer for a physiologically relevant 10.5 mM bicarbonate buffer has been previously reported for drug molecules in the absence of excipients.[16] Using Krieg, et al. as to provide a starting point, a weakly acidic compound like HPMCAS, at pH 7.0, the expected equivalent phosphate buffer concentration should range between 2.5-10 mM. Bicarbonate buffer and its effect on surface pH does not only affect drug molecules, but can also be useful in evaluating other pH dependent excipients, mainly pH dependent polymers such as HPMCAS. Some of these polymers have pH-controlled solubility due to carboxylic acid groups which are non-ionized at low pH. These polymers can be used as enteric coatings. Enteric coatings can be applied to drug products to delay drug release until reaching the intestinal tract. A review by Al-Gousous et al. states that, despite use since before the turn of the 20th century, disintegration and dissolution of enteric coatings beyond the stomach has not been well defined.[17] The review continues by suggesting the use of bicarbonate buffers to determine discrepancies between in vitro and in vivo performance of products with enteric coats.[17] Conventional in vitro tests have shown relatively fast disintegration and dissolution compared to the in vivo processes. However, with appropriate buffer systems, in vitro systems have shown promise in predicting in vivo performance.[18] Bicarbonate buffer has also been shown to provide rank order dissolution evaluation to discern between differing enteric coats for prednisolone, a BCS Class I drug.[19] One study by Kararli, Kirchkoff and Truelove showed that increasing ionic strength in vitro caused increased dissolution rate for enteric coated formulations.[20] The goal of this

study is to determine the role of buffer species and concentration, ionic strength, and pH as part of ASD dissolution both with respect to Compound A and the role of HPMCAS in determining overall drug dissolution. Our hypothesis is that HPMCAS as a weak acid determines the overall dissolution of API (Compound A), a weak base, and that a low buffer capacity phosphate buffer with physiologically realistic ionic strength will successfully mimic physiologically relevant bicarbonate buffer with a physiologically realistic ionic strength. Furthermore, a more complete understanding of the mechanism of dissolution under physiologic conditions will provide greater insight into in vivo performance of ASDs.

2.2. Materials and Methods

2.2.1. Materials

Active pharmaceutical ingredient (Compound A) solid dispersion were used for all dissolution experiments. The solid dispersion was formed by dissolving API in a pH-sensitive polymer matrix using hot-melt extrusion technology; the API was mixed with HPMCAS (1:3, w/w) for the hot-melt extrusion process. For standard solutions, analytical grade Compound A was used. All other materials used were of analytical grade or greater. Purified water was used for all experiments.

2.2.2. Dissolution Experimental Conditions

Dissolution experiments were performed under the conditions shown in Table 2.1. Phosphate buffer solutions used as dissolution media were prepared using sodium monobasic phosphate and sodium phosphate dibasic anhydrous to the desired concentration and initial bulk pH. Sodium chloride was added as needed to adjust ionic strength. Polysorbate 80 was added to each buffer solution at a ratio of 1.3% w/v. After addition of polysorbate, the solution was allowed to mix until dissipation of foam. Addition of polysorbate 80 was necessary to prevent crystallization of drug and ensure dissolution of drug under physiologic pH conditions where it is non-ionized and

therefore very insoluble. Crystalline form solubility in polysorbate 80 concentration was very low and could not contribute to the extent of the dissolution. All dissolution experiments were performed with media maintained at 37°C. USP <711> Apparatus 2 was used, and dissolution media volume was fixed at 900 mL with a paddle speed of 50 rpm. Solid dispersion was accurately weighed to achieve target dose of compound A and added to each dissolution vessel. While monitoring the pH over the course of the experiment, dilute solutions of hydrochloric acid and sodium hydroxide were used through manual addition to maintain the pH with 0.1 pH units.

2.2.3. Bicarbonate Buffer

The buffer capacity of an open carbon dioxide system has been described mathematically as shown in Equation 1.[21]

$$\beta_{op} = 2.303[HCO_3^-] \tag{2.1}$$

Where β_{op} is the buffer capacity of the solution and [HCO3-] is the molar concentration of bicarbonate.[21] The buffer capacity of bicarbonate is typically sufficient to maintain bulk pH when continuously sparging with carbon dioxide. However, the pH at the dissolving surface of a particle dictates the dissolution of ionizable drugs and excipients. At the surface of a dissolving particle or tablet, a pH gradient occurs as dissolving solute (drug or polymer) alters the pH such that the bicarbonate buffer is unable to maintain the bulk pH at the surface of the dissolving substance.16,19Bicarbonate buffer solutions were prepared by continuously sparging a mix of 100% compressed air and 100% dry carbon dioxide (Metro Welding, Ann Arbor, MI), using gas flow controllers (King Instrument Company, CA, USA) to make the desired bicarbonate concentration in a 0.9% w/v sodium chloride solution. Throughout the experiment, percentage of aqueous carbon dioxide and pH were monitored using a CO2 monitor (YSI 8500, Yellow Springs, OH) and a pH meter (Beckman Φ 40, Brea, CA), respectively. Solid sodium hydroxide was added to adjust the initial pH. For all dissolution experiments, samples of approximately 2 mL of media were withdrawn from the vessel and filtered (Millex 1.0 μm glassfiber syringe filter, 25 mm diameter, EMD Millipore, Burlington, MA). The

filtrate was then diluted at a 1:1 ratio with acetonitrile in an HPLC autosampler vial. Standard vials were prepared in a similar manner.

2.2.4. HPLC Method

Sample solutions were analyzed by an isocratic reverse phase HPLC method (Agilient 1100 Series, Santa Clara, CA) using an Agilent Zorbax SB-Phenyl column (4.6 x 150mm, 3.5um particles). Mobile phase was prepared at a 36:64:0.15 v:v:v ratio of acetonitrile:water:85% o-phosphoric acid. The column was maintained at 40°C with a mobile phase flow rate of 2.0mL/minute. UV detection was performed at 254 nm. A standard solution was prepared at 0.3mg/mL approximating the final concentration of sample solutions.

2.2.5. NMR Sample Preparation

Deuterium oxide (D2O) was purchased from Cambridge Isotope Laboratories and was used as received. 1.7 mm NMR tubes were acquired from Bruker (Bruker Biospin, Rheinstetten, Germany). Acetonitrile (ACN) was purchased from Fisher Scientific (Thermo Fisher Scientific, Waltham, MA, USA) and was used as received.
Samples for NMR analysis were prepared using the following workflow. The reason for utilizing this workflow is discussed in more detail in the discussion section. One mL samples from dissolution testing were added to HPLC vials. 500 µL of each sample was transferred to a 96-well, low-volume plate (1.5 mL). Water was removed from the samples using a GeneVac® EZ-2 centrifugal evaporator (GeneVac Ltd., Ipswich, United Kingdom) prior to extraction with deuterated phosphate buffer, pH 6.5 acetonitrile (50:50, v/v) using a Scilogex MX-M microplate mixer (Scilogex, LLC., Rocky Hill, CT). Using a Gilson® GX-274 liquid handling system (Gilson, Inc., Middleton, WI, USA), 45 µL of solution was then transferred to 1.7 mm NMR tubes (60 µL total volume) in a SampleJet cassette (Bruker Biospin, Rheinstetten, Germany) for automated NMR analysis.

2.2.6. NMR Spectroscopy

All NMR experiments were performed on a Bruker AV-III 500 MHz spectrometer equipped with a 1.7 mm TCI z-gradient cryoprobe and SampleJet automated sample changer (Bruker Biospin, Rheinstetten, Germany). 1H NMR spectra were acquired at 298.0 K using the zg30 pulse sequence (Bruker Biospin, Rheinstetten, Germany) at a pulse width of 13.5 s. 65,536 points were acquired through 320 scans with a spectral width of 8 kHz, constant receiver gain, an acquisition time of 2 s, and relaxation delay of 3 s. Data were acquired with TopSpin™ software (Bruker Biospin, Rheinstetten, Germany) and processed using MestReNova 11.0 software (Mestrelab Research S. L. Santiago de Compostela, Spain).

2.3. Results and Discussion

2.3.1. Comparison of Conventional Dissolution Media to Bicarbonate Buffer

Dissolution of the ASD was performed in conventional dissolution media: 50 mM phosphate buffer, pH 6.8, 200 mM ionic strength; and in 10.5 mM bicarbonate buffer at two different pH conditions, 7.0 and 6.5 and results are shown in Figure 2.1. The dissolution of the ASD in the conventional phosphate buffer media was substantially faster than dissolution in the bicarbonate buffer. In bicarbonate buffer, dissolution did not reach completion after two hours at either pH condition.

2.3.2. Determination of Equivalent Phosphate Buffer at pH 7.0

As previously discussed in the introduction, the expected equivalent phosphate buffer concentration for HPMCAS approximating physiologically relevant bicarbonate buffer at pH 7.0 is between 2.5 and 10 mM. This estimation is based on the low solubility of HPMCAS and its pKa of approximately 5.16 Using this equivalent phosphate concentration as a basis, the bicarbonate dissolution profile was compared to three phosphate concentrations in that range: 2.5 mM, 5.0 mM and 7.5mM, as shown in

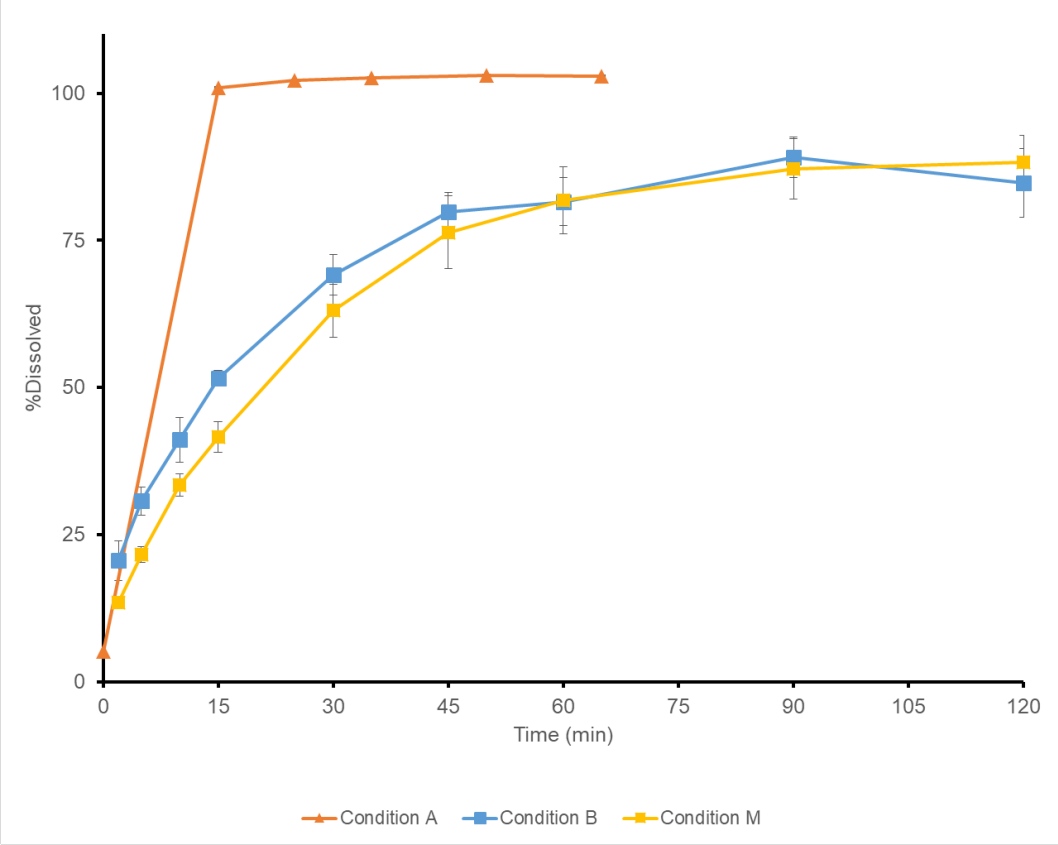

Figure 2.1: Comparison of conventional dissolution media at pH 6.8 (Condition A) to bicarbonate buffer at pH 7.0 and 6.5 (Conditions B and D, respectively). See Table 2.1 for full descriptions of each condition

Figure 2.2 (conditions E, G and M, respectively). The profile for 2.5 mM phosphate buffer was most similar to the bicarbonate buffer in both rate and extent of dissolution. Two expected equivalent phosphate buffer concentrations were used to further characterize impact of ionic strength and set of experiments were carried out by varying ionic strength: 2.5mM and 7.5mM. Under those buffer concentrations, ionic strength was controlled using varied levels of sodium chloride for ionic strengths between 50 and 150 mM. Figure 2.3, in the left panel, shows a comparison of 2.5 mM phosphate buffer at varying ionic strengths to 10.5 mM bicarbonate buffer at 150 mM ionic strength the right panel compares 7.5 mM phosphate buffer at varying ionic

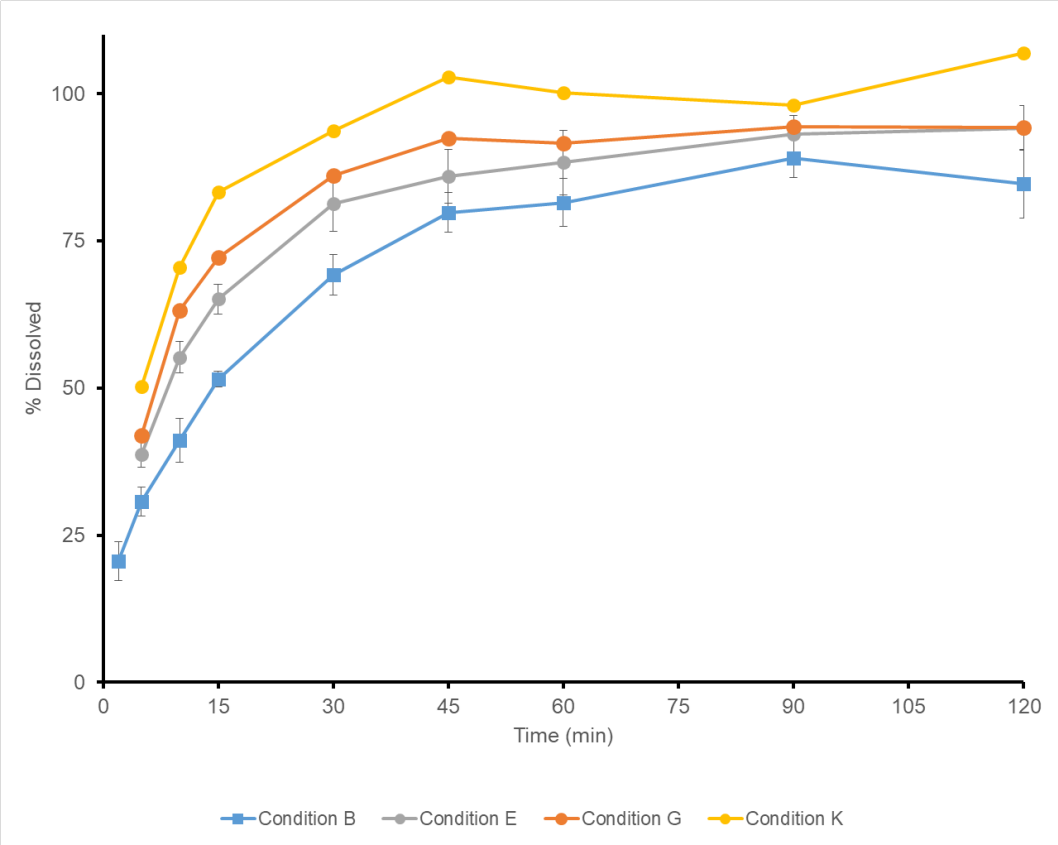

Figure 2.2: Comparison of pH 7.0 bicarbonate buffer (Condition B) to varying phosphate concentrations at pH 7.0, (E: 2.5mM, G: 5mM, K: 7.5mm). See Table 2.1 for full descriptions of each condition.

strengths to the same 10.5 mM bicarbonate buffer. These data demonstrate the important role of ionic strength on the extent and rate of drug ASD dissolution. With increasing ionic strength, the extent of dissolution of drug ASD increases. This effect on extent of dissolution with increasing ionic strength appears to reach a maximum effect at 150 mM with little increase in extent of dissolution beyond 100 mM ionic strength, as shown when comparing Conditions E-G in the right panel of Figure 2.3. Understanding HPMCAS dissolved in sample solution provides a more clear view of the drug dissolution behavior in media with differing ionic strength. Several chromatography approaches such as reverse phase and size exclusion were evaluated to determine

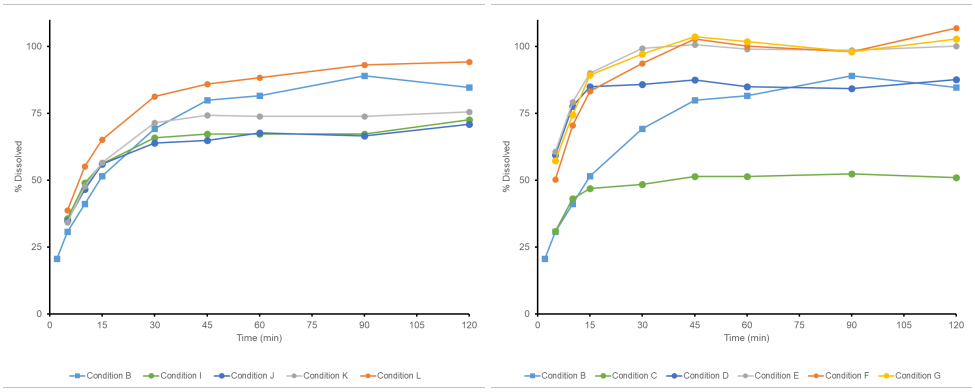

Figure 2.3: Comparison of bicarbonate buffer (Condition B) at pH 7.0 to 2.5 mM (left) and 7.5mM (right) phosphate buffer at different ionic strengths (left, I: 50 mM, J: 75 mM, K: 100 mM, L: 150 mM; right, C: 40 mM, D: 75 mM, E: 100 mM, F: 150 mM, G: 200 mM) See Table 2.1 for full descriptions of each condition.

amount of HPMCAS in sample solution dissolved over time. Presence of polysorbate 80 complicated the determination of HPMCAS levels using High Performance Liquid chromatography, hence NMR analysis was used. The dissolution experiments were conducted in water which can reduced the sensitivity of NMR analysis and introduces higher noise. Therefore, water was removed from the samples using a centrifugal evaporator and after water removal extraction was performed with deuterated phosphate buffer, pH 6.5 /acetonitrile (50:50, v/v). Figure 2.4 shows that with lower ionic strength (75mM versus 150 mM), there is decreased dissolution rate of HPMCAS and typically reduced drug dissolution. The dissolution rate of HPMCAS is decreased at lower ionic strength, resulting in a reduced extent of dissolution for drug and HPMCAS. The decreased drug dissolution may be due in part to a lower concentration of HPMCAS dissolved in solution, thus reducing the precipitation inhibition effect that HPMCAS has on the solution and drug. Using equal ionic strengths in both buffer systems is important to ensuring an accurate determination of equivalent phosphate. At pH 7.0, the dissolution rates of both drug and HPMCAS are most similar to the bicarbonate buffer system with 2.5 mM phosphate buffer and 150 mM ionic strength. This equivalent buffer concentration is consistent with the dissolution of the low solubility, weak acid HPMCAS.

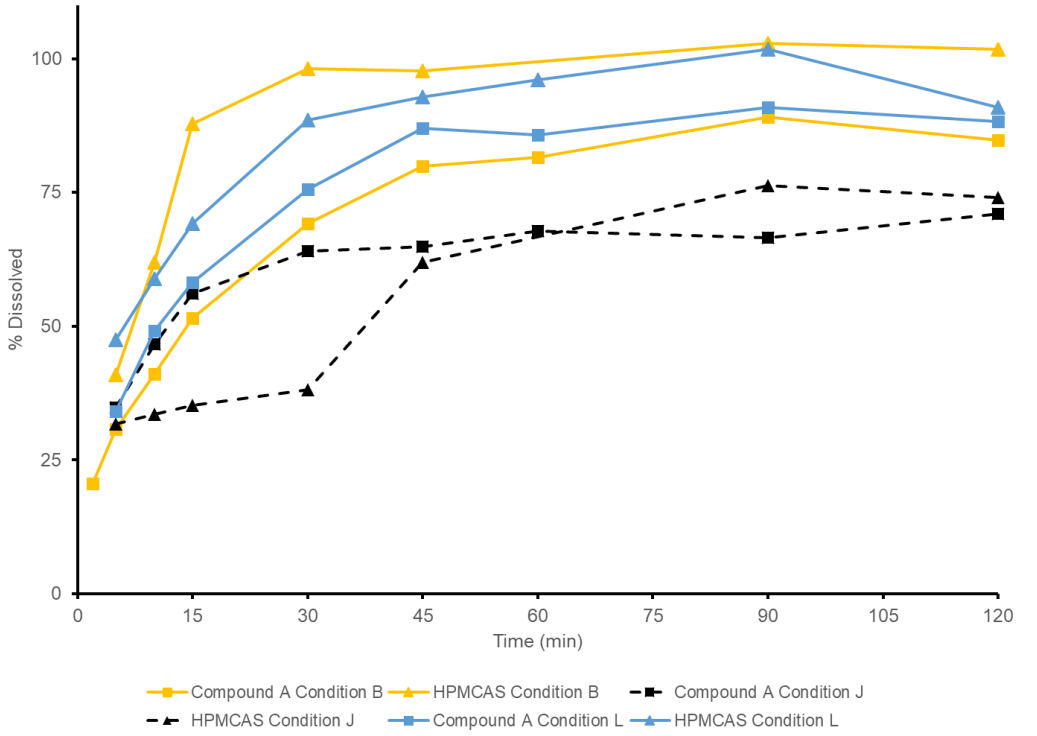

Figure 2.4: Comparison of HPMCAS and Compound A Dissolution at pH 7.0. Condition B is 10.5mM bicarbonate buffer with 150 mM ionic strength. Both conditions J and L are 2.5 mM phosphate buffer with varied ionic strengths: 75 mM for Condition J, 150 mM for Condition L. See Table 2.1 for full descriptions of each condition.

2.3.3. Determination of Equivalent Phosphate Buffer at pH 6.5

HPMCAS and drug dissolution was also determined at pH 6.5. These results are shown in Figure 2.5. As with pH 7.0, the dissolution rates at pH 6.5 of both drug and HPMCAS are comparable between the bicarbonate buffer system and 2.5 mM phosphate buffer with 150 mM ionic strength. This equivalent buffer concentration is also consistent with the dissolution of the low solubility, weak acid HPMCAS.

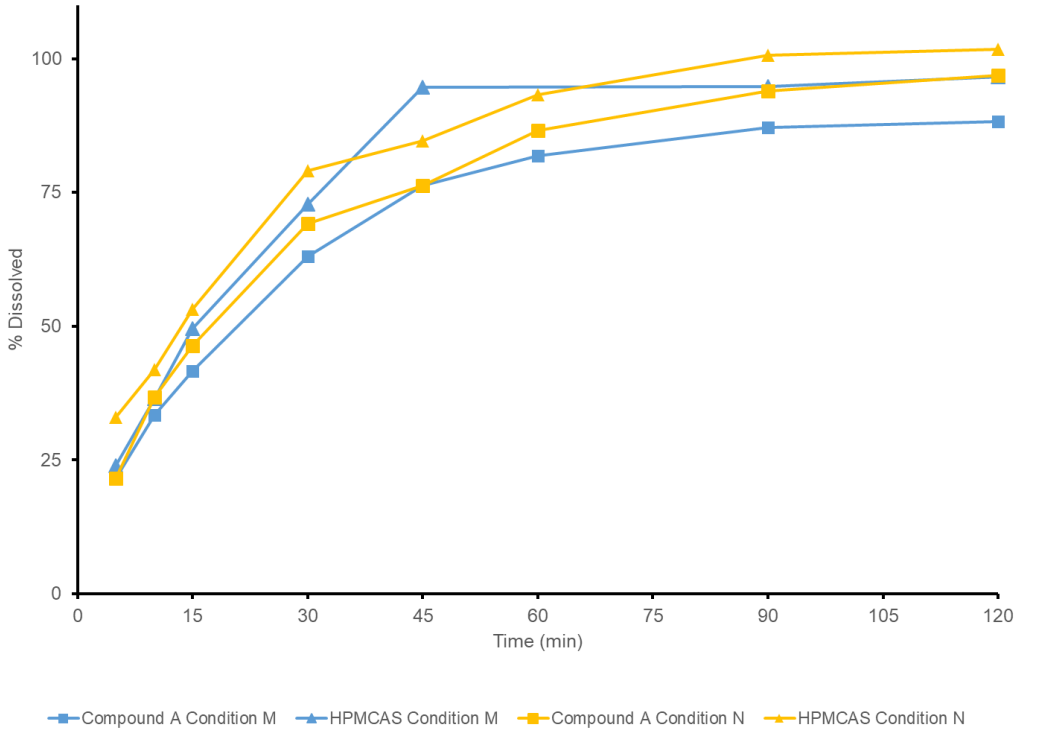

Figure 2.5: Comparison of HPMCAS and Compound A Dissolution at pH 6.5. Condition M is 10.5 mM bicarbonate buffer with 150 mM ionic strength. Condition N is 2.5 mM phosphate buffer with 150 mM ionic strength. See Table 2.1 for full descriptions of each condition.

2.3.4. Discussion

These results demonstrate that conventional in vitro dissolution conditions with high buffer capacity phosphate can substantially increase the dissolution rate and extent of dissolution for ASDs utilizing HPMCAS. When compared to a biorelevant buffer system like bicarbonate, the dissolution rate of the model drug-HPMCAS ASD is substantially higher in conventional media at the same pH conditions. Additionally, the ionic strength of solution also affects the rate and extent of dissolution of HPMCAS and drug in weakly buffered media. This is likely due in part to the enhanced solubility of HPMCAS which can inhibit precipitation of the metastable amorphous form drug present in the ASD and thus provides solubility enhancement above the intrinsic

solubility. These results are consistent with the hypothesis that HPMCAS is dictating the overall dissolution rate of drug-HPMCAS granules in physiologically relevant buffer. The equivalent phosphate buffer for the ASD determined was 2.5 mM for both pH 6.5 and pH 7.0 conditions and 150 mM ionic strength, consistent with the expected equivalent phosphate concentration for low solubility, weak acid HPMCAS polymer. For this formulation, congruent dissolution rates were observed between the polymer and drug under isotonic conditions. Drug dissolution therefore appears to be controlled by the dissolution of HPMCAS.

2.4. Conclusions

These results emphasize the value of in vivo relevant media in conducting mechanistic in vitro testing. The dissolution rate of the model drug-HPMCAS ASD is substantially higher in conventional media compared to physiologically relevant bicarbonate buffer system. Ionic strength also plays an important role in the rate and extent of dissolution of HPMCAS and drug in weakly buffered media. Under biorelevant conditions utilizing either physiologically relevant bicarbonate buffer concentration or low buffer capacity phosphate buffer at approximately isotonic conditions (150 mM ionic strength) drug dissolution is controlled by the dissolution of HPMCAS.
Further evaluation of optimal polymer to drug ratios could be explored using bicarbonate buffer or its equivalent phosphate buffer. These results are promising for improved evaluation of ASDs and could provide a means to predict an optimal ASD formulation during the pre-clinical phase of development.

2.5. Acknowledgements

I would like to thank W. Peter Wuelfing, and Justin Pennington from Merck & Co., Inc., Kenilworth, NJ, USA for support regarding this work. I would also like to thank William Forrest, Andre Hermans, and Sanjaykumar Patel for the many conversations and discussions about the development of this work. Research reported in this publication was partially supported by Merck Sharp & Dohme Corp., a subsidiary of

Merck & Co., Inc., Kenilworth, NJ, USA. I also gratefully acknowledge partial financial support from the College of Pharmacy, University of Michigan.

2.6. References

1. Tsume Y, Mudie DM, Langguth P, Amidon GE, Amidon GL 2014. The Biopharmaceutics Classification System: subclasses for in vivo predictive dissolution (IPD) methodology and IVIVC. Eur J Pharm Sci 57:152-163.

2. Amidon GL, Lennernäs H, Shah VP, Crison JR 1995. A Theoretical Basis for a Biopharmaceutic Drug Classification: The Correlation of in Vitro Drug Product Dissolution and in Vivo Bioavailability. Pharmaceutical Research 12(3):413-420.

3. B. MS, J. PM, M. SR, H. BR 2010. Solubility advantage of amorphous pharmaceuticals: I. A thermodynamic analysis. Journal of Pharmaceutical Sciences 99(3):1254-1264.

4. Hancock BC, Parks M 2000. What is the True Solubility Advantage for Amorphous Pharmaceuticals? Pharmaceutical Research 17(4):397-404.

5. Parks GS, Huffman HM, Cattoir FR 1928. Studies on glass. II. The transition between the glassy and liquid states in the case of glucose. The Journal of Physical Chemistry 32(9):1366-1379.

6. Murdande SB, Pikal MJ, Shanker RM, Bogner RH 2010. Solubility Advantage of Amorphous Pharmaceuticals: II. Application of Quantitative Thermodynamic Relationships for Prediction of Solubility Enhancement in Structurally Diverse Insoluble Pharmaceuticals. Pharmaceutical Research 27(12):2704-2714.

7. Sandrien J, Guy VdM 2009. Review: physical chemistry of solid dispersions. Journal of Pharmacy and Pharmacology 61(12):1571-1586.

8. Frank DS, Matzger AJ 2018. Probing the Interplay between Amorphous Solid Dispersion Stability and Polymer Functionality. Mol Pharm 15(7):2714-2720.

9. Alonzo DE, Gao Y, Zhou D, Mo H, Zhang GGZ, Taylor LS 2011. Dissolution and precipitation behavior of amorphous solid dispersions. J Pharm Sci 100(8):3316-3331.

10. Konno H, Handa T, Alonzo DE, Taylor LS 2008. Effect of polymer type on the dissolution profile of amorphous solid dispersions containing felodipine. Eur J Pharm Biopharm 70(2):493-499.

11. Tanno F, Nishiyama Y, Kokubo H, Obara S 2004. Evaluation of hypromellose acetate succinate (HPMCAS) as a carrier in solid dispersions. Drug Dev Ind Pharm 30(1):9-17.

12. Mudie DM, Amidon GL, Amidon GE 2010. Physiological Parameters for Oral Delivery and in Vitro Testing. Molecular Pharmaceutics 7(5):1388-1405.

13. Lindahl A, Ungell A-L, Knutson L, Lennernäs H 1997. Characterization of fluids from the stomach and proximal jejunum in men and women. Pharmaceutical research 14(4):497-502.

14. Banwell J, Gorbach S, Pierce N, Mitra R, Mondal A 1971. Acute undifferentiated human diarrhea in the tropics: II. Alterations in intestinal fluid and electrolyte movements. The Journal of clinical investigation 50(4):890-900.

15. Fadda H, Basit A 2005. Dissolution of pH responsive formulations in media resembling intestinal fluids: bicarbonate versus phosphate buffers. Journal of drug delivery science and technology 15(4):273-279.

16. Krieg BJ, Taghavi SM, Amidon GL, Amidon GE 2015. In Vivo Predictive Dissolution: Comparing the Effect of Bicarbonate and Phosphate Buffer on the Dissolution of Weak Acids and Weak Bases. Journal of Pharmaceutical Sciences 104(9):2894-2904.

17. Al-Gousous J, Tsume Y, Fu M, Salem, II, Langguth P 2017. Unpredictable Performance of pH-Dependent Coatings Accentuates the Need for Improved Predictive in Vitro Test Systems. Mol Pharm 14(12):4209-4219.

18. Al-Gousous J, Amidon GL, Langguth P 2016. Toward Biopredictive Dissolution for Enteric Coated Dosage Forms. Mol Pharm 13(6):1927-1936.

19. Liu F, Merchant HA, Kulkarni RP, Alkademi M, Basit AW 2011. Evolution of a physiological pH 6.8 bicarbonate buffer system: application to the dissolution testing of enteric coated products. Eur J Pharm Biopharm 78(1):151-157.

20. Kararli TT, Kirchhoff CF, Truelove JE 1995. Ionic strength dependence of dissolution for Eudragit S-100 coated pellets. Pharmaceutical research 12(11):1813-1816.

21. Butler JN. 1991. Carbon dioxide equilibria and their applications / James N. Butler. ed.: Lewis Publishers.

Chapter 3.

Gastro-Intestinal Simulator-2 Device Design and Method Validation

3.1. Introduction

For oral drug formulations, the efficacy of the formulation on the individual is dependent on many physiological processes and variables. For most drug products, the formulation must disintegrate, undissolved mass must empty from the stomach and into the upper Gastrointestinal (GI) tract, the drug must dissolve and then absorb across the intestinal wall to reach systemic circulation.[1] In addition, the GI fluid is a complex multi-component system.[2,3] One of the difficulties in a pre-clinical setting is capturing the relevant processes and variables in order to relatively rapidly evaluate formulations. Despite understanding of relevant processes, conventional in vitro methods only capture part of one of these processes by performing dissolution at one pH, without any other processes acting on the formulation. Therefore, in order to produce relevant dissolution data in vitro for the goal of producing predictions of in vivo performance, the processes involved in vivo must be considered when designing a new dissolution device. These processes should be selected based on the drug molecules physical properties, such as using their BCS class and subclass as a guide, in order to provide the optimal test. In this work, the consideration of these processes is discussed and examined when designing a four-compartment dissolution device[4,5], the

Gastro-Intestinal Simulator-2 (GIS-2). The USP-2 dissolution device is ubiquitous in the dissolution field. This dissolution technology is frequently used for quality control applications, where simplicity and consistency of results is more important than in vivo relevance. The system can be used to evaluate the effect of variations in manufacturing conditions on in vitro performance. It is also part of in vitro testing necessary for waivers for bioequivalence studies for immediate release products.[6] However, for molecules that exhibit pH-dependent solubility, the shift in pH from the stomach to small intestine is relevant to their dissolution.[5] Thus, a dissolution technology for evaluation of molecules requires a change in pH. A change in pH can be achieved by multiple routes, by adjusting the pH of the media in a single vessel with the addition of sodium hydroxide (either solid or solution)[7,8] or a highly concentrated buffer solution[8-10], or by transferring fluid between compartments.[11-25,29] Fluid transfer between compartments, not only allows for the pH-shift to occur, but also the gastric emptying process can occur in a way that simulates the in vivo process. A variety of multi-compartmental dissolution devices exist and have been shown to be a valuable piece of a pharmaceutical scientist's toolkit in formulation design, troubleshooting and optimization. These devices include: the TNO TIM-1[11-13], the artificial stomach-duodenum (ASD)[14-17], the Golem apparatus[18], and the Gastro-Intestinal Simulator (GIS)[19-22] and other un-named systems based on modified USP dissolution apparatuses.[23-25] These systems range in design philosophy from complex systems attempting to directly mimic the physiologic conditions (TNO TIM-1) and systems that try to emulate in vivo dissolution conditions while maintaining a simple easy-to-use dissolution system that can be run multiple times in one day by a single analyst (GIS/ASD). For the sake of this work, the original GIS, or GIS-1, is examined and used as a basis for designing GIS-2. One necessary decision for the design of GIS-2 is utilizing recent research on the hydrodynamics of the gastrointestinal tract. Lindfors, 2015 showed that hydrodynamics in the small intestine are not a critical factor for micronized particles or disaggregation of drug particle aggregates.[26] However, GI hydrodynamics factor into disintegration of large particles and tablets.[27] The shear rate is also important for large non-micronized particles dissolution as shear effect increases with increasing particle size.[29] Lastly, shear has been shown to act as an enhancement

to mass transfer beyond pure diffusion. This enhancement can be applied to mass transport equations with use of the Sherwood number. The Sherwood number is a dimensionless number that is the ratio between total mass flux from the solid particle surface and flux from that solid by pure diffusion. In terms of conventional equations used for estimating drug dissolution, the Sherwood number can also be used to describe the ratio between particle radius and diffusion layer thickness, these equations are compared in Equation 3.1.

$$\frac{dm}{dt} = Sh(4\pi r)D\Delta C \tag{3.1}$$

Where dm/dt is the change in mass of an individual particle, Sh is the Sherwood number, r is the particle radius, D is the diffusion coefficient of the drug molecule and ΔC is the difference in concentration between the particle surface (saturation) and the bulk solution. Per the work of, Wang and Brasseur the enhancement from pure diffusion can be described as ΔSh units for confinement, shear and convection effects, as shown in Equation 3.2.[30-32]

$$Sh = 1 + \Delta Sh_{confine} + \Delta Sh_{shear} + \Delta Sh_{convection} + \ldots \tag{3.2}$$

where $\Delta Sh_{confine}$ is the enhancement due to the confinement effect, ΔSh_{shear} is the enhancement due to shear on the fluid surround the particle and $\Delta Sh_{convection}$ is the enhancement due to convective forces. For particles of 100 μm diameter, the approximate Sherwood number is in the range of 1.4-4.2 under increasing shear rates.[30] In addition to shear effects on dissolution, another consideration for hydrodynamics is maintain well suspended particles. Dissolution can be unintentionally inhibited if particles are not well suspended and are stationary on the base of the dissolution vessel. This also alters the solution homogeneity and prevents accurate prediction of dissolution due to inconsistent undissolved particle transfer between vessels. Hydrofoil impellers (or hydrofoils) are axial flow impellers that generate particle lift by generating turbulent eddies on the base of vessel.[33-36] For industrial reactor applications, hydrofoils are a common choice for suspended solid particles and are a good fit for a dissolution device for maintain particle suspension.

3.2. Materials and Methods

3.2.1. Materials

All materials were of analytical grade or higher, unless otherwise specified. Acetonitrile for HPLC analysis was HPLC Grade (Fisher Scientific) and trifluoroacetic acid was LC/MS-grade (Sigma-Aldrich, St. Louis, MO).

3.2.2. GIS-1 Method Optimization

GIS-1 Method

GIS-1 is an existing device described in literature, Throughout the optimization stage, the method was in a state of flux to find the optimal method. Listed are initial and final methods to represent the improvements made over the course of the optimization. For any deviations from these two methods, a note has been made in the results section to address those deviations. Initial and final methods are described in Table 3.1, below.

3.3. Determination of the Critical Micellular Concentration of Sodium Dodecyl Sulfate at pH 2.0 with Ibuprofen

Solutions of varying sodium dodecyl sulfate (0-8 mM) were prepared in 0.01N hydrochloric acid. Solution was added to a scintillation vial in triplicate and ibuprofen was added in excess. Control solutions of ibuprofen without SDS were also prepared in triplicate. Solutions were mixed in a shaker bath at 37C for 24 hours. After 24 hours had elapsed, an aliquot of the solution was removed and filtered. Filtered solution was analyzed by HPLC. CMC was determined by the calculating the intercept of the control concentration with the linear regression of all solutions that showed an increase in concentration, using Microsoft Excel (Microsoft, Redmond, WA).

Parameter	Original Condition	Final Condition
Stirring Conditions		
Stomach Stirring	50 RPM with Burst Mixing at 500 RPM every 26 seconds	250 RPM constant
Duodenum Stirring	50 RPM with Burst Mixing at 500 RPM every 26 seconds	120 RPM constant
Jejunum Stirring	100 RPM with stir plate	75 RPM
Initial Vessel Conditions		
Stomach Initial Medium	50 mL of 0.01N Hydrochloric Acid & 250 mL of purified water (300 mL total)	50 mL of 2mM SDS in 0.01N Hydrochloric Acid & 250 mL 2mM SDS in water (300 mL total)
Stomach Secretion Medium	0.01N Hydrochloric Acid	2mM SDS in 0.01N Hydrochloric Acid
Duodenum Initial Medium	50 mL of 50 mM phosphate buffer at pH 7.0	50 mL of 50 mM phosphate buffer at pH 6.5
Duodenum Secretion Medium	100 mM phosphate buffer at pH 7.0	100 mM phosphate buffer at pH 7.0
Jejunum Initial Medium	Empty	100 mL of 50 mM phosphate buffer at pH 6.5
Other Experimental Conditions		
Jejunum Beaker Shape	1 L low form Pyrex beaker	900 mL USP-2 Round Bottom Water Jacketed Vessel
Jejunum Temperature Control	Manually monitored while heated on heated stir plate	Controlled by circulating water bath
Sampling volume	500 µL sampled, centrifuged and supernatant diluted for HPLC analysis	1.5 mL filtered and diluted for HPLC analysis
Media Replacement	No	Yes, Replaced Sampled volume with secretion media
Stomach Volume Maintained	No	Yes at 10 mL

Table 3.1: Comparison of pre-optimization and post-optimization parameters for GIS-1 experiments.

3.4. Just Suspended Speed Determination

Just suspended speed was performed based on the procedure originally described by Zwietering and modified by Ayranci and Kresta.[36,37] The water bath was removed and the vessels were elevated using a lab jack. Normal stirrer clearance was checked. The water bath was removed to allow for better visibility of the base of the vessels. Saturated ibuprofen solution was introduced to the vessel at room temperature. A known volume of ibuprofen suspension was introduced to the vessel. The stir speed was increased incrementally, allowing one to two minutes to reach steady state. After this time period, the bottom of the vessel was observed for about 30 seconds. The speed was increased until no particle was observed to be stationary on the base of the vessel. This procedure was repeated at three volume conditions in the stomach and two in the duodenum. Four observers were used to increase sample size and to verify the results. The just suspended speed was then averaged for the sample group and rounded up to the nearest 10 RPM.

3.5. Apparent Sherwood Number/Mass Transfer Enhancement

3.5.1. Particle Size Distribution

Particles used in the suspension for the dissolution test were viewed via brightfield microscopy. The particles were viewed through polarized light and digital images were taken. Images of ibuprofen particles were then processed using ImageJ (NIH, Bethesda, MD). Based on the rectangular dimensions of the particles, the third dimension was estimated by taking half of the smallest dimension and multiplying it by the two visible dimensions to calculate the particle volume. The effective spherical particle size was then estimated based on this volume. A particle size distribution was generated based on the effective spherical particle sizes observed across observations.

3.5.2. Dissolution Data

In order to properly predict dissolution in the GIS using mass transport models, an apparent Sherwood number was determined. Ibuprofen suspension was introduced to 0.01N hydrochloric acid at the appropriate volume for the vessel and the media was stirred at the determined just suspended speed. Manual samples were taken at regular intervals, aliquoting 1.5 mL from each vessel. Aliquots were filtered through a 0.45 um syringe filter, discarding the first 0.5 mL. Remaining filtrate was diluted as necessary for HPLC analysis. Media removed from each vessel was replaced with appropriate secretion media to maintain volume.

3.5.3. Apparent Sherwood Number

Using the experimental data, the apparent Sherwood number was calculated, using equation 3.1. The predicted dissolution was performed post hoc and fit to the observed dissolution data by varying the Sherwood number to reduce absolute residuals.

3.6. GIS-2 Device & Dissolution Method

3.6.1. 3D Print Material & Tubing Partitioning Study

One cm diameter spheres were printed on a Stratays J750 3D printer (Startasys, Eden Prairie, MN) using Veroclear transparent photopolymer. Spheres were dried at 105C overnight to ensure all volatile material had been removed. After allowing to cool to room temperature in a desiccator, the spheres were weighed and the diameter was recorded using calipers. One sphere was added to an ibuprofen solution of known concentration. The spheres were stirred at 37C for 72 hours, taking timepoints at 12, 24, 48 and 72 hours. Samples were assayed as described above. After 72 hours, the spheres were removed and dried in the oven again overnight. Spheres were weighed to determine any weight increases. This procedure was also applied to tubing for the Ismatec pumps, with the modification of only 72-hour time points being taken.

3.6.2. Device

The GIS-2 is a computer-controlled, four-vessel dissolution device for testing oral formulations. The four vessels represent the stomach, duodenum, jejunum, and ileum. The conditions of the experiment can be adjusted, including initial volumes, stomach emptying profile, secretion rates, temperature, pH, buffer capacity and ionic strength. pH is continuously monitored throughout the experiment. The vessels are flat-bottomed cylindrical glass jacketed vessels. The vessels are mixed using top-down stirring, controlled by digital motors (Myostat Motion Control Inc., Newmarket, ON Canada). The stirrers use appropriately sized 3-blade hydrofoils (Manufacturer, Location).

3.6.3. Method

The devices was controlled by software developed in Labview (National Instruments, Austin, TX). Screenshots of the GUI of the GIS-2 software can be found in Appendix A, along with the operating procedure. Stirring was maintained at speed, cycling between a lower speed to suspend most particles, with a one second burst, every sixty seconds to re-suspend any particles that may have settled to the bottom of the vessel. All fluid transfer was controlled by Ismatec Reglo ICC peristaltic pumps (Cole-Parmer GmbH, Wertheim, Germany). Pumps were standardized with water on day of analysis before analysis. Initial conditions can be found in Table 3.2. The stomach emptied from 300 mL, initially, to 75 mL with first-order kinetics (t1/2: 30 min). Volume was maintained at 50 mL in the duodenum and jejunum. The ileum accumulated all excess volume to maintain the first three vessels. After the stomach reached 75 mL, the experiment continued for one hour, with secretions only, with the stomach, duodenum, and jejunum volumes held constant. Formulations were pre-disintegrated in the stomach, by stirring at 120 RPM for 10 minutes, before fluid transfer was initiated.
Manual samples were taken at regular intervals, aliquoting 1.5 mL from each vessel. Aliquots were filtered through a 0.45 um syringe filter, discarding the first 0.5 mL. Remaining filtrate was diluted as necessary for HPLC analysis. Media removed from each vessel was replaced with appropriate secretion media to maintain volume.

Vessel	Initial Volume and Media	Stir Speed (RPM)	Burst Speed (RPM)	Secretion Buffer and Rate
Stomach	300 mL: 250 mL of 2mM SDS 50 mL of 0.01N HCl w/ 2mM SDS	120	240	2.5 mL/min: 50 mL of 0.01N HCl w/2mM SDS
Duodenum & Jejunum	50 mL of 50 mM Phosphate Buffer pH 6.5	175	350	1 mL/min: 100 mM Phosphate Buffer pH 6.5
Ileum	250 mL of 50 mM Phosphate Buffer pH 6.5	75	150	NA

Table 3.2: Standard GIS-2 media and stirring conditions for experiments.

3.6.4. Stomach Emptying Rate & Maintain Phase Validation

With the introduction of new stomach emptying methods and the ability to maintain stomach volume post-gastric emptying, those new processes required validation. For the new software, three emptying profiles were implemented: 1st order, Weibull and User-Defined. The pre-defined profiles are shown for a 300 mL starting volume in Figure 3.1. In order to validate the emptying profiles, each profile (and the maintain phase) was appropriately setup in the software and each vessel was replaced with an appropriate vessel in order to monitor. The stomach, duodenum and jejunum manually monitored gravimetrically and the ileum was monitored using a graduated cylinder. The initial volume of the stomach was reduced from the typical starting volume to 250 mL due to balance limitations, the duodenum and jejunum were at 50 mL. The gravimetrically monitored vessels were tared before initializing the pumps and their weight was recorded incrementally and concomitantly from stomach to ileum. The difference from tare weight was then used to calculate the observed volume and how the observed volume deviated from the expected volume.

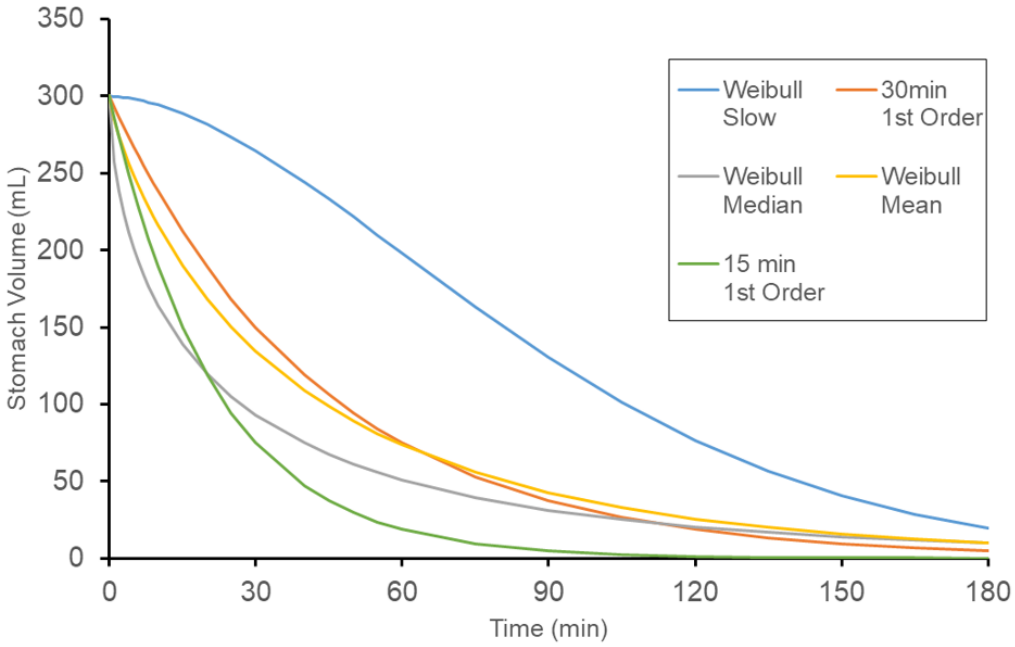

Figure 3.1: Standard GIS-2 media and stirring conditions for experiments.

3.6.5. Titration

Predictions

Predictions for titration methods were generated using MatLAB (Mathworks, Natick, MA). Using the Henderson-Hasselbach equation and maintaining constant volume in the duodenum vessel, total buffer concentration, individual buffer species concentrations and pH were estimated across small time increments (< 1 second). Based on those inputs the amount of titrant was calculated, depending on the method being tested. Code can be found in Appendix B.

Experimental

Titration methods were tested by calibrating the first unused pump channel and priming it with 0.01N sodium hydroxide. Stomach and duodenum conditions were set as described in Table 3.2, with the exception of the duodenum media and secretion which

were 5 mM and 50 mM phosphate buffers, respectively. Throughout the experiment, pH was monitored and recorded. An 800 mg ibuprofen tablet was introduced to the stomach at the beginning of the experiment to simulate a weakly acidic drug.

3.6.6. HPLC Method

Filtered and diluted samples were analyzed by an isocratic reverse phase HPLC method (Agilient 1100 Series, Santa Clara, CA) using an Agilent C-18 column (3.5µm x 4.6µm x 150mm). Mobile phase was a 60:40 mix of acetonitrile:water with 0.1% trifluoroacetic acid. The column was maintained at 40°C with a mobile phase flow rate of 1.0mL/minute. UV detection was performed at 220 nm. A standard curve was prepared bracketing the sample solutions.

3.7. Results

3.7.1. GIS-1 Method Optimization

Concerns for Requiring Method Optimization

Figure 3.2 shows the total mass dissolved in the GIS-1 following a 1-hour experiment. Following 1 hour about 40% of the total dose was dissolved in the system. This experiment showed poor mass recovery in the system and required improvements in order to ensure repeatable and quality data is generated when using GIS-1. This was also necessary to determine what design considerations are needed when designing a next generation device, where improvements can be made.

The first improvement was extending the length of the experiment out to two hours. This was initially achieved in GIS-1 by preventing the volume in the stomach to fall below 10 mL by raising the height of the transfer tube. This was later done by updating the software of the GIS. Next, the sampling procedure needed to be changed. The previous method allowed for inconstant results to be obtained due poor pelletizing of centrifuged samples. If a small drug particle was transferred to the HPLC vial for dilution, results were skewed. To prevent drug particles from being dissolved in the

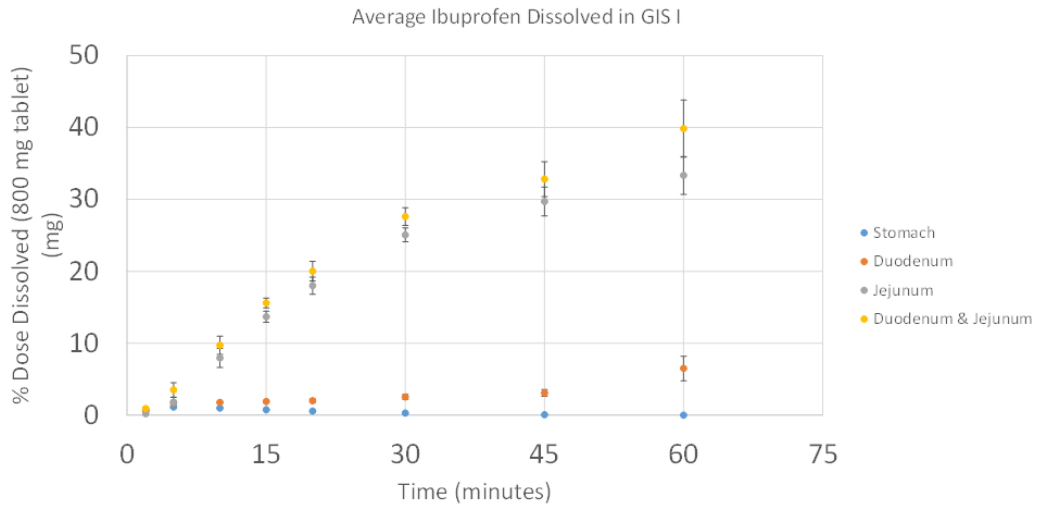

Figure 3.2: Performance of GIS-1 dissolution of an 800 mg ibuprofen tablet using pre-existing methods.

HPLC vial, a 1.5 mL sample was removed and filtered. To compensate for the larger volume removed, equivalent media was replaced into the dissolution vessels to ensure consistent volumes. Third, the pumps were rearranged and tubing was cut to limit particle settling in the transfer tubing lengths. Additionally, transfer pumps and the stomach and duodenum vessels were rinsed after analysis to capture any undissolved drug for mass balance. Next, the jejunum vessel was replaced with a jacketed USP-2 vessel. This helped with maintaining volume and temperature in the jejunum with the assistance of a lid and the recirculating water bath. Lastly, the pump procedure was changed in updated software to be based on a known number of revolutions of the pump and the measured mass of water transferred. This ensures that the pumps are pumping at the correct volumetric flow rate instead of relying on the previous calibration factor to estimate how much volume was transferred. The length of the pre-calibration pump priming cycles and the calibration cycles and calibration speeds were also adjusted to improve calibration. A summary of purge and calibration conditions can be found in Table 3.3.

Pump Type	Purge Conditions	Calibration Conditions
Secretion Pump	45 RPM for 10 min	10 RPM for 3 min
Transfer Pump	90 RPM for 10 min	50 RPM for 3 min

Table 3.3: Summary of pump purging and calibration conditions.

3.7.2. Determination of the critical micellular concentration of sodium dodecyl sulfate at pH 2.0 with Ibuprofen

Figure 3.3 shows change in ibuprofen concentration with increasing concentrations of sodium dodecyl sulfate. There was inconclusive literature data on the CMC of SDS at pH 2. Surfactant was explored because during the disintegration of the ibuprofen tablet, solid adhesion was absorbed on the glass walls of the stomach beaker. This adhesion was severe enough to make the glass beaker nearly opaque. This was another suspected source of loss of ibuprofen to the system. By adding surfactant, drug wetting was improved slightly and the solid adhesion to the walls of the beaker was greatly reduced. The CMC was determined to be the SDS concentration when the linear regression of the elevated ibuprofen concentration intersects the concentration of the control. This intercept was 3.060 mM of SDS. In order to ensure the media remained below the CMC while preventing solid adhesion to the walls of the vessels, 2 mM SDS was selected as an acceptable concentration of SDS.

3.7.3. GIS-1 Hydrodynamics

Just Suspended Speed in GIS-1 Stomach and Duodenum

Just suspended speed was determined by addition of ibuprofen particles to GIS-1 vessels. Table 3.4 summarizes the results of the just suspended speed experiments in the GIS-1 stomach and duodenum vessels. In order to ensure full suspension of particles, the stir speeds can be during operation of the GIS-1.

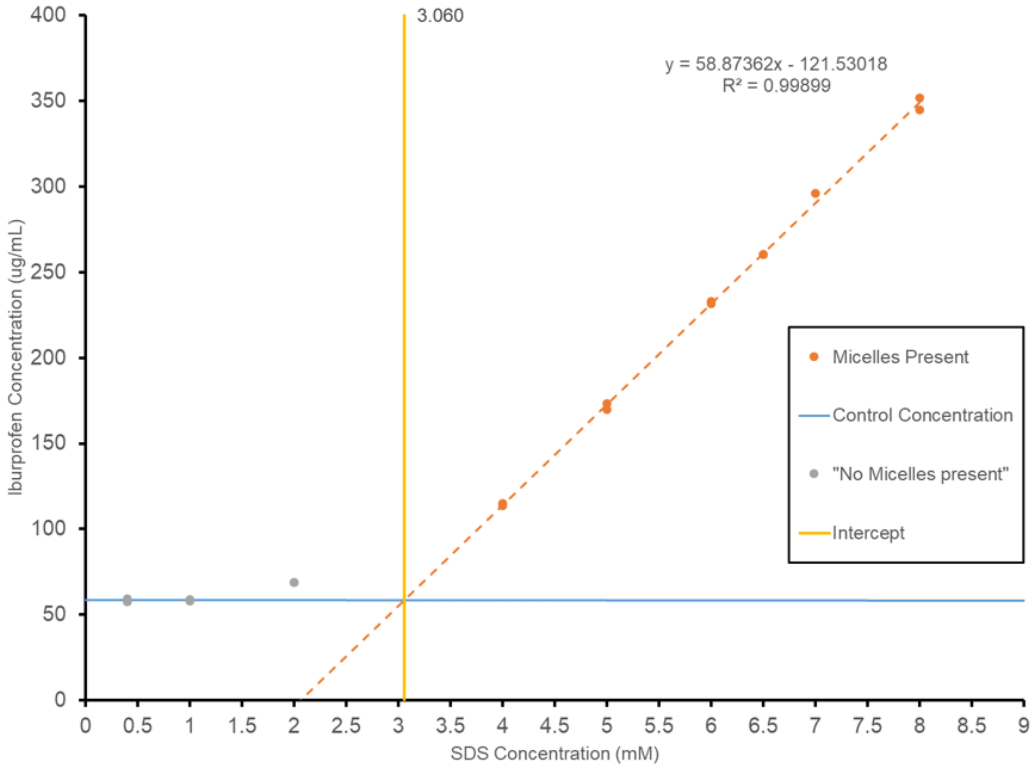

Figure 3.3: Ibuprofen concentration when increasing sodium dodecyl sulfate in order to determine the critical micellular concentration (CMC). CMC was determined to be the SDS concentration when the linear regression of the elevated ibuprofen concentration intersects the concentration of the control (the intrinsic solubility)

Volume (mL)	RPM	SEM
Stomach (n=3)		
300 mL	250	5.6
200 mL	238	11.5
100 mL	242	16.8
Duodenum (n=4)		
50 mL	118	4.0
25 mL	111	8.1

Table 3.4: Summary of the just suspended speed observations and the standard error of the mean for the replicates.

3.7.4. GIS-1 Post-Method Optimization

Following the above optimizations on GIS-1, the results of an 800 mg dissolution experiment can be seen in Figure 3.4. The experiment resulted in 90% of the dose dissolved in the GIS-1 vessels after two hours. This gave confidence in the entire procedure, which could be transferred over to the new device.

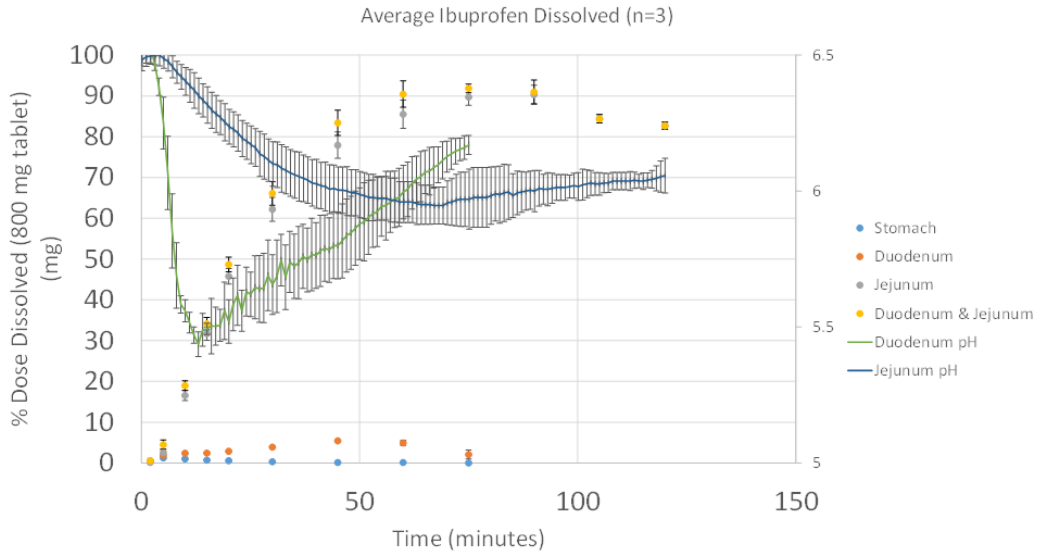

Figure 3.4: Dissolution of 800 mg ibuprofen tablet in GIS-1 after method optimization. This also includes pH monitor of the duodenum and jejunum compartments

3.8. GIS-2 Design

3.8.1. Vessel Design

Initial vessels were rapid prototyped using 3D printing. To validate the design decisions, dissolution experiments were attempted in the 3D printed vessel designs, but had aberrant results. In order to determine the cause, partitioning studies were performed on the 3D printing material.

3D-Print Prototypes & Partitioning

Table 3.5 summarizes the LogD of ibuprofen in the 3D print material. Since ibuprofen had high permeability in the 3D print material it was unsuitable for use in GIS-2 and glass was chosen as a replacement material

pH	LogD
2.0	1.94
6.5	0.37
8.0	-0.37

Table 3.5: Summary of pH-dependent LogD of ibuprofen in the Veroclear 3D print material. All items in this table are unitless

Glass Dimensions

The ileum vessel was replaced with a glass water-jacketed USP-2 vessel. For the stomach and the vessels were custom water-jacketed flat-bottomed vessels with dimensions described in Table 3.6. These dimensions are close to the prototypes and were used for the remainder of experiments. For the stomach and ileum, 3-blade two-inch diameter stainless steel hydrofoils were selected for mixing and for the duodenum and jejunum 3-blade one-and-one-half-inch diameter stainless steel hydrofoils were selected.

Vessel	Diameter	Minimum Height
Stomach	74 mm	>100 mm
Duodenum	46 mm	> 40 mm

Table 3.6: Dimensions of GIS-2 vessels. Minimum height is listed for each vessel type

3.8.2. Vessel Hydrodynamics

Following the finalization of the vessels, the just suspended speed was determined for the three vessel types. The results of the just suspended speed study are shown in both stirring directions in Table 3.7. Since clockwise stirring had lower just suspended

speeds, the vessels were stirred in a clockwise direction. After determining the just

Vessel	Counter-Clockwise	Clockwise
Stomach (300 mL)	120 RPM	160 RPM
Duodenum/Jejunum (50 mL)	175 RPM	220 RPM
Ileum (250 mL)	75 RPM	N/A

Table 3.7: Summary of just suspended speed in GIS-2 for all vessels

suspended speed, the apparent Sherwood number was determined for these stirring speeds at two different solution volumes. The results of the apparent Sherwood number estimation are shown in Table 3.8. These apparent Sherwood numbers can be used to predict dissolution in the GIS-2 system.

Vessel and Volume (mL)	Apparent Sherwood Number
Stomach – 300	3.75
Stomach – 100	2.8
Duodenum – 50	1.33
Duodenum – 25	3.33

Table 3.8: The apparent Sherwood number for ibuprofen suspension dissolution determined in each dissolution vessel at high and low volume. The apparent Sherwood number is a unitless quantity.

3.8.3. Tubing Selection

In order to achieve faster stomach emptying rates and the additional secretion rates of three vessels with secretion, the GIS-2 device needed new tubing. Three tubing types were evaluated for drug partitioning, Tygon HC, Pharmed and Viton. The results are summarized in Table 3.9. The Viton tubing had the lowest partitioning coefficient and was selected at its greatest available inner diameter for use in the transfer pumps. In order to limit the length of tubing exposed to drug solution, stainless steel tubing was cut to bridge the distance between the vessels and the pumps. For the secretion channels, stainless steel tubing was used for the length inside the vessel, as no drug should be exposed to the secretion tubing.

Tubing	Partition Coefficient per Length of Tubing log[(ug/cm) / (ug/mL)]
Tygon HC	1.62
Pharmed	1.11
Viton	0.75

Table 3.9: Length normalized partition coefficient for the three proposed tubing materials. Partition coefficient is a unitless quantity.

3.8.4. Stomach Emptying Rates/Pump Validation

Stomach emptying rates needed to be validated as some issues in GIS-1 were related to incorrect calculation of emptying rates. Three gastric emptying profile types were validated: 1st order, Weibull and User-Defined. The volume in each vessel was observed over the course of at least 60 minutes and compared to the theoretical values. The residuals of each vessel were also calculated. The observed profile and residuals for first order, Weibull Mean and User-Defined are seen in Figures 3.5, 3.6 and 3.7, respectively. The user-defined gastric emptying profile that was input into the software can be found in Appendix 3. All 3 methods lacked any systematic issues and any deviation from theoretical volume is likely related to error in determining the calibration factor for the pumps.

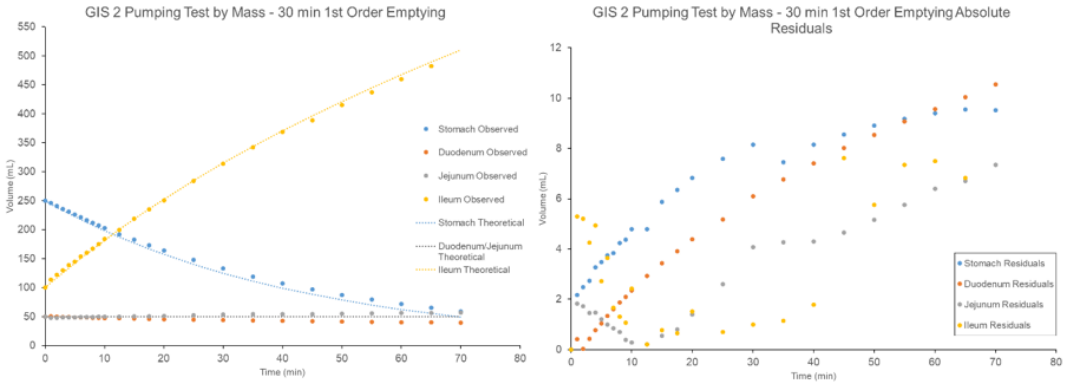

Figure 3.5: With a gastric emptying profile of 1st Order, 30 minute half emptying time, the Observed Volume over time in the GIS-2 Vessels compared to the theoretical volumes (left) and the residuals of the observed volumes for each vessel compared the theoretical volumes (right)

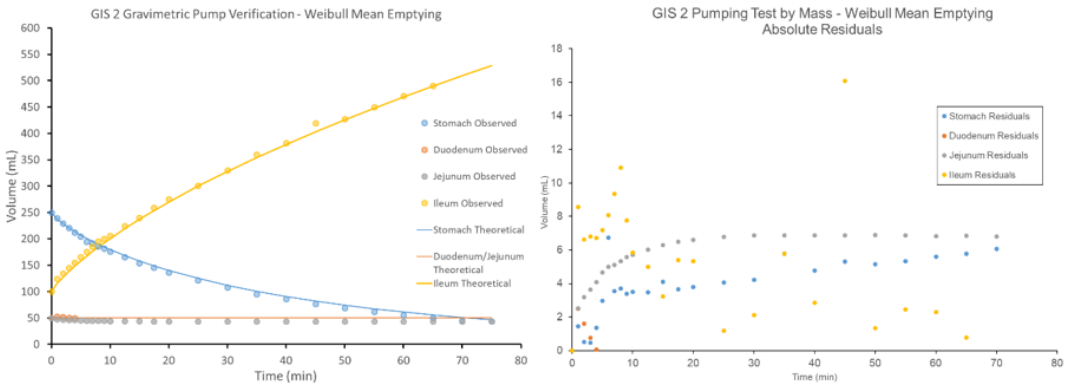

Figure 3.6: With a gastric emptying profile the Weibull Mean (ν=39.4; β=0.81), the Observed Volume over time in the GIS-2 Vessels compared to the theoretical volumes (left) and the residuals of the observed volumes for each vessel compared the theoretical volumes (right)

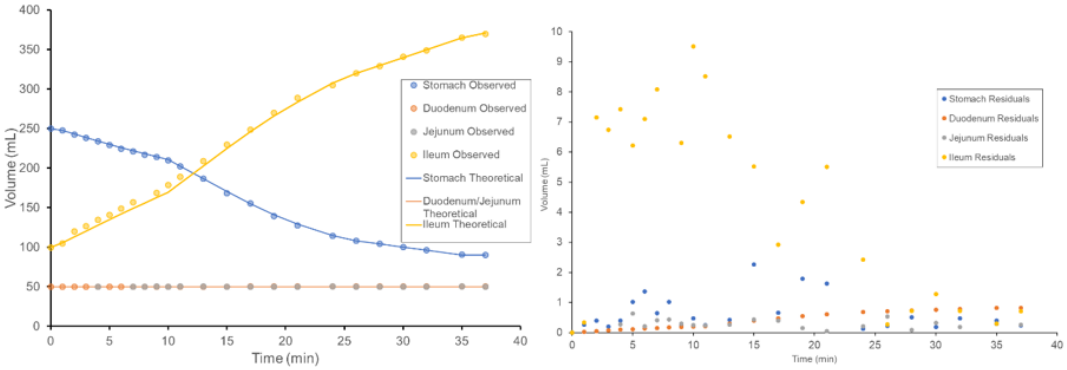

Figure 3.7: Using a user-defined gastric emptying profile, the Observed Volume over time in the GIS-2 Vessels compared to the theoretical volumes (left) and the residuals of the observed volumes for each vessel compared the theoretical volumes (right)

3.8.5. Titration

Titration is required to maintain bulk pH in the duodenum vessel when lower buffer concentration media was used. In order to determine the best method for maintain pH, three methods were proposed: constant titrant infusion, titrant bolus and a hybrid of the two, where constant titrant infusion occurs, and if the pH falls below a recommended pH a bolus addition is triggered. A simulation of the bolus method is

shown in Figure 3.8. In implementation, despite being the most complex, the hybrid

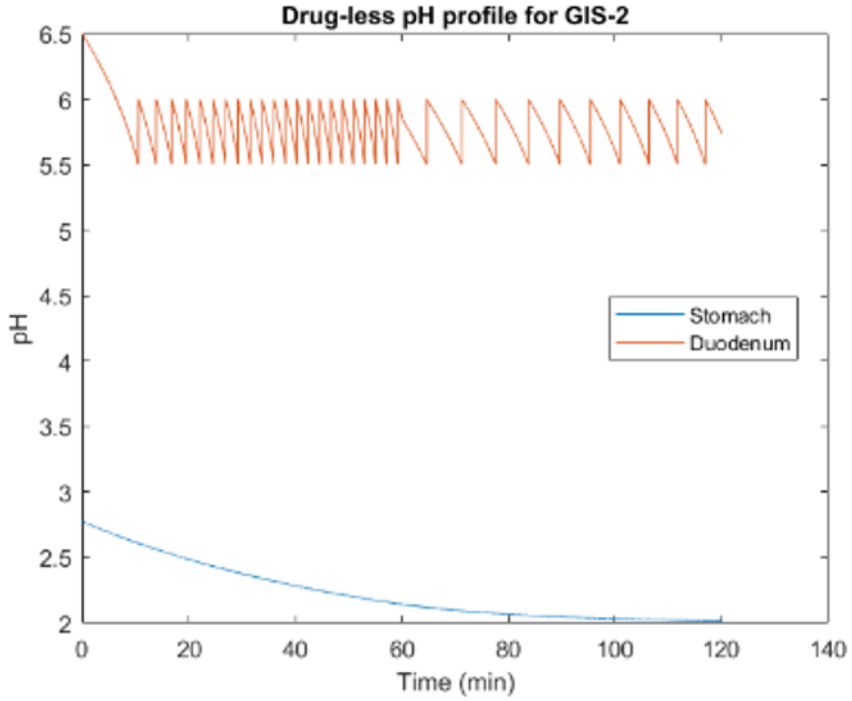

Figure 3.8: Simulated pH for stomach and duodenum with titration maintain pH in the duodenum. pH in the duodenum is maintained between 5.5 and 6.0 during the simulation.

solution allowed for slow constant infusion of titrant once below a set-point to maintain pH. As necessary, the bolus addition allowed the bulk pH to be recovered if the infusion was unable to maintain bulk pH. To test this titration method GIS-2 dissolution experiment was performed with an 800mg ibuprofen tablet and a Weibull Mean gastric emptying profile. The pH data for the stomach and duodenum vessels is shown in Figure 9. The duodenum pH profile resembles the predicted scheme as shown in Figure 8. The variations in the first 10 minutes is likely due to non-instantaneous pH readings and rapid acid flux in from the stomach causing the titration system to be unable to maintain pH as effectively as needed. Also, the calculations in the GIS-2 software to predict acid flux into the duodenum do not account for undissolved ibuprofen molecules dissolving in the media and adding protons to solution. However, this process did maintain pH as intended and is an acceptable titration function for the GIS-2 software.

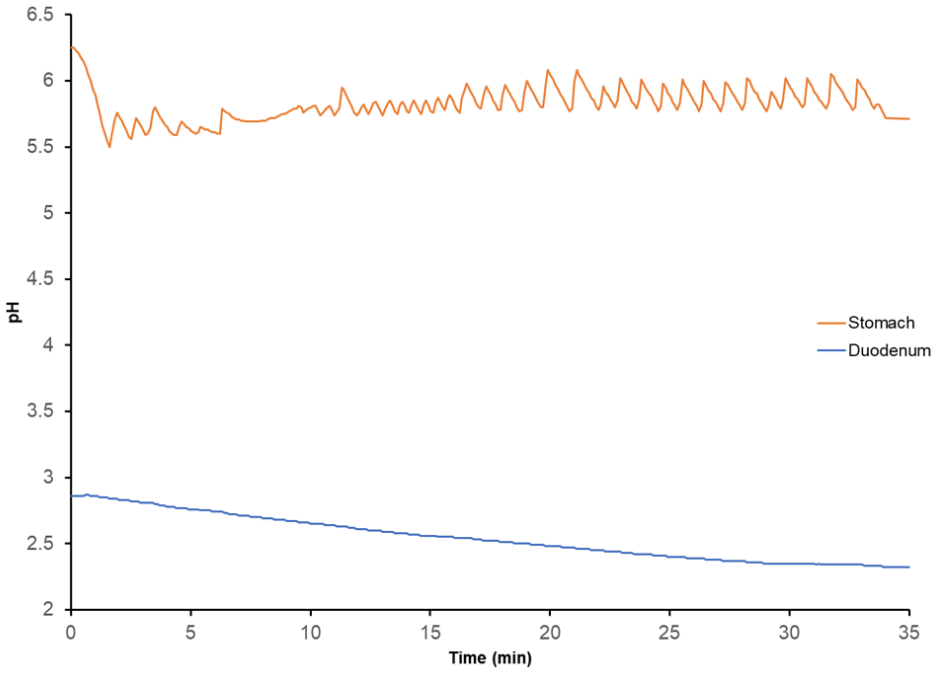

Figure 3.9: Stomach and Duodenum pH measured in GIS-2 with hybrid titration. Weibull mean gastric emptying profile.

3.9. Discussion

Multi-vessel and pH-shift dissolution studies have proven to be a good tool for in vitro evaluation of oral formulations. However, the adaptation of the artificial-stomach duodenum into the GIS-1 required some changes to the system that were not originally planned. When first working with the GIS-1 system, there were a myriad of problems with repeatability and ease of analysis. In order to design a new system, it was necessary to determine what issues were inherent to the system and which were only experimental issues that rose from tribalistic learning passed from one analyst to the next. Simple method refinements (Tables 3.1 & 3.2) removed inconsistencies in sampling and vessel volume control and allowed for more consistent results and improved mass recovery (Figures 3.2 & 3.4). In order to prevent drug loss to the vessel walls, accurate measurement of the CMC of SDS was required to prevent solubility enhancement due

to micelles (Figure 3.3). The addition of surfactant to gastric fluid quantitively decreased the amount of undissolved drug that remained in the stomach vessel at the end of the experiment. However, the physical constraints of the GIS-1 device limited further refinement and improvements. Thus, with an established method on GIS-1 in place, the design of GIS-2 could move forward. GIS-2 was developed using 3D printing of rapid prototypes, in order to visualize and test the dimensions. Following aberrant dissolution experiments, the partitioning of the 3D print material was determined and the 3D print material was deemed unsuitable for future experiments (Table 3.5). For this reason, GIS-2 vessels were fabricated out of glass with similar dimensions as those prototyped (Table 3.6). Glass allowed for easier observation of the system and assured no drug partitioning into the vessels. With the vessels and stirrers in place, hydrodynamics in the vessels could be determined. First, the just suspended speed for an ibuprofen suspension was determined (Table 3.7). This ensures that particles are well-suspended in the vessel fluid, without excessive stirring. However, these stir speeds alone do not provide necessary information to predict dissolution in the system. In order to predict dissolution, the mass transfer enhancement, or Sherwood number, was determined (Table 3.8). This Sherwood number is purely empirical and is for the particle size used in the determination but should provide a good starting point for estimating dissolution in the system. With the vessels and stirring in place and characterized, the remainder of the system needed design, evaluation, and validation. The new software to control the GIS-2 was developed to add new functions to the system. The first was the addition of new emptying profiles. In order to accommodate faster emptying profiles and prevent solid drug particles from clogging transfer tubing, larger tubing for the pumps were selected. In order to ensure lack of drug loss, three tubing materials were selected based on their available internal diameters and chemical compatibility. These tubing materials were tested for drug portioning using ibuprofen and the Viton material was selected based on the lowest partitioning coefficient (Table 3.9). With tubing selected, the emptying profiles could be validated. Since the new software for GIS-2 was built without using previous versions of the software all emptying profile types were validated. Three emptying profiles were present in the new GIS-2 software: 1st order, Weibull profile, and user-defined. Emptying profiles were

validated by measuring the volume in the vessels gravimetrically, by mass difference. These volumes were compared to theory and were assessed for any systematic issues (Figures 3.5-7). Any deviations from theoretical volumes were negligible and were likely due to small errors in the accuracy in determining the calibration factor and not related to the implementation of the emptying profiles in the software. Lastly, titration functions were added to the software, in order to allow for lower buffer concentrations while maintaining the pH of the bulk solution. The final titration method selected uses a hybrid of constant titrant addition and small volume instantaneous titrant additions to maintain the pH within a set range (figures 3.8 & 3.9).

3.10. Conclusions

This work set out to improve upon the existing GIS-1 dissolution device. In order to improve upon the actual device, the cause of perceived issues with the device were split into two categories, method-based and device-based. Once the issues were categorized both method and device improvements could be made. These improvements allow for a fast, easy, and reliable dissolution test that provides dissolution data from a 4-vessel system. The system captures the processes relevant to in vivo dissolution including disintegration, particle transfer and emptying from the stomach, dissolution in the stomach and intestinal fluids, and the changes in dissolution rate and solubility associated with the change in pH across the system. The system is not meant to be a perfect analogue of each process, but a simplified version that allows for in vitro testing. Multi-compartment dissolution devices have long existed. However, the design of GIS-2 provides customizability that is not present in other systems and the amount of control of experimental parameters in the software provide infinite possibilities in designing a dissolution experiment. Future work in the GIS-2, including work included in this dissertation, can show the capabilities of the GIS-2 as a formulation evaluation tool.

3.11. Acknowledgements

This entire project hinged on the work of two people, Roy Wentz and Randy Wald. Roy Wentz is the University of Michigan Chemistry Glass Blower and fabricated the vessels used in the GIS-2 device. Randy Wald is a close collaborator and designed the GIS-2 Software in Labview. Randy was a great help when troubleshooting issues with the device and a great person to discuss ideas for implementation into the GIS-2, particularly with the titration function. Next, I would like to thank the early GIS-2 design team, Hiro Tsume, Deanna Mudie, Patrick Sinko and Niloufar Salehi. Pat and Niloufar were particularly helpful in doing some of the early work in vessel and stirrer shapes and hydrodynamics work that drove some of the design decisions discussed abouve. Niloufar was also a great help in debugging MatLAB code that I wrote or modified from her own base code. Her help, patience and diligence was a huge help in this project. I can't write enough thanks to Niloufar for all of her amazing work. I would also like to thank Meagan Dean, Pam Meyer and Troy Halseth. Meagan was instrumental in the optimization of the GIS-1. Her attention to detail, patience and stubbornness helped refine that method to the point that GIS-2 was able to have something functional to be based off of. Pam assisted in some of the early validation tests on GIS-2, both with emptying rate validation and titration function. Troy, along with Meagan and Pat, were also additional observors for the GIS-1 just suspended speed trials. Lastly, I'd like to acknowledge the support for this project from the FDA funding HHSF223201510157C and HHSF223201310144C, without which none of this would be possible.

3.12. References

1. Culen, M., Rezacova, A., Jampilek, J., & Dohnal, J. (2013). Designing a dynamic dissolution method: a review of instrumental options and corresponding physiology of stomach and small intestine. Journal of Pharmaceutical Sciences, 102(9), 2995-3017.

2. Mudie, D. M., Samiei, N., Marshall, D. J., Amidon, G. E., & Bergström, C. A. (2020). Selection of In Vivo Predictive Dissolution Media Using Drug Substance and Physiological Properties. The AAPS Journal, 22(2), 34.

3. Mudie, D. M., Amidon, G. L., & Amidon, G. E. (2010). Physiological parameters for oral delivery and in vitro testing. Molecular pharmaceutics, 7(5), 1388-1405.

4. Amidon, G. L., Lennernäs, H., Shah, V. P., & Crison, J. R. (1995). A theoretical basis for a biopharmaceutic drug classification: the correlation of in vitro drug product dissolution and in vivo bioavailability. Pharmaceutical research, 12(3), 413-420.

5. Tsume, Y., Mudie, D. M., Langguth, P., Amidon, G. E., & Amidon, G. L. (2014). The Biopharmaceutics Classification System: subclasses for in vivo predictive dissolution (IPD) methodology and IVIVC. European Journal of Pharmaceutical Sciences, 57, 152-163. FDA, US. (2017). Waiver of in vivo bioavailability and bioequivalence studies for immediate-release solid oral dosage forms based on a biopharmaceutics classification system. Guidance for industry.

6. Locher, K., Borghardt, J. M., Frank, K. J., Kloft, C., & Wagner, K. G. (2016). Evolution of a mini-scale biphasic dissolution model: impact of model parameters on partitioning of dissolved API and modelling of in vivo-relevant kinetics. European Journal of Pharmaceutics and Biopharmaceutics, 105, 166-175.

7. Frank, K. J., Locher, K., Zecevic, D. E., Fleth, J., & Wagner, K. G. (2014). In vivo predictive mini-scale dissolution for weak bases: advantages of pH-shift in combination with an absorptive compartment. European Journal of Pharmaceutical Sciences, 61, 32-39.

8. Uekusa, T., Oki, J., Omori, M., Watanabe, D., Inoue, D., & Sugano, K. (2020). Effect of buffer capacity on dissolution and supersaturation profiles of pioglitazone hydrochloride. Journal of Drug Delivery Science and Technology, 55, 101492.

9. Gesenberg, C., Mathias, N. R., Xu, Y., Crison, J., Savant, I., Saari, A., ... & Zheng, N. (2019). Utilization of In Vitro, In Vivo and In Silico Tools to Evaluate the pH-Dependent Absorption of a BCS Class II Compound and Identify a pH-Effect Mitigating Strategy. Pharmaceutical research, 36(12), 164.

10. Hens, B., Brouwers, J., Anneveld, B., Corsetti, M., Symillides, M., Vertzoni, M., ... & Augustijns, P. (2014). Gastrointestinal transfer: in vivo evaluation and implementation in in vitro and in silico predictive tools. European journal of pharmaceutical sciences, 63, 233-242.

11. Blanquet, S., Zeijdner, E., Beyssac, E., Meunier, J. P., Denis, S., Havenaar, R., & Alric, M. (2004). A dynamic artificial gastrointestinal system for studying the behavior of orally administered drug dosage forms under various physiological conditions. Pharmaceutical research, 21(4), 585-591.

12. Minekus, M., Marteau, P., & Havenaar, R. (1995). Multicompartmental dynamic computer-controlled model simulating the stomach and small intestine. Alternatives to laboratory animals: ATLA.

13. Carino, S. R., Sperry, D. C., & Hawley, M. (2010). Relative bioavailability of three different solid forms of PNU-141659 as determined with the artificial stomach-duodenum model. Journal of pharmaceutical sciences, 99(9), 3923-3930.

14. Polster, C. S., Atassi, F., Wu, S. J., & Sperry, D. C. (2010). Use of artificial stomach–duodenum model for investigation of dosing fluid effect on clinical trial variability. Molecular pharmaceutics, 7(5), 1533-1538.

15. Polster, C. S., Wu, S. J., Gueorguieva, I., & Sperry, D. C. (2015). Mechanism for enhanced absorption of a solid dispersion formulation of LY2300559 using the artificial stomach duodenum model. Molecular pharmaceutics, 12(4), 1131-1140.

16. Carino, S. R., Sperry, D. C., & Hawley, M. (2006). Relative bioavailability estimation of carbamazepine crystal forms using an artificial stomach-duodenum model. Journal of pharmaceutical sciences, 95(1), 116-125.

17. Čulen, M., Tuszyński, P. K., Polak, S., Jachowicz, R., Mendyk, A., & Dohnal, J. (2015). Development of in vitro-in vivo correlation/relationship modeling approaches for immediate release formulations using compartmental dynamic dissolution data from "golem": A novel apparatus. BioMed research international, 2015.

18. Tsume, Y., Takeuchi, S., Matsui, K., Amidon, G. E., & Amidon, G. L. (2015). In vitro dissolution methodology, mini-Gastrointestinal Simulator (mGIS), predicts better in vivo dissolution of a weak base drug, dasatinib. European Journal of Pharmaceutical Sciences, 76, 203-212.

19. Matsui, K., Tsume, Y., Amidon, G. E., & Amidon, G. L. (2015). In vitro dissolution of fluconazole and dipyridamole in gastrointestinal simulator (GIS), predicting in vivo dissolution and drug–drug interaction caused by acid-reducing agents. Molecular pharmaceutics, 12(7), 2418-2428.

20. Tsume, Y., Igawa, N., Drelich, A. J., Ruan, H., Amidon, G. E., & Amidon, G. L. (2019). The in vivo predictive dissolution for immediate release dosage of donepezil and danazol, BCS class IIc drugs, with the GIS and the USP II with biphasic dissolution apparatus. Journal of Drug Delivery Science and Technology, 100920.

21. Tsume, Y., Amidon, G. L., & Takeuchi, S. (2013). Dissolution effect of gastric and intestinal pH fora BCS class II drug, pioglitazone: new in vitro dissolution system to predict in vivo dissolution. J Bioequiv Availab, 5(6), 224-7.

22. Milanowski, B., Hejduk, A., Bawiec, M. A., Jakubowska, E., Urbańska, A., Wiśniewska, A., ... & Lulek, J. (2020). Biorelevant In Vitro Release Testing and In Vivo Study of Extended-Release Niacin Hydrophilic Matrix Tablets. AAPS PharmSciTech, 21(3), 83.

23. Souliman, S., Beyssac, E., Cardot, J. M., Denis, S., & Alric, M. (2007). Investigation of the biopharmaceutical behavior of theophylline hydrophilic matrix tablets using USP methods and an artificial digestive system. Drug development and industrial pharmacy, 33(4), 475-483.

24. Lee, C. M., Luner, P. E., Locke, K., & Briggs, K. (2017). Application of an artificial stomach-duodenum reduced gastric pH dog model for formulation principle assessment and mechanistic performance understanding. Journal of pharmaceutical sciences, 106(8), 1987-1997.

25. Lindfors, L., Jonsson, M., Weibull, E., Brasseur, J. G., & Abrahamsson, B. (2015). Hydrodynamic effects on drug dissolution and deaggregation in the small intestine—a study with felodipine as a model drug. Journal of pharmaceutical sciences, 104(9), 2969-2976.

26. Abrahamsson, B., Pal, A., Sjöberg, M., Carlsson, M., Laurell, E., & Brasseur, J. G. (2005). A novel in vitro and numerical analysis of shear-induced drug release from extended-release tablets in the fed stomach. Pharmaceutical research, 22(8), 1215-1226.

27. Sheng, J. J., Sirois, P. J., Dressman, J. B., & Amidon, G. L. (2008). Particle diffusional layer thickness in a USP dissolution apparatus II: a combined function of particle size and paddle speed. Journal of pharmaceutical sciences, 97(11), 4815-4829.

28. Lennernäs, H., Aarons, L., Augustijns, P., Beato, S., Bolger, M., Box, K., ... & Frank, K. J. (2014). Oral biopharmaceutics tools–time for a new initiative–an introduction to the IMI project OrBiTo. European Journal of Pharmaceutical Sciences, 57, 292-299.

29. Wang, Y., & Brasseur, J. G. (2019). Enhancement of mass transfer from particles by local shear-rate and correlations with application to drug dissolution. AIChE Journal, 65(8), e16617.

30. Wang, Y., Abrahamsson, B., Lindfors, L., & Brasseur, J. G. (2012). Comparison and analysis of theoretical models for diffusion-controlled dissolution. Molecular pharmaceutics, 9(5), 1052-1066.

31. Wang, Y., Abrahamsson, B., Lindfors, L., & Brasseur, J. G. (2015). Analysis of Diffusion-Controlled Dissolution from Polydisperse Collections of Drug Particles with an Assessed Mathematical Model. Journal of pharmaceutical sciences, 104(9), 2998-3017.

32. Grenville, R. K., Mak, A. T. C., & Brown, D. A. R. (2015). Suspension of solid particles in vessels agitated by axial flow impellers. Chemical Engineering Research and Design, 100, 282-291.

33. Ayranci, I., Machado, M. B., Madej, A. M., Derksen, J. J., Nobes, D. S., & Kresta, S. M. (2012). Effect of geometry on the mechanisms for off-bottom solids suspension in a stirred tank. Chemical Engineering Science, 79, 163-176.

34. Sardeshpande, M. V., Sagi, A. R., Juvekar, V. A., & Ranade, V. V. (2009). Solid suspension and liquid phase mixing in solid– liquid stirred tanks. Industrial & engineering chemistry research, 48(21), 9713-9722.

35. Spogis, N., & Nunhez, J. R. (2009). Design of a high-efficiency hydrofoil through the use of computational fluid dynamics and multiobjective optimization. AIChE journal, 55(7), 1723-1735.

36. Zwietering, T. N. (1958). Suspending of solid particles in liquid by agitators. Chemical engineering science, 8(3-4), 244-253.

37. Ayranci, I., Ng, T., Etchells III, A. W., & Kresta, S. M. (2013). Prediction of just suspended speed for mixed slurries at high solids loadings. Chemical Engineering Research and Design, 91(2), 227-233.

Chapter 4.

Preliminary Determination of in vitro-in vivo correlations (IVIVC) in the Gastro-Intestinal Simulator-2 (GIS-2)

4.1. Introduction

Oral drug formulations must undergo multiple processes for its active ingredient to reach the site of action. These processes can vary from person to person and their interactions between the drug molecule and those processes. In order to determine in vivo performance, animal and human studies are conducted to directly determine that performance. However, in order to prevent unnecessary and uninformed in vivo experiments from commencing, in vitro dissolution tests are a valuable part of the formulator's toolkit. Thus, an in vitro device that is informed by the in vivo processes can be used to predict in vivo performance. Culen et al. states that in order to achieve an in vitro-in vivo relationship, physiologically relevant dissolution results are necessary.[1] The Gastro-Intestinal Simulator-2 (GIS-2) was designed based on the physiological processes and conditions of the in vivo physiology.[2,3] In order to determine its applications, in vitro-in vivo correlations (IVIVC) were attempted to be

determined from in vitro dissolution on the GIS-2 compared to existing in vivo plasma data from the literature. Ibuprofen is a BCS-II drug and a weakly acidic molecule. Clinical data has shown that intestinal solution concentrations are the driving force for absorption rates into the plasma.[4,5] Furthermore, dissolution depends on luminal pH, gastric motility events and gastric emptying rate, in both fed and fasted states.[4,5] According to FDA guidance, in vitro-in vivo correlations are a valuable tool in quantifying drug release into systemic circulation.[6] This is especially useful in replacing a costly in vivo bioequivalence study with a simple, cost-effective in vitro test. IVIVCs have multiple correlation levels: Level A, B and C. Level-A has the strongest level of correlation, with a point to point relationship between dissolution rate and plasma profile. Level B compares parameters associated with each instance, say mean dissolution time in vitro testing to mean residence time from the in vivo profile. Level C compares data from a single timepoint of the in vitro data to a value from the in vivo data. Level A is the only valid correlation for replacing bioequivalence studies as levels B & C cannot directly predict the entire plasma profile. In order to apply in vivo relevant dissolution to existing plasma data, an understanding of the pharmacokinetics is necessary.[6] Once ibuprofen reaches systemic circulation, it has been shown to follow a two-compartment pharmacokinetic model, but one-compartment model has been shown to be applicable in certain circumstances.[4] In some circumstances, where onset of in vitro dissolution occurs more rapidly than the drug is observed in the plasma in vivo, time scaling may be applied to the data in order to improve the fit.[7-10] Typically time scaling is applied with the development of a Levy Plot.[7] In addition, for multi-compartment dissolution devices, single vessel dissolution profiles can be correlated with plasma concentration-time profiles using time scaling with some success.[1]

4.2. Materials and Methods

4.2.1. Materials

All materials were of analytical grade or higher, unless otherwise specified. Acetonitrile for HPLC analysis was HPLC Grade (Fisher Scientific) and trifluoroacetic acid was LC/MS-grade (Sigma-Aldrich, St. Louis, MO).

4.2.2. GIS-2 Device & Dissolution Method

The GIS-2 is a computer-controlled, four-vessel dissolution device for testing oral formulations. The four vessels represent the stomach, duodenum, jejunum, and ileum. The conditions of the experiment can be adjusted, including initial volumes, stomach emptying profile, secretion rates, temperature, pH, buffer capacity and ionic strength. pH was continuously monitored throughout the experiment. The vessels are flat-bottomed cylindrical glass jacketed vessels. The vessels are mixed using top-down stirring, controlled by digital motors (Myostat Motion Control Inc., Newmarket, ON Canada). The stirrers are appropriately sized 3-blade hydrofoils (Manufacturer, Location). Stirring was maintained at speed, cycling between a lower speed to suspend most particles, with a one second burst, every sixty seconds to re-suspend any particles that may have settled to the bottom of the vessel. All fluid transfer was controlled by Ismatec Reglo ICC peristaltic pumps (Cole-Parmer GmbH, Wertheim, Germany). Pumps were standardized with water on day of analysis before analysis. Initial conditions can be found in Table 4.1. The stomach emptied from 300 mL, initially, to 75 mL with first-order kinetics (t1/2: 30 min). Volume was maintained at 50 mL in the duodenum and jejunum. The ileum accumulated all excess volume to maintain the first three vessels. After the stomach reached 75 mL, the experiment continued for one hour, with secretions only, with the stomach, duodenum, and jejunum volumes held constant. Formulations were pre-disintegrated in the stomach, by stirring at 120 RPM for 10 minutes, before fluid transfer was initiated. Manual samples were taken at regular intervals, aliquoting 1.5 mL from each vessel. Aliquots were filtered through a 0.45 um syringe filter, discarding the first 0.5 mL. Remaining filtrate was diluted as necessary for

Vessel	Initial Volume and Media	Stir Speed (RPM)	Burst Speed (RPM)	Secretion Buffer and Rate
Stomach	300 mL: 250 mL of 2mM SDS 50 mL of 0.01N HCl w/ 2mM SDS, 100 mM ionic strength (adjusted with NaCl)	120	240	2.5 mL/min: 50 mL of 0.01N HCl w/2mM SDS,100 mM ionic strength (adjusted with NaCl)
Duodenum & Jejunum	50 mL of 50 mM Phosphate Buffer pH 6.5, 150 mM ionic strength (adjusted with NaCl)	175	350	1 mL/min: 100 mM Phosphate Buffer pH 6.5, 150 mM ionic strength (adjusted with NaCl)
Ileum	250 mL of 50 mM Phosphate Buffer pH 6.5, 150 mM ionic strength (adjusted with NaCl)	75	150	NA

Table 4.1: Standard GIS-2 media and stirring conditions for experiments.

HPLC analysis. Media removed from each vessel was replaced with appropriate secretion media to maintain volume.

4.2.3. USP-2 Dissolution Method

500 mL of 50 mM Phosphate Buffer pH 6.5 was added to a standard 900 mL USP-2 dissolution vessel and allowed to equilibrate to 37°C. Once equilibrated, the tablets were introduced to the media. Manual samples were taken at regular intervals, aliquoting 1.5 mL from each vessel. Aliquots were filtered through a 0.45 µm syringe filter, discarding the first 0.5 mL. Remaining filtrate was diluted as necessary for HPLC analysis. Media removed from each vessel was replaced with appropriate secretion media to maintain volume.

4.2.4. HPLC Method

Filtered and diluted samples were analyzed by an isocratic reverse phase HPLC method (Agilient 1100 Series, Santa Clara, CA) using an Agilent C-18 column (3.5µm x 4.6µm x 150mm). Mobile phase was a 60:40 mix of acetonitrile:water with 0.1% trifluoroacetic acid. The column was maintained at 40°C with a mobile phase flow rate of 1.0mL/minute. UV detection was performed at 220 nm. A standard curve was prepared bracketing the sample solutions.

4.2.5. Formulations

Formulations used in the experiment were Motrin IB (McNeil Consumer Healthcare, Fort Washington, PA) and ibuprofen sodium (Pfizer, Madison, NJ). Two tablets were introduced to the experiment for a total dose of 400 mg ibuprofen.

4.2.6. Compartmental Approaches to IVIVC

Pharmacokinetic parameters for Wagner-Nelson and Loo-Riegelman deconvolution and convolution were calculated using the PKSolver add-in for Microsoft Excel.[11] These

parameters are summarized in Table 4.2. Fraction absorbed (Fa) was estimated using Wagner-Nelson and Loo-Riegelman deconvolution methods performed in Excel using the parameters from Table 4.1, with the area under the curve (AUC) estimated by the trapezoid method. Levy plots were generated using interpolated times for increments of Fa and fraction dissolved (Fd).

Wagner-Nelson Parameters		Loo-Riegelman Parameters	
K_e (1/hr)	0.63	K_{10} (1/hr)	0.79
V_d (L)	5.2	K_{12} (1/hr)	2.79
		K_{21} (1/hr)	3.73

Table 4.2: Summary of PK parameters as determined by PKSolver add-in for Microsoft Excel

4.2.7. Predictability Evaluation

In order to determine the validity of the correlations generated below, the predictability was evaluated by calculating the prediction error for the area under the curve (AUC) and Cmax. The prediction error is calculated by equation 4.1, below:

$$PE(\%) = \frac{|Observed - Predicted|}{Observed} * 100 \tag{4.1}$$

All prediction error values calculated are for internal predictability, as both formulations are used to create the correlation. FDA guidance for internal predictability requires average absolute prediction error to be less than 10% for both parameters and no individual formulation can have PE exceed 15%.[6]

4.3. Results

4.3.1. Dissolution Data

GIS-2

Ibuprofen formulations were introduced to the stomach of the GIS-2 and dissolution was observed over a two-hour experiment. The dissolution of ibuprofen from the Motrin IB formulation is shown in Figure 4.1. Over the course of the same experiment, pH was continuously monitored in all four dissolution vessels, as shown in Figure 4.2.

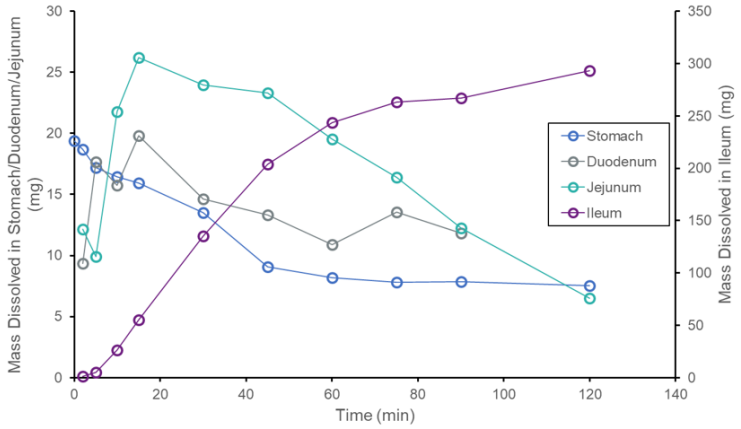

Figure 4.1: GIS-2 dissolution profiles for Motrin IB, in each vessel [Stomach (●), Duodenum (●), Jejunum (●), and Ileum(●)]. Dissolution data for Ileum vessel is plotted on the secondary y-axis for clarity of the other vessels.

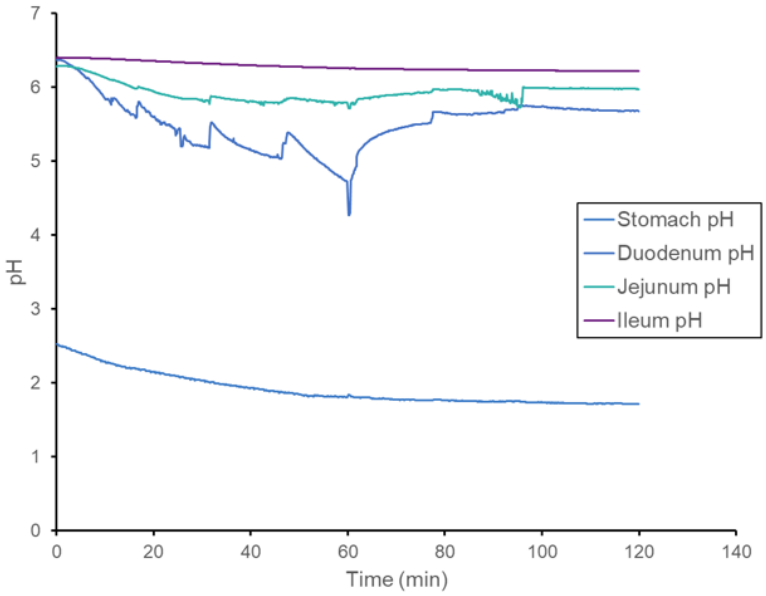

Figure 4.2: GIS-2 pH Data for Motrin IB, in each vessel [Stomach (–), Duodenum (–), Jejunum (–), and Ileum(–)].

Figure 4.3 shows the comparison of total dissolution of ibuprofen between the two formulations, Motrin-IB (ibuprofen) and the ibuprofen sodium tablets in the intestinal vessels of GIS-2. These data are co-plotted on two y-axes to represent the mass dissolved and fraction dissolved (F_d) on the left and right, respectively. The F_d from these data are used in determining the correlations to in vivo data. Ibuprofen sodium dissolved more quickly and to a greater extent due to the higher solubility of the sodium salt under low bulk pH conditions. This allowed less solid material to remain in the stomach and prevented the loss of undissolved material to the system (i.e. filtration of samples).

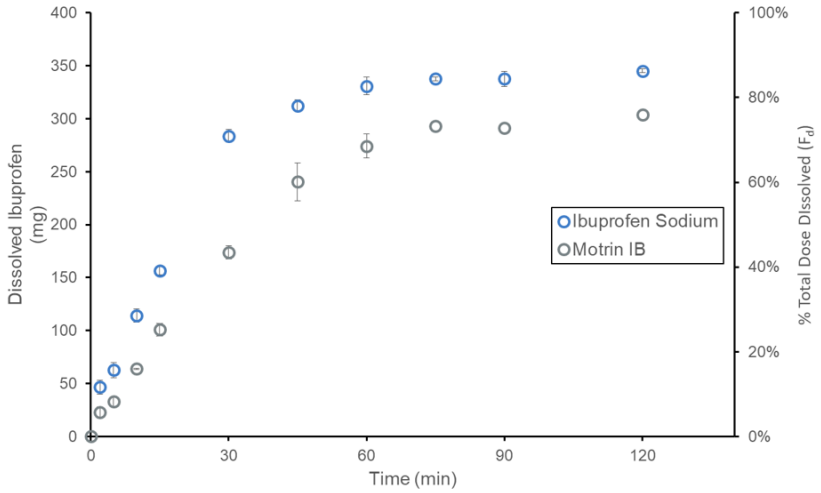

Figure 4.3: Total ibuprofen dissolved in the intestinal vessels of the GIS for the Ibuprofen Sodium (●) and Motrin IB (●) formulations.

USP-2

Figure 4.4 shows the comparison of total dissolution of ibuprofen between the two formulations, Motrin-IB (ibuprofen) and the ibuprofen sodium tablets from USP-2 dissolution. These data are co-plotted on two y-axes to represent the mass dissolved and fraction dissolved (F_d) on the left and right, respectively. The F_d from these data are used in determining the correlations to in vivo data. Ibuprofen sodium dissolved more quickly than the Motrin formulation. This is likely due to the faster observed disintegration time for that formulation as there is a limited solubility difference between ibuprofen and its sodium salt at pH 6.5.

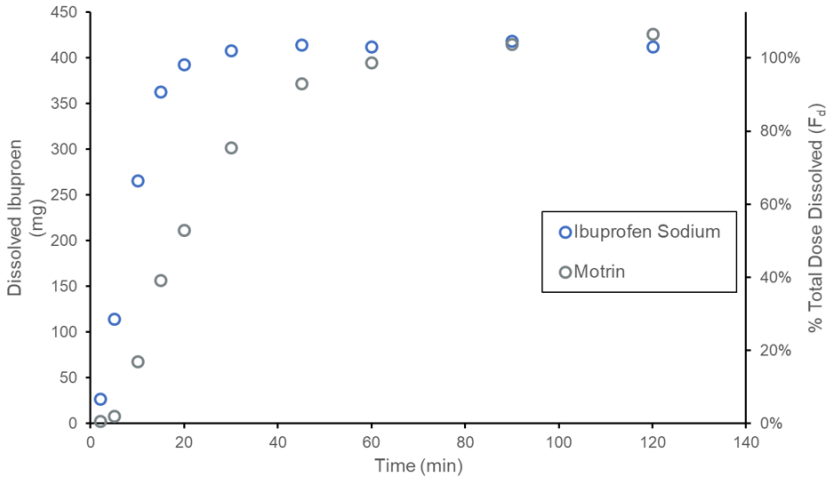

Figure 4.4: Total ibuprofen dissolved in the 500 mL USP-2 dissolution for the Ibuprofen Sodium (●) and Motrin IB (●) formulations.

4.3.2. Loo-Riegelman

Figure 4.5 shows the results of deconvolution of ibuprofen and ibuprofen sodium plasma profiles, as determined by Dewland, Reader & Berry and the PK parameters shown in Table 4.2.[12] The results of this deconvolution resulted in a fraction absorbed exceeding 100% for both formulations. This is likely due to the sourcing of data from literature and the nature of two-compartment pharmacokinetic modeling. Since the PK parameters determined from infusion data separate from the oral dosed data used for deconvolution, it's likely that error was introduced into the prediction of fraction absorbed. Additionally, Lockwood, et al. showed that pharmocokinetic parameters for two-compartment models have high variability within the sample population (shown by large confidience intervals for each parameter) and inter-study comparisons show large differences between determined values. This is especially true with both parameters involving the peripheral compartment, where the amount of drug in the peripheral compartment must be estimated and poor estimation of those values can lead to systemic error. This deconvolution is incongruent with expectations for fraction absorbed. However, for the sake of the exercise of determining an IVIVC for the dissolution data using a two-compartment model, these deconvoluted data will be used in place of improving the data with population matched infusion and oral dosed human subjects.

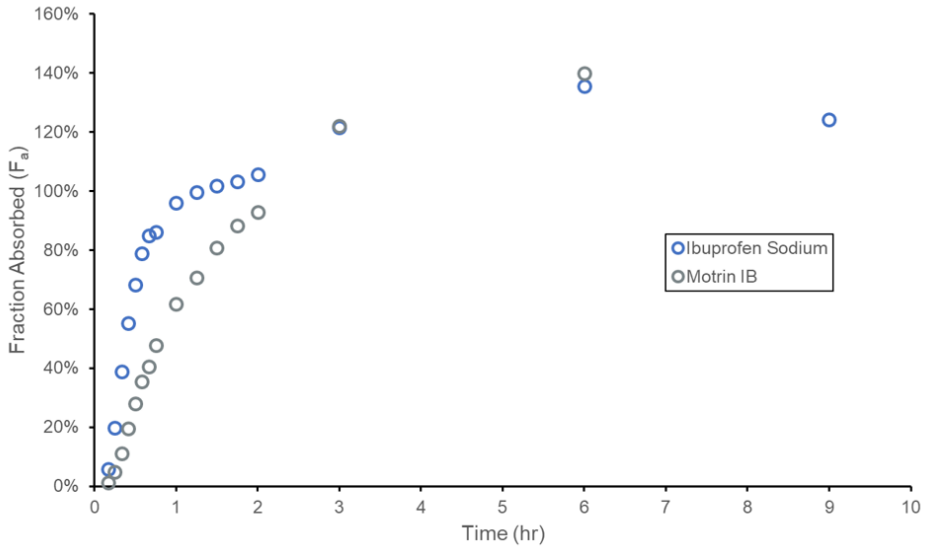

Figure 4.5: Deconvolution using the Loo-Riegelman model from plasma profiles of Ibuprofen Sodium (●) and ibuprofen (●) formulation.[12]

Figure 4.6 shows the nonlinear fitting of fraction absorbed in vivo and fraction dissolved in vitro (GIS-2). A non-linear fit is allowed under FDA guidance and provided a higher level of correlation than a linear fit.

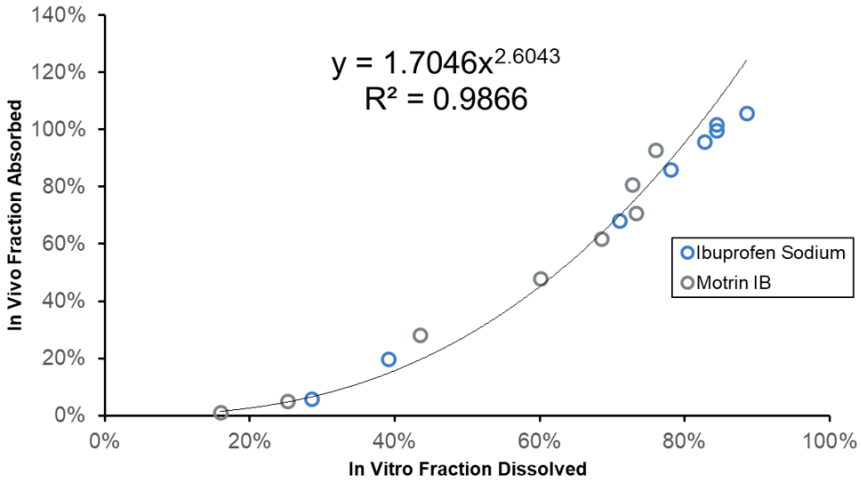

Figure 4.6: IVIVC plot for fraction absorbed from Loo-Riegelman deconvoluted plasma profiles of Ibuprofen Sodium (●) and ibuprofen (●) and the fraction dissolved from GIS-2 intestinal dissolution .

Using the correlation shown in Figure 4.6, the dissolution data determined using GIS-2 was used to predict Fa values at each time point. These Fa values were used to predict plasma profiles for both formulations by Loo-Riegelman convolution. These predicted plasma profiles are shown in Figures 4.7 & 4.8. The predicted values for Cmax and AUC of each formulation were compared to the observed values for both parameters. The validity of the correlation was tested by calculating the prediction error, as shown in Table 4.3. The correlation met the criteria for both Cmax values and the AUC for the Motrin formulation, but failed to meet the FDA criteria for the AUC of ibuprofen, so the correlation was rejected.

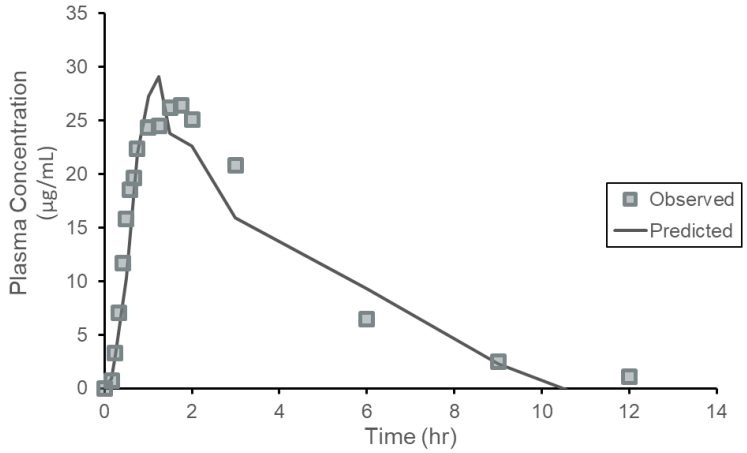

Figure 4.7: Loo-Riegelman predicted plasma profile for the Motrin IB formulation (–) compared to the observed plasma profile (■) from (Dewland, et al.)[12].

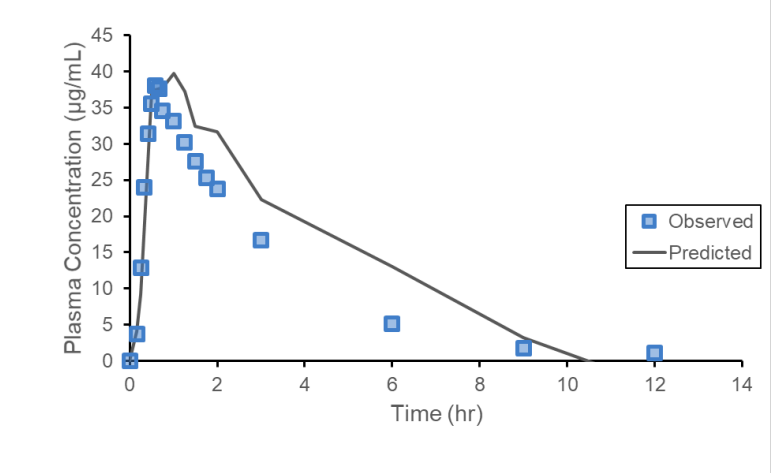

Figure 4.8: Loo-Riegelman the predicted plasma profile for the ibuprofen sodium formulation (–) compared to the observed plasma profile (■) from (Dewland, et al.)[12].

Parameter	Observed	Predicted	%Prediction Error
CMax (motrin IB) (µg/mL)	26.37	29.13	10.4
AUC (motrin IB) (µg/mL·hr)	121.22	111.89	7.7
CMax (Ibuprofen Sodium) (µg/mL)	38.04	39.79	4.6
AUC (Ibuprofen Sodium) (µg/mL·hr)	120.71	164.32	36.0

Table 4.3: Summary of Prediction Error from Loo-Riegelman Correlations and Predictions

4.3.3. Wagner-Nelson

As described by Bermejo, 2018, though ibuprofen is typically described by a two-compartment model, a one-compartment model can be used to sufficiently analyze ibuprofen with a similar level of accuracy. Deconvolution of the same plasma profiles as in Figure 4.5 is shown below in Figure 4.9.

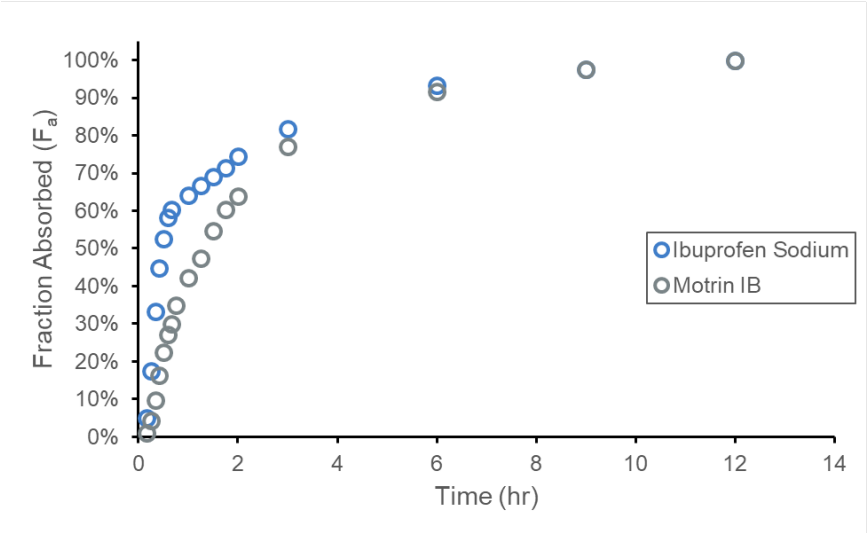

Figure 4.9: Deconvolution using the Wagner-Nelson model from plasma profiles of Ibuprofen Sodium (●) and ibuprofen (●) formulation.[12]

Figure 4.10 shows the linear fit of fraction absorbed in vivo and fraction dissolved in vitro (GIS-2) with a correlation of R2 = 0.9585.

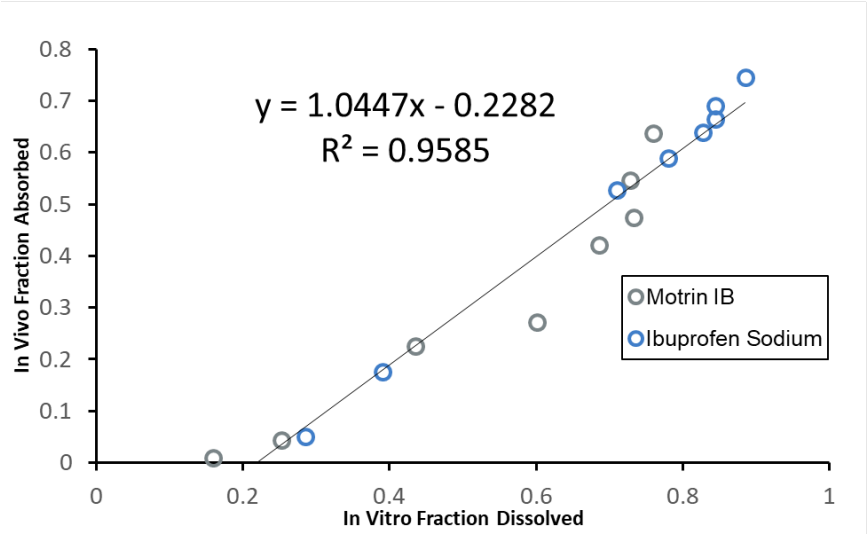

Figure 4.10: IVIVC plot for fraction absorbed from Wagner-Nelson deconvoluted plasma profiles of Ibuprofen Sodium (●) and ibuprofen (●) and the fraction dissolved from GIS-2 intestinal dissolution.

Using the correlation shown in Figure 4.10, the dissolution data determined using GIS-2 was used to predict Fa values at each time point. These Fa values were used to predict plasma profiles for both formulations by Wagner-Nelson convolution. These predicted plasma profiles are shown in Figures 4.11 & 4.12. The predicted values for Cmax and AUC of each formulation were compared to the observed values for both parameters. The validity of the correlation was tested by calculating the prediction error, as shown in Table 4.4. The correlation failed to meet the FDA criteria for prediction error for three of the four predicted parameters, with only the Cmax of the ibuprofen sodium formulation meeting the criteria and the correlation was rejected.

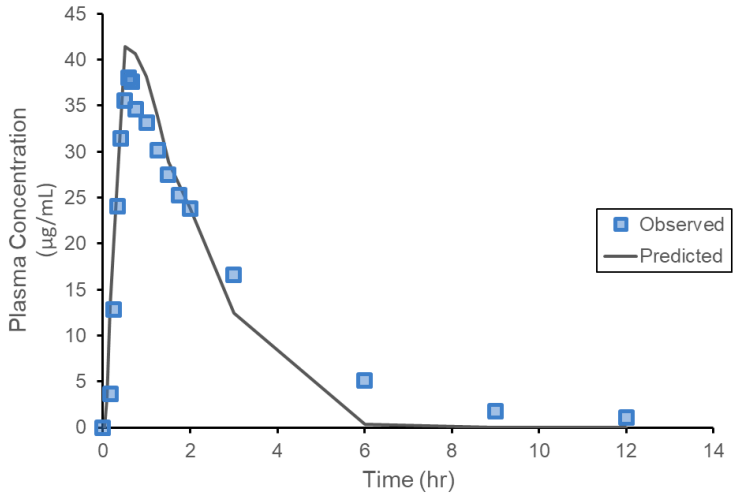

Figure 4.11: Wagner-Nelson predicted plasma profile for the Motrin IB formulation (–) compared to the observed plasma profile (■) from (Dewland, et al.)[12].

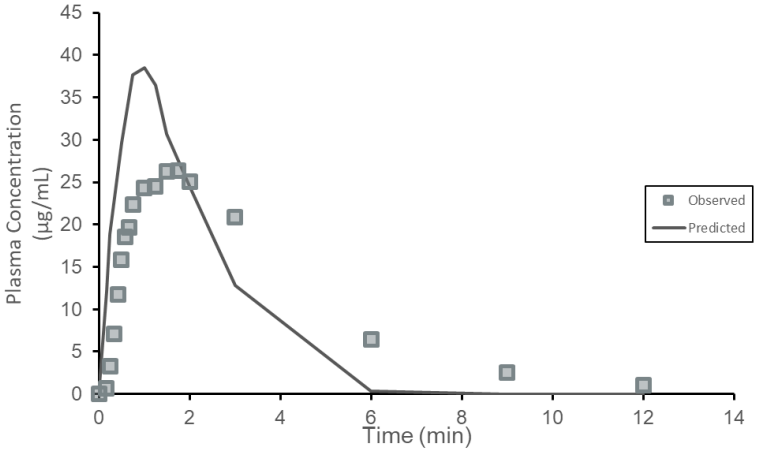

Figure 4.12: Wagner-Nelson predicted plasma profile for the ibuprofen sodium formulation (–) compared to the observed plasma profile (■) from (Dewland, et al.)[12].

Parameter	Observed	Predicted	%Prediction Error
CMax (motrin IB) (µg/mL)	26.37	38.49	46.0
AUC (motrin IB) (µg/mL·hr)	121.22	96.98	20.1
CMax (Ibuprofen Sodium) (µg/mL)	38.04	41.40	8.8
AUC (Ibuprofen Sodium) (µg/mL·hr)	120.71	98.0	18.8

Table 4.4: Summary of Prediction Error from Wagner-Nelson Correlations and Predictions

4.3.4. Levy Plot

Neither the Wagner-Nelson model nor the Loo-Riegelman model resulted in correlations that successfully met FDA requirements. However, both correlations showed in vivo lag time due to some other physiological or formulation characteristic,9 which can be corrected for using a Levy Plot. The following section used Levy Plots to attempt to improve upon the correlations from above.

Loo-Riegelman

A levy plot was generated by linear interpolation of the F_A and F_D data for both formulations, pairing the times of F_A and F_D values from 0-100% in increments of 10% . The levy plot for the Loo-Riegelman F_A values (from Figure 4.1) and GIS-2 intestinal dissolution F_D data is shown in Figure 4.13. The two formulations show distinct individual slopes for their respective paired time points, which is evident by the poor correlation (R^2 = 0.5036). This levy plot was not usable to create a predictions of plasma concentrations from the F_D data and was rejected.

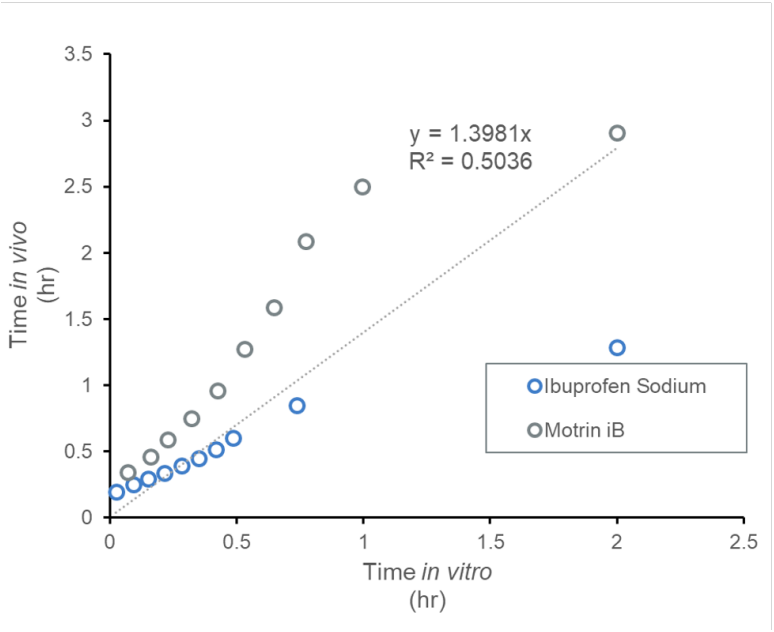

Figure 4.13: Levy Plot for time in vivo to specified Fa from Loo-Riegelman deconvolution of Ibuprofen Sodium (●) and ibuprofen (●) and the time in vitro for fraction dissolved matched to the in vivo time.

Wagner-Nelson

A levy plot was generated by linear interpolation of the F_A and F_D data for both formulations, pairing the times of F_A and F_D values in increments of 10%. For Wagner-Nelson one-compartment model, levy plots were generated for both total dose normalized FDAnd final mass dissolved in the intestinal compartments ($F_{diss\text{-}inf}$)

Dose Normalized

The levy plot for the Wager-Nelson F_A values (from Figure 4.9) and GIS-2 intestinal dissolution F_D data normalized to the dose is shown in Figure 4.14. The fraction for each formulation is truncated at 70% and 80% for Motrin IB and ibuprofen sodium formulations, respectively. This truncation is due to the maximum F_D observed during the experiment when normalizing to the dose. The two formulations similar slopes with a correlation of R^2 = 0.8924. Using this levy plot the plasma profiles can be

predicted by using the correlation to produce the equivalent time in vivo (T_A) associated to the F_D at time in vitro (T_D)

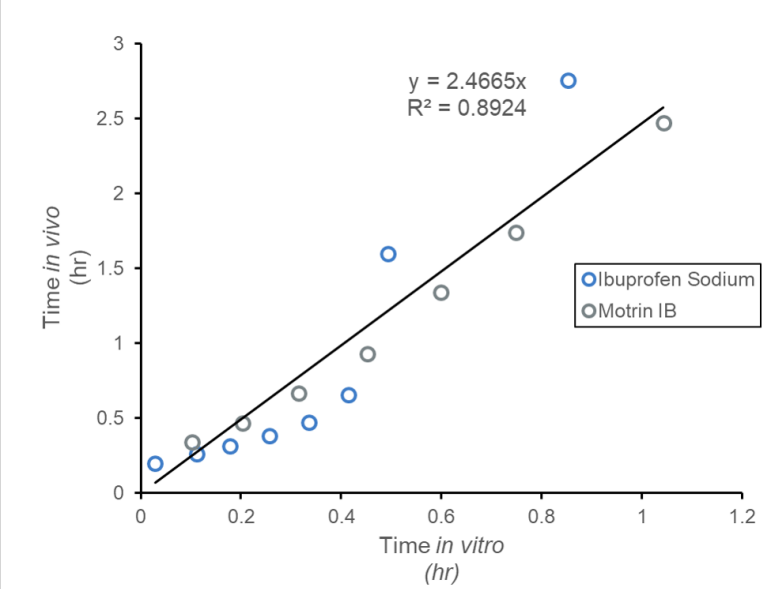

Figure 4.14: Levy Plot for time in vivo to specified Fa from Wagner-Nelson deconvolution of Ibuprofen Sodium (●) and ibuprofen (●) and the time in vitro for fraction dissolved, normalized to dose, matched to the in vivo time.

Using the Levy Plot, shown in Figure 4.14, the dissolution data determined using GIS-2 was used as Fa values with each time point scaled using the relationship from the Levy Plot. These Fa values were used to predict plasma profiles for both formulations by Wagner-Nelson convolution. These predicted plasma profiles are shown in Figures 4.15 & 4.16. The predicted values for Cmax and AUC of each formulation were compared to the observed values for both parameters. The validity of the correlation was tested by calculating the prediction error, as shown in Table 4.5. The correlation met the criteria for both AUC values and the Cmax for the ibuprofen sodium formulation but failed to meet the FDA criteria for the Cmax of ibuprofen, so the correlation was rejected.

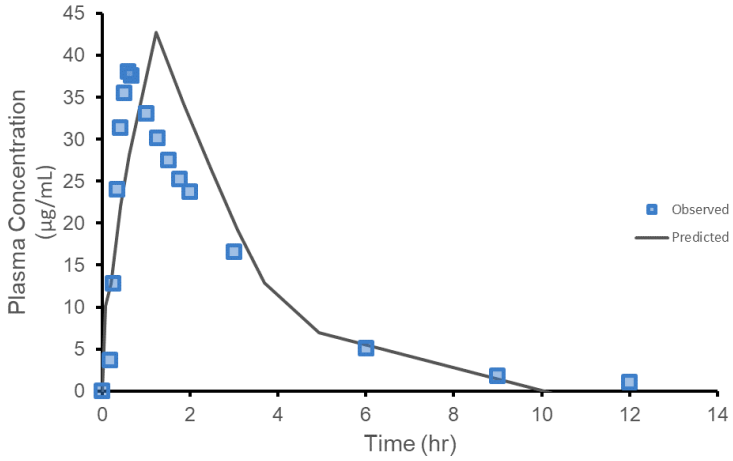

Figure 4.15: Time-scaled Wagner-Nelson (dose normalized) predicted plasma profile for the Motrin IB formulation (–) compared to the observed plasma profile (■) from (Dewland, et al.)[12].

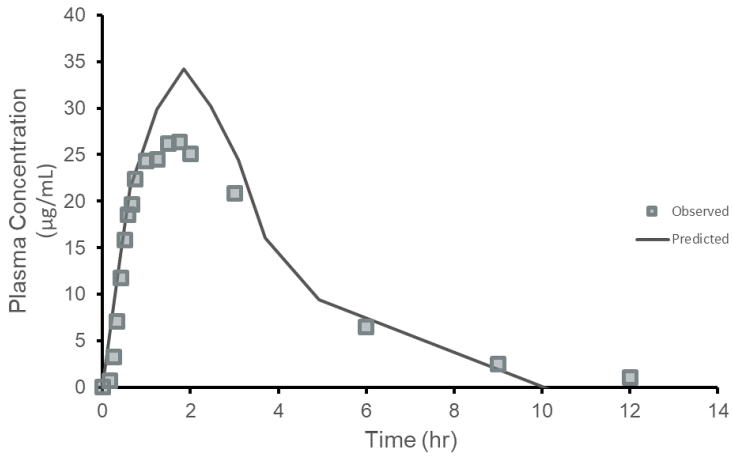

Figure 4.16: Time-scaled Wagner-Nelson (dose normalized) predicted plasma profile for the ibuprofen sodium formulation (–) compared to the observed plasma profile (■) from (Dewland, et al.)[12].

Parameter	Observed	Predicted	%Prediction Error
CMax (motrin IB) (µg/mL)	26.37	34.23	29.8
AUC (motrin IB) (µg/mL·hr)	121.22	127.69	5.3
CMax (Ibuprofen Sodium) (µg/mL)	38.04	42.78	12.5
AUC (Ibuprofen Sodium) (µg/mL·hr)	120.71	126.18	4.5

Table 4.5: Summary of Prediction Error from Time-scaled Wagner-Nelson (dose normalized) Correlations and Predictions

Final Amount Dissolved Normalized

The levy plot for the Wager-Nelson F_A values (from Figure 4.9) and GIS-2 intestinal dissolution F_D data normalized to the final mass dissolved ($F_{Diss\text{-}inf}$) is shown in Figure 4.17. The two formulations similar slopes with a correlation of R^2 = 0.9484. Using this levy plot the plasma profiles can be predicted by using the correlation to produce the equivalent time in vivo (T_A) associated to the FDAt time in vitro (T_D).

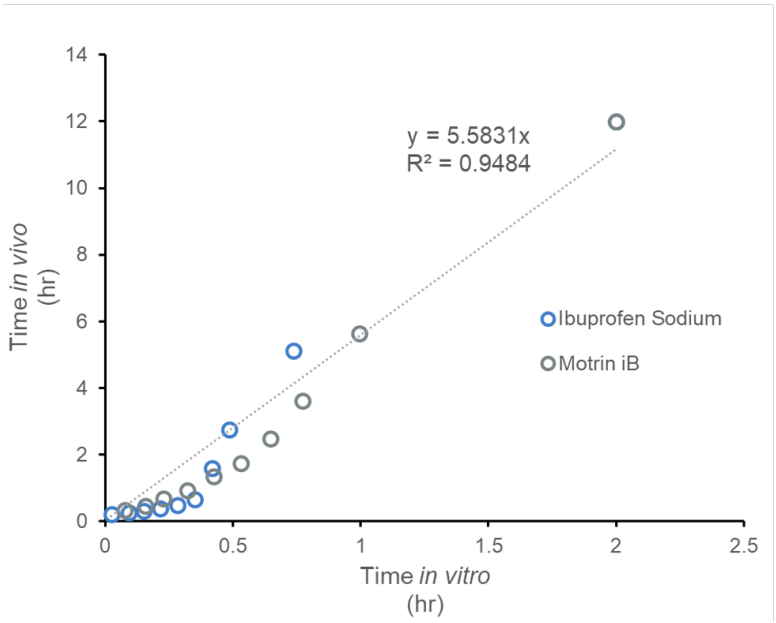

Figure 4.17: Levy Plot for time in vivo to specified Fa from Wagner-Nelson deconvolution of Ibuprofen Sodium (●) and ibuprofen (●) and the time in vitro for fraction dissolved, normalized to final mass dissolved, matched to the in vivo time.

Using the Levy Plot, shown in Figure 4.17, the process from the previous section is repeated to predict plasma profiles for both formulations. These predicted plasma profiles are shown in Figures 4.18 & 4.19. The predicted values for Cmax and AUC of each formulation were compared to the observed values for both parameters. The validity of the correlation was tested by calculating the prediction error, as shown in Table 4.6. The correlation met the criteria for both AUC values and but failed to meet the FDA criteria for both Cmax values, so the correlation was rejected.

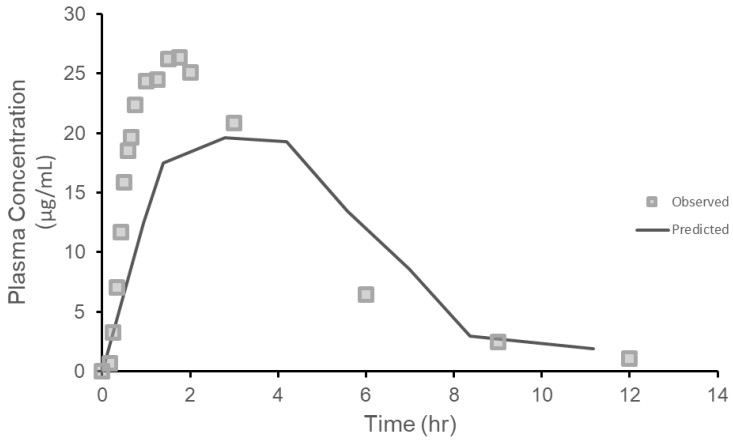

Figure 4.18: Time-scaled Wagner-Nelson (normalized to final mass dissolved) predicted plasma profile for the Motrin IB formulation (–) compared to the observed plasma profile (■) from (Dewland, et al.)[12].

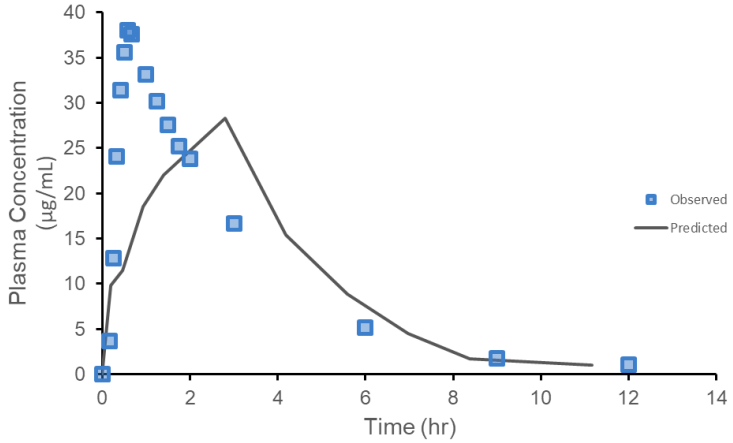

Figure 4.19: Time-scaled Wagner-Nelson (normalized to final mass dissolved) predicted plasma profile for the ibuprofen sodium formulation (–) compared to the observed plasma profile (■) from (Dewland, et al.)[12].

Parameter	Observed	Predicted	%Prediction Error
CMax (motrin IB) (µg/mL)	26.37	19.64	26.8
AUC (motrin IB) (µg/mL·hr)	121.22	120.24	0.8
CMax (Ibuprofen Sodium) (µg/mL)	38.04	35.11	16.5
AUC (Ibuprofen Sodium) (µg/mL·hr)	120.71	121.08	0.1

Table 4.6: Summary of Prediction Error from Time-scaled Wagner-Nelson (normalized to final mass dissolved) Correlations and Predictions

USP-2 (Wagner-Nelson)

A levy plot was generated by linear interpolation of the F_A and F_D data for both formulations, pairing the times of F_A and F_D values from 0-100% in increments of 10%. The levy plot for the Wagner-Nelson F_A values (from Figure 4.1) and dissolution in the USP-2 dissolution vessel F_D data is shown in Figure 4.13. The two formulations show distinct individual slopes for their respective paired time points, which is evident by the poor correlation (R¬2 = 0.6841). This levy plot was not usable to create a predictions of plasma concentrations from the F_D data and was rejected.

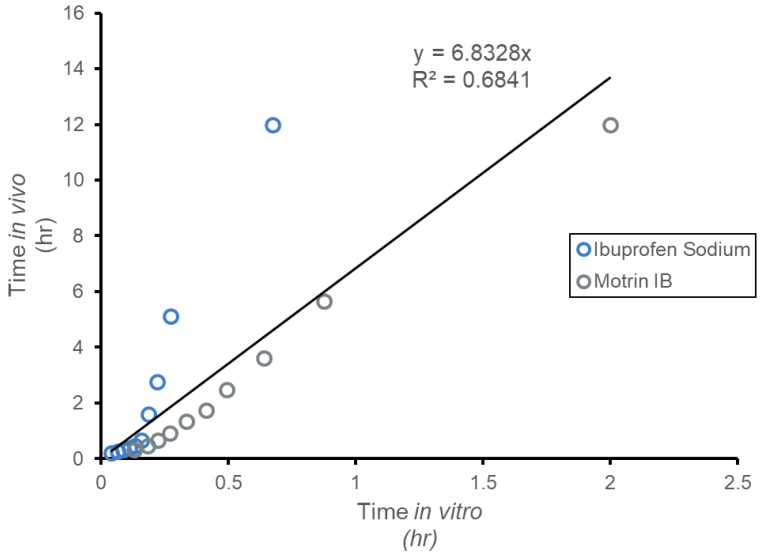

Figure 4.20: IVIVC plot for fraction absorbed from Wagner-Nelson deconvoluted plasma profiles of Ibuprofen Sodium (●) and ibuprofen (●) and the fraction dissolved from USP-2 dissolution.

4.4. Discussion

When designing an in vitro device, utilizing the knowledge of the in vivo processes that act on an oral formulation can be an improvement over conventional dissolution. Multi-compartment dissolution devices have demonstrated good correlation with in vivo data.1 The Gastro-Intestinal Simulator 2 (GIS-2) is a system that applies those processes to produce in vivo¬ based dissolution conditions. In order to test the capability of the GIS-2 to be in vivo-like, IVIVCs were developed and evaluated, using two different compartment models.

Dissolution data for USP-2 and GIS-2 dissolution shows varied kinetics and extent for dissolution (Figures 4.1 & 4.3). Using these dissolution data and the fraction absorbed from in vivo plasma data for similar formulations the correlations were generated, as in Figure 4.10. Using these correlations, plasma profiles were predicted for each correlation. Neither model met the requirements for IVIVC per FDA guidance without

time scaling. The Loo-Riegelman correlation had more parameters meet FDA requirements with three of the four parameters meeting requirements. However, the shape of the plasma profile has an odd jut at the three hour mark, likely due to the difficulty in predicting peripheral drug concentration in the Loo-Riegelman method and the large confidence interval related to PK parameters in the two-compartment model of ibuprofen. Moreover, both correlations show in vivo lag, where the correlation was shifted right on the x-axis instead of intersecting near the origin. Therefore, time scaling was a necessary step to attempt to improve the correlation.

With the introduction of time scaling, by use of a Levy Plot, the two formulations were shown to have separate slopes and the low-quality correlation for the Loo-Riegelman method. This likely related to the difficulties in estimating a two-compartment model without infusion data and oral plasma data from the same subject group in order to accurately estimate the pharmacokinetic parameters. This is exacerbated by the inclusion of time-scaling, which relies on fraction absorbed values to remain within the bounds of 0-100%. When the same time scaling procedure was applied to the fraction absorbed data from Wagner-Nelson deconvolution, linearity was found. When using this time scaling to predict plasma concentrations, the lowest average predicted error across all models for AUC were observed, but failed to predict the Cmax within the FDA criterion. Therefore, the correlations were rejected. Although the Cmax failed to meet requirements, this may not be directly the fault of the correlation method. Due to the interpolation necessary for the time scaling of the Levy Plot, insufficient data may have been gathered in vitro to allow for full coverage of the early absorption phase leading up to the Cmax resulting in the predicted plasma curves to be plateau shaped or with depressed peaks (Figures 4.18 & 4.19). In comparison to conventional dissolution, (USP-2) the in vivo-inspired GIS-2 was far more successful at correlating to in vivo data. The Levy Plot generated from USP-2 dissolution data had similar issues as the Loo-Riegelman Levy plot for GIS-2, where the formulations had divergent slopes. However, this does not take away from the usefulness of USP-2 dissolution, just under these circumstances the GIS-2 in its current state has some advantages.

With the lack of evidence of a correlation between GIS-2 dissolution and in vivo plasma data, some improvements could be made to the studies described. First, the

formulations used have identical absorption kinetics since they are the same parent drug molecule. However, the formulations are the free acid and sodium salt, which have different dissolution behavior due to differences in their pH-dependent solubilities. Thus, different formulations of the same drug molecule should be tested to improve the quality of correlations.

Next, the PK data and parameters for the models were based on separate sources of data from literature. Ideally, the PK parameters and the plasma profiles being correlated with from oral dosing of the drug would be generated from the same subjects in order to reduce subject variability. As shown in Lockwood, et al., for ibuprofen the confidence interval for the PK parameters for both inter-study and intra-study are quite wide.[13] Thus, performing PK studies may be necessary to truly have correlative dissolution.

Third, the GIS-2 dissolution method is far from optimized. These data were generated as proof of concept dissolution studies and were then applied to the in vivo data without any optimization to the method. Areas of improvement for the method include: 1) using more in vivo relevant gastric emptying times; 2) increasing the number of sampling timepoints in the early stages of the experiment to improve resolution of the dissolution data; 3) reducing the pre-disintegration time; 4) using biorelevant buffers (bicarbonate or equivalent phosphate buffer) in the duodenum and jejunum vessels; and 5) using titration to maintain duodenal (and jejunal) bulk pH within a relevant range over the course of the experiment. With these method improvements in mind, future dissolution experiments in the GIS-2 may provide better correlations to in vivo data.

Last, when considering ibuprofen, a BCS IIa compound, the processes that limit absorption are: disintegration of the dosage form, drug particle emptying/transit from the stomach into the duodenum and jejunum, and dissolution in the intestinal fluid, as limited dissolution will occur in the acidic conditions of the stomach. However, a weakly basic drug with high permeability (BCS IIb) could benefit from study in the GIS-2, as the pH change from gastric conditions into the intestine; thus, allowing for capture of the supersaturation and precipitation behavior that occurs in vivo for that class of molecules. The GIS-2 is tailored for low solubility drugs in its current state. However, when supersaturation and precipitation occur, for weakly basic drugs, an absorption process for the GIS-2 may be necessary to capture differences in

supersaturation and precipitation behavior as supersaturation may be maintained for longer when absorption is allowed to occur at supersaturated drug concentrations. The above discussed method improvements are one of the benefits of the GIS-2 system, the simplicity and modularity of its design allows for the dissolution test to be tailored to the needs of the API and formulation(s) being tested.

4.5. Conclusions

The capability of a dissolution device that provides discriminative and in vivo correlative dissolution could be a powerful tool in development of oral dosage forms. The GIS-2 was designed to incorporate the processes in vivo that affect drug dissolution and absorption. Although the results of this work lack evidence of correlative dissolution, the results do provide a promising framework for the future correlative dissolution. The system has the capability for further optimization, which could allow for improved correlations, including media selection, gastric emptying, and introduction an absorption compartment. The study also lacked quality or distinct data for each formulation. Rather, in vivo data was used from literature for the purpose of this study and was not produced directly from the formulations used in the GIS-2 dissolution experiments. Additionally, PK parameters were derived from IV infusion data separate from the source of the oral dosage PK profiles. Despite the difficulties described above, the GIS-2 has the potential to be used as a benchtop evaluator of formulations and with further refinement should be capable of predicting their behavior in vivo.

4.6. Acknowledgements

I would like to thank Dr. Marival Bermejo for her assistance in understanding the Wagner-Nelson and Loo-Riegelman deconvolution and convolution. I would also like to thank Brian Thompson for his assistance with confirmatory work in WinNonLin.

4.7. References

1. Čulen, M., Tuszyński, P. K., Polak, S., Jachowicz, R., Mendyk, A., & Dohnal, J. (2015). Development of in vitro-in vivo correlation/relationship modeling approaches for immediate release formulations using compartmental dynamic dissolution data from "golem": A novel apparatus. BioMed research international, 2015.

2. Mudie, D. M., Samiei, N., Marshall, D. J., Amidon, G. E., & Bergström, C. A. (2020). Selection of In Vivo Predictive Dissolution Media Using Drug Substance and Physiological Properties. The AAPS Journal, 22(2), 34.

3. Mudie, D. M., Amidon, G. L., & Amidon, G. E. (2010). Physiological parameters for oral delivery and in vitro testing. Molecular pharmaceutics, 7(5), 1388-1405.

4. Bermejo, M., Paixão, P., Hens, B., Tsume, Y., Koenigsknecht, M. J., Baker, J. R., ... & Shedden, K. (2018). Linking the Gastrointestinal Behavior of Ibuprofen with the Systemic Exposure between and within Humans—Part 1: Fasted State Conditions. Molecular pharmaceutics, 15(12), 5454-5467.

5. Paixão, P., Bermejo, M., Hens, B., Tsume, Y., Dickens, J., Shedden, K., ... & Lionberger, R. (2018). Linking the Gastrointestinal Behavior of Ibuprofen with the Systemic Exposure between and within Humans—Part 2: Fed State. Molecular pharmaceutics, 15(12), 5468-5478.

6. FDA (1997) Guidance for industry. Extended release oral dosage forms: development, evaluation and application of in vitro/in vivo correlations. Center for Drug Evaluation and Research (CDER), US Department of Health and Human Services

7. Levy, G., Leonards, J. R., & Procknal, J. A. (1965). Development of in vitro dissolution tests which correlate quantitatively with dissolution rate-limited drug absorption in man. Journal of Pharmaceutical Sciences, 54(12), 1719-1722.

8. Cardot, J. M., Beyssac, E., & Alric, M. (2007). In vitro-in vivo correlation: importance of dissolution in IVIVC. Dissolution technologies, 14(1), 15.

9. Cardot, J. M., & Davit, B. M. (2012). In vitro–in vivo correlations: tricks and traps. The AAPS journal, 14(3), 491-499.

10. Sjögren, E., Abrahamsson, B., Augustijns, P., Becker, D., Bolger, M. B., Brewster, M., ... & Holm, R. (2014). In vivo methods for drug absorption–comparative physiologies, model selection, correlations with in vitro methods (IVIVC), and applications for formulation/API/excipient characterization including food effects. European Journal of Pharmaceutical Sciences, 57, 99-151.

11. Zhang, Y., Huo, M., Zhou, J., & Xie, S. (2010). PKSolver: An add-in program for pharmacokinetic and pharmacodynamic data analysis in Microsoft Excel. Computer methods and programs in biomedicine, 99(3), 306-314.

12. Dewland, P. M., Reader, S., & Berry, P. (2009). Bioavailability of ibuprofen following oral administration of standard ibuprofen, sodium ibuprofen or ibuprofen acid incorporating poloxamer in healthy volunteers. BMC clinical pharmacology, 9(1), 19.

13. Lockwood, G. F., Albert, K. S., Wagner, J. G., & Szpunar, G. J. (1984). Pharmacokinetics of ibuprofen in man IV: Absorption and disposition.

Chapter 5.

Formulation Evaluation – Comparison of Conventional Tests to Gastrointestinal Simulator-2

5.1. Introduction

Regardless of route of administration, optimization of a drug formulation is crucial across all steps of the development process. Fonner, Buck, and Banker, some of the first applications of mathematical optimization techniques to pharmaceutical systems, state that determining the effects of controllable variables on the response variable accurately requires a statistically well designed and extensive series of experiments. Further complicating matters is that certain design objectives are competing, such as tablet friability and disintegration time, or tablet hardness and drug dissolution rate.[1] This means that most formulation behaviors are constrained variables, that is, that variable cannot be optimized for ad infinitum without consideration towards the effect on another. Although the system for drug dissolution of an oral formulation is governed by observable laws, the system is so complicated that an empirical approach is necessary, as is true for most industrial systems.[2,3] This optimization involves a set of designed experiments and determining a mathematical model that describes the effects of each process variable on the response variable in order to determine the optimal

levels for each process variable.[1,4,5] On such statistical design for experiments is the Placket-Burman design.[6] Plackett-Burman is screening experiments designed to use the minimum amount of experiments to determine the main effects of interest. The design is typically used for screening as multi-factor interactions are assumed to be negligible and the results are confounded by any multi-factor interactions. Conventional in vitro evaluation techniques for the optimization of oral formulations are: disintegration, tablet hardness, dissolution, friability.[1,4,5] Though separately these experiments are important for determining manufacturing variability, they lack in vivo relevance that another test may have. However, in order to test the viability of the GIS-2 system as a potential system for evaluating formulations, a comparison between it and conventional tests is necessary. Therefore, the goal of this study is to determine the sensitivity of GIS-2 dissolution to a set of process variables compared to the USP disintegration test and modified non-compendial USP-2 dissolution, with the end goal of GIS-2 determining what factors are important to a particular drug. For this study, ibuprofen will be used along with excipients typically found in on-the-market ibuprofen oral formulations.

5.2. Materials and Methods

5.2.1. Materials

All materials were of analytical grade or higher, unless otherwise specified. Acetonitrile for HPLC analysis was HPLC Grade (Fisher Scientific) and trifluoroacetic acid was LC/MS-grade (Sigma-Aldrich, St. Louis, MO).

5.2.2. Preparation of Formulations

Pure ibuprofen was sieved through a set of sieves and the solids from a portion of sieves was collected. The sieved ibuprofen was used in all formulations. Formulations were designed based on a Plackett-Burman design with seven factors and eight formulations. The Plackett-Burman array is shown in Table 1 of Appendix 1. Note that formulation #9

is a repeat of formulation #5 for the sake of determining experimental error. Formulations were made as 25 g batches, as described in Table 2 of Appendix 1. All excipients, except magnesium stearate, and ibuprofen were weighed and screened through an 18-mesh sieve. The sieved components were mixed in a V-blender for 5 minutes. After V-blending, 5g of the mix was added to the weighed magnesium stearate and screened through the 18-mesh sieve twice. This sieve mixture was re-added to the V-blender and mixed for 2 minutes. Mixture was transferred to a plastic bag for storage before compression. Into a 9.5mm diameter circular convex tablet punch and die, 220 mg of the formulation mixture was added. Compression force was varied per compressed tablet until the desired solid fraction was achieved. Procedure was repeated until twenty tablets were produced for each formulation.

5.2.3. Disintegration Method

Disintegration was performed in a USP disintegration apparatus. The procedure was based on USP general chapter <701>.[7] Into each tube of the basket, one tablet was added. The basket was allowed to cycle up and down in approximately 750 mL of water for 10 minutes at 30 cycles per minute. Time was recorded for each individual tablet when it had been determined to full disintegrated. Average and standard error for each formulation was calculated and reported.

5.2.4. USP-2 Dissolution Method

Dissolution procedure was modified from the USP general chapter <711> for dissolution.[8] 500 mL of 50 mM phosphate buffer pH 6.5, with ionic strength adjusted to 150 mM with sodium chloride, was added to a standard 900 mL USP-2 dissolution vessel and allowed to equilibrate to 37C. Once equilibrated, the tablets were introduced to the media. Manual samples were taken at regular intervals, aliquoting 1.5 mL from each vessel. Aliquots were filtered through a 0.45 um syringe filter, discarding the first 0.5 mL. Remaining filtrate was assayed by HPLC. Media removed from each vessel was replaced with appropriate secretion media to maintain volume. Procedure was repeated in triplicate for each formulation.

5.2.5. GIS-2 Device & Dissolution Method

Device

The GIS-2 is a computer-controlled, four-vessel dissolution device for testing oral formulations. The four vessels represent the stomach, duodenum, jejunum, and ileum. The conditions of the experiment can be adjusted, including initial volumes, stomach emptying profile, secretion rates, temperature, pH, buffer capacity and ionic strength. pH is continuously monitored throughout the experiment. The vessels are flat-bottomed cylindrical glass jacketed vessels. The vessels are mixed using top-down stirring, controlled by digital motors (Myostat Motion Control Inc., Newmarket, ON Canada). The stirrers use appropriately sized 3-blade hydrofoils (MXD, Louisville, KY).

Method

The device was controlled by software developed in Labview (National Instruments, Austin, TX). Stirring was maintained at speed, cycling between a lower speed to suspend most particles, with a one second burst, every sixty seconds to re-suspend any particles that may have settled to the bottom of the vessel. All fluid transfer was controlled by Ismatec Reglo ICC peristaltic pumps (Cole-Parmer GmbH, Wertheim, Germany). Pumps were standardized with water on day of analysis before analysis. Initial conditions can be found in Table 5.1. The stomach emptied from 300 mL, initially, to 75 mL with first-order kinetics (t1/2: 30 min). Volume was maintained at 50 mL in the duodenum and jejunum. The ileum accumulated all excess volume to maintain the first three vessels. After the stomach reached 75 mL, the experiment continued for one hour, with secretions only, with the stomach, duodenum, and jejunum volumes held constant. Formulations were pre-disintegrated in the stomach, by stirring at 120 RPM for 10 minutes, before fluid transfer was initiated. Manual samples were taken at regular intervals, aliquoting 1.5 mL from each vessel. Aliquots were filtered through a 0.45 um syringe filter, discarding the first 0.5 mL. Remaining filtrate was assayed by HPLC. Media removed from each vessel was replaced with appropriate secretion media to maintain volume.

Vessel	Initial Volume and Media	Stir Speed (RPM)	Burst Speed (RPM)	Secretion Buffer and Rate
Stomach	300 mL: 250 mL of 2mM SDS 50 mL of 0.01N HCl w/ 2mM SDS, 100 mM ionic strength (adjusted with NaCl)	120	240	2.5 mL/min: 50 mL of 0.01N HCl w/2mM SDS,100 mM ionic strength (adjusted with NaCl)
Duodenum & Jejunum	50 mL of 50 mM Phosphate Buffer pH 6.5, 150 mM ionic strength (adjusted with NaCl)	175	350	1 mL/min: 100 mM Phosphate Buffer pH 6.5, 150 mM ionic strength (adjusted with NaCl)
Ileum	250 mL of 50 mM Phosphate Buffer pH 6.5, 150 mM ionic strength (adjusted with NaCl)	75	150	NA

Table 5.1: Standard GIS-2 media and stirring conditions for experiments.

HPLC Method

Filtered and diluted samples were analyzed by an isocratic reverse phase HPLC method (Agilient 1100 Series, Santa Clara, CA) using an Agilent C-18 column (3.5µm x 4.6µm x 150mm). Mobile phase was a 60:40 mix of acetonitrile:water with 0.1% trifluoroacetic acid. The column was maintained at 40°C with a mobile phase flow rate of 1.0mL/minute. UV detection was performed at 220 nm. A standard curve was prepared bracketing the sample solutions.

Statistical Analysis

Statistical analysis was performed on the results from each analysis in order to determine the effects of each formulation factor on the performance of the formulations. Using the FrF2 package in R, a part of the DoE.base package for analyzing the design of experiments.[9,10] Statistical significance was determined by a two-sided t-test.

5.3. Results

5.3.1. Disintegration Results

Results from disintegration testing are shown in Table 5.2. The effects of each formulation factor are shown in Figure 5.1 with the effects and p-values shown in Table 5.3. Copovidone level was the only statistically significant factor in disintegration time, with increasing copovidone increasing disintegration time. All other factors did not show statistical significance.

Formulation	Average Disintegration Time (sec)	Standard Error (sec)
1	95.0	13.7
2	31.0	2.5
3	311.4	16.9
4	155.6	13.1
5	241.3	13.3
6	110.7	4.6
7	551.9	0.7
8	17.6	5.3
9	253.1	23.9

Table 5.2: Summary of results from disintegration testing. The average disintegration time and standard error are shown for all formulations

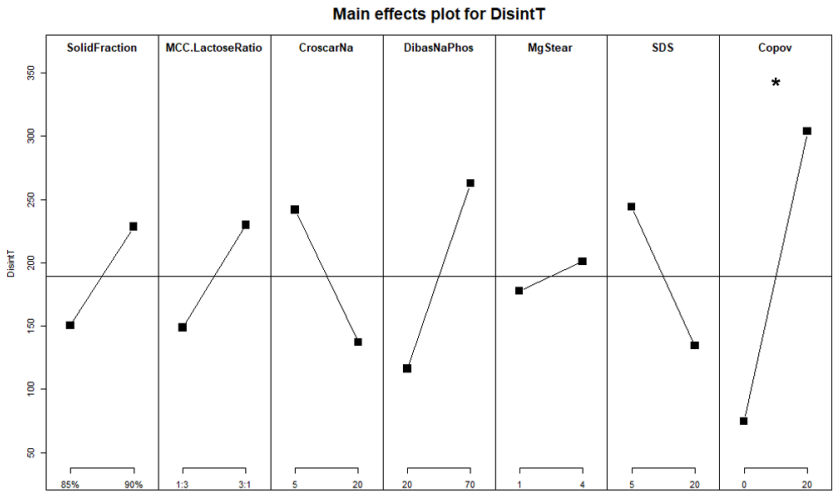

Figure 5.1: Main Effects for each factor for total disintegration time. $p < 0.05$ = *

Effect	β_0	$\beta_{Solid\ Frac}$	β_{Ratio}	$\beta_{Croscar}$	β_{PO4}	β_{MgStrt}	β_{SDS}	β_{CoPov}	ε
Value (min)	189.31	38.99	40.49	-52.29	73.16	11.51	-54.66	**114.51**	5.9
p-value	-	0.096	0.092	0.072	0.051	0.302	0.068	**0.033**	-

Table 5.3: Summary of Main Effects values for Disintegration Time and their associated p-value

5.3.2. USP-2 Results

USP-2 dissolution showed some formulation to formulation discrimination, with the possibility of forming a rank order of the performance of the formulations. Figure 5.2 shows the mass dissolved over time for the nine formulations. However, when determining effects of the individual factors, none of the formulations showed a statistically significant effect on dissolution time to 50% of final amount dissolved. The effect plots for the formulation factors is shown in Figure 5.3.

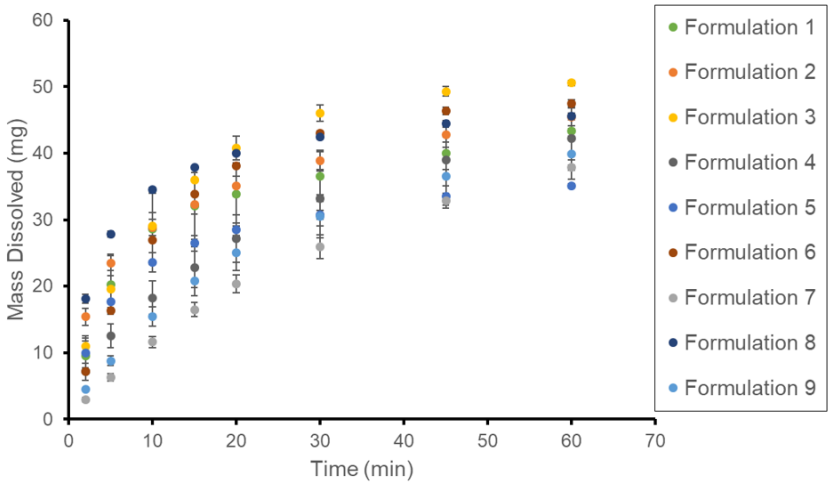

Figure 5.2: Mass dissolved over time plot of the Plackett-Burman array of formulations in the USP-2 dissolution experiments.

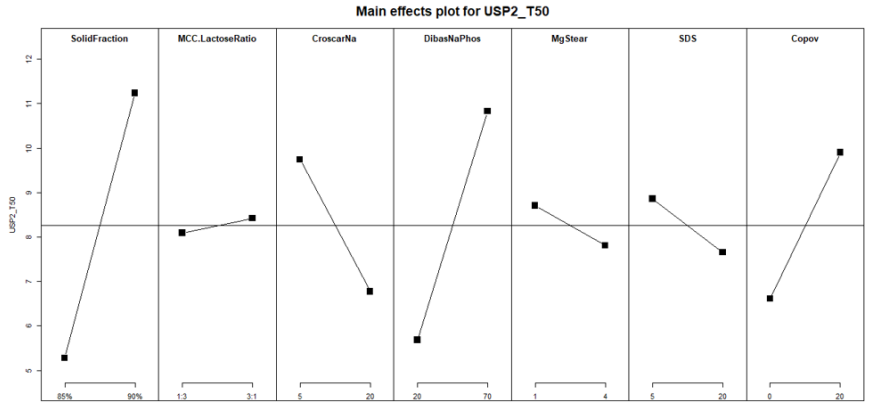

Figure 5.3: Main effect plots for each factor for time to 50% of final amount dissolved.

Effect	B_0	$\beta_{Solid\ Frac}$	β_{Ratio}	$\beta_{Croscar}$	β_{PO4}	β_{MgStrt}	β_{SDS}	β_{CoPov}	ε
Value (min)	8.256	2.977	0.162	-1.482	2.571	-0.449	-.6001	1.643	7.31
p-value	-	0.754	0.986	0.872	0.785	0.961	0.948	0.859	-

Table 5.4: Summary of Main Effects values for time to 50% in the USP-2 dissolution and their associated p-value

5.3.3. GIS-2 Dissolution

GIS-2 showed some discrimination between formulations, as shown in Figure 5.4. With the duplicate formulations (5 & 9) show the greatest dissolution after 90 minutes and similar profiles of the course of the experiment. By contrast, formulation 2 had less extent of dissolution. The remaining formulations fell between those two sets of formulations. When examining the effects of the formulation factors, copovidone levels and croscarmellose sodium levels had statistically significant effects on dissolution performance in the GIS-2 device, as shown in Figure 5.5. Dissolution performance was examined for time to 80% of final mass dissolved.

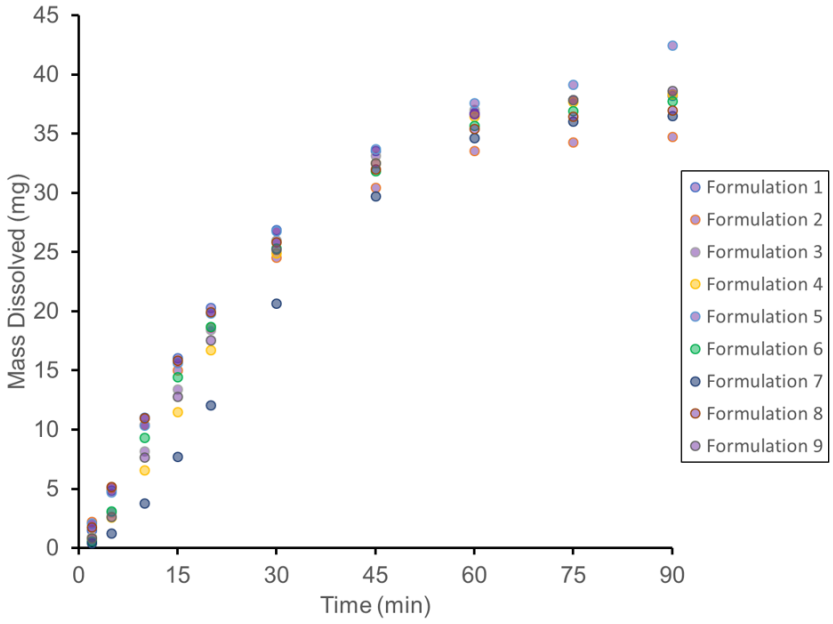

Figure 5.4: Mass dissolved over time plot of the Plackett-Burman array of formulations in the intestinal vessel of the GIS-2

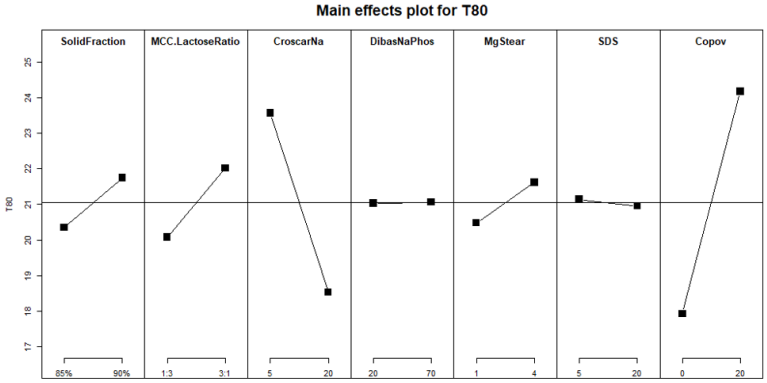

Figure 5.5: Main Effects for each factor for time to 80% of final amount dissolved in the intestinal vessels of the GIS-2. $p < 0.05$ = *

Effect	**B_0**	**$\beta_{Solid\ Frac}$**	**β_{Ratio}**	**$\beta_{Croscar}$**	**β_{PO4}**	**β_{MgStrt}**	**β_{SDS}**	**β_{CoPov}**	**ε**
Value (min)	21.045	0.695	0.970	**-2.518**	0.013	0.573	-0.090	**3.123**	0.93
p-value	-	0.115	0.083	**0.032**	0.935	0.139	0.607	**0.026**	-

Table 5.5: Summary of Main Effects values for time to 80% in the intestinal vessels of GIS-2 and their associated p-value

5.4. Discussion

Three techniques for evaluating formulations were examined using a Plackett-Burman array. When determining significant effects USP-2 Dissolution showed no significant effects, though two effects did show high magnitude of effect. This is due to high experimental variability determined when comparing the duplicated formulation (5 & 9). The USP disintegration test determined the copovidone level had a significant effect on disintegration time. This is not unexpected, as copovidone is a tablet binder. Therefore, increasing copovidone level, would increase the time to disintegration. The GIS-2 test showed the most statistically significant factors. Copovidone was again shown to be a statistically significant effect, while croscarmellose sodium was also statistically significant. This result was also expected as croscarmellose sodium is a disintegrant. Thus, increasing croscarmellose sodium decreases disintegration time for the tablet and allows undissolved drug particles to reach the duodenum compartment to dissolve more quickly than at when croscarmellose sodium is at a lower level. It is surprising that this was not shown to be statistically significant in the disintegration test. This also shows a potential main mechanism for ibuprofen dissolution in GIS-2. Ibuprofen dissolution is driven mostly by tablet disintegration stomach emptying. This is likely why most formulations had similarities in time to 80% dissolved. Since GIS-2 was designed to have in vivo-like dissolution conditions, the observations in effects on dissolution performance are most likely to transfer over to in vivo performance of drug formulations.

5.5. Conclusions

GIS-2 was shown to better discern between effects that cause changes in dissolution behavior. However, these studies were designed for semi-optimized formulations. Further studies in formulation optimization could be performed in order to determine further optimization. By widening the range of levels for the factors, more significant effects may become apparent. Also, due to the nature of Plackett-Burman design, the interactions between formulation effects were not examined. A design of experiments

that examines secondary interactions between effects but could be examined with additional experiments to determine if the GIS-2 is able to detect any secondary effects. Lastly, since ibuprofen is a BCS IIa drug, its solubility is high in neutral pH conditions, so disintegration and gastric emptying drive intestinal dissolution. For other compounds, like BCS class IIb drugs, the processes acting upon the drug molecule are more complex, including supersaturation in the intestinal compartments. These additional processes may be more sensitive to formulation changes and could be an area of study for formulation optimizations in the GIS-2 device.

5.6. Acknowledgements

I would like to thank Yuhan Wang for her contributions to this entire chapter, including the preparation of the formulations and the disintegration and USP-2 dissolution studies.

5.7. References

1. Fonner Jr, D. E., Buck, J. R., & Banker, G. S. (1970). Mathematical optimization techniques in drug product design and process analysis. Journal of pharmaceutical sciences, 59(11), 1587-1596.
2. Davies, O. L. (1954). The design and analysis of industrial experiments. The design and analysis of industrial experiments.
3. Banker, G. S., Siepmann, J., & Rhodes, C. (Eds.). (2002). Modern pharmaceutics. CRC Press.
4. Schwartz, J. B., Flamholz, J. R., & Press, R. H. (1973). Computer optimization of pharmaceutical formulations I: General procedure. Journal of pharmaceutical sciences, 62(7), 1165-1170.
5. Dick, C. F., Klassen, R. A., & Amidon, G. E. (1987). Determination of the sensitivity of a tablet formulation to variations in excipient levels and processing

conditions using optimization techniques. International journal of pharmaceutics, 38(1-3), 23-31.

6. Plackett, R. L., & Burman, J. P. (1946). The design of optimum multifactorial experiments. Biometrika, 33(4), 305-325.

7. United States Pharmacopeia and National Formulary (USP 43-NF 38). General Chapter <701>. Rockville, MD: United States Pharmacopeial Convention; Nov 1, 2019.

8. United States Pharmacopeia and National Formulary (USP 43-NF 38). General Chapter <701>. Rockville, MD: United States Pharmacopeial Convention; Nov 1, 2019.

9. Grömping U (2014). R Package FrF2 for Creating and Analyzing Fractional Factorial 2-Level Designs. Journal of Statistical Software, 56(1), 1-56. URL http://www.jstatsoft.org/v56/i01/.

10. Grömping U (2018). "R Package DoE.base for Factorial Experiments." Journal of Statistical Software, 85(5), 1-41. doi: 10.18637/jss.v085.i05 (URL: https://doi.org/10.18637/jss.v085.i05)

Chapter 6.

Conclusions and Future Directions

The goal of this thesis was to develop a new dissolution device that is mechanistically designed and encapsulates the in vivo processes and conditions and oral dosage form experiences. The system is based off of the GIS-1, a three-vessel device previously used for evaluating in vivo performance. The GIS-2 is a four-vessel device, with improved stirring conditions, gastric emptying profiles based on in vivo emptying kinetics, titration to allow for use of lower buffer capacity media and empirically determined hydrodynamics that can be used for dissolution predictions in the GIS-2 device. The device is designed for modularity with vessels that can be swapped out for other types of vessels, which allows for user-customizability to match the needs of the drug molecule and its formulation. With a well-characterized, validated dissolution device in place, the system can be used for many applications. Based on existing in vitro data from literature for two ibuprofen formulations, in vitro data was used to attempt to form a correlation between the data. This was performed in order to determine if the in vitro-in vivo relevance that is claimed for GIS-2, and systems like GIS-2, was applicable. No correlations were determined that meet the requirements of the FDA guidance for Level A correlations. However, the exercise in developing these correlations showed promise for method development that could lead to improved correlations. Additionally, correlations were attempted between two different forms of the active drug molecule, the free acid and a sodium salt. Though they had different plasma profiles, their dissolution kinetics differed. Population averages were used to determine

pharmacokinetic parameters, which has been shown to have large confidence intervals and lead to issues in developing correlations. Also, the sample groups for the PK parameters and the plasma data for the two formulations were separate sample groups. Despite all of these challenges, GIS-2 shows promise in its ability to determine in vivo-in vitro correlations and with improved data inputs could reliably generate valuable data. Formulations were evaluated under a Plackett-Burman design, by disintegration, USP-2 dissolution and GIS-2 dissolution in order to determine what formulation variables affect performance, with the expectation that improved performance in these in vitro tests can be related to in vivo performance. Since GIS-2 was designed to have in vivo-like dissolution conditions, any observed effects on dissolution performance are most likely to transfer over to in vivo performance of drug formulations. The GIS-2 test showed the most statistically significant factors compared to the other two testing methods. However, these studies were designed for semi-optimized formulations, by constraining the excipient levels to typical levels used in manufacturing. Further studies in formulation optimization could be performed in order to determine further optimization of the formulation. By widening the range of levels for the factors, more significant effects may become apparent. Also, due to the nature of Plackett-Burman design, the interactions between formulation effects were not examined. Further studies in the GIS-2 device could also be designed based on the experiments performed herein. For all BCS II-IV drugs, the GIS-2 can be modified in order to meet the needs of the drug molecule. Due to the modular design, an absorption compartment could be installed to assist in sustaining supersaturation. This is true for weakly basic drugs, which decrease in solubility as it progresses through the system, but may also apply to co-crystals, salts and amorphic drug forms. Additionally, the stomach pH can be modified to mimic drug-drug interactions caused by acid reducing agents and proton pump inhibitors, which typically affect weakly basic drugs. The GIS-2 system is an excellent and exciting basis for exploring the oral formulation space.

Appendix A.

Operating Procedure for GIS-2 Software

Materials and Equipment Preparation

1. Buffer/Solutions
    a) Buffer preparation will vary depending on the experiment and drug/formulation being tested.
    b) Example solutions include 0.01N HCl solution with 2mM sodium dodecyl sulfate and 50 mM phosphate buffer at pH 6.5
2. General Set-up
    a) Confirm hydrofoils and other parts are all visibly clean
    b) Turn on the water bath such that media temperatures are 37°C. This may require setting the water bath temperature slightly higher than 37C.
    c) Gather materials needed for experiment
    d) Check Tubing prior to each experiment
        i. Tubing should be replaced when it appears to be permanently crinkled, very flat or deformed. Visual and physical inspection should be used. Ideally all tubing should be replaced at the same time. A log of replacement of GIS 2 tubing should be kept.

ii. New tubing should be conditions for at least 10 minutes by flowing water

e) Set up pumping system

i. Attach labeled tubing to tubing clamps following guide on the tubing for proper placement.

ii. Insert tubing clamps into their appropriate labelled locations, based on the locations described in the software

f) Calibrate pH meter according to the user manual and on-screen directions

Set up of GIS 2 software and equipment prior to experiment start

1. General information

a) GIS software icon is located on the desktop

b) Software is periodically updated. Always use the most recently updated version

c) The following instructions will discuss actions required for each screen

2. Screen One: Set Experimental Parameters and Initialize Equipment/Sensors

a) Choose one of the options in the "Choose a Method for the Gastric emptying Phase" drop down menu. This list may not be all inclusive

b) Choose one of the options in the "Choose the Post-Emptying Phase Action". This list may not be all inclusive

i. End GIS-1 after Gastric Emptying Phase

ii. Keep STIRRERS ON (Pumps OFF; Main & Burst stir speeds)

iii. MAINTAIN the S, D, & J volumes w/Stirring (Tx1 = S secretion; Tx2 = S + D secretions; Main & Burst Stirring)

A. This feature allows the stomach, duodenum & jejunum volumes to be maintained at your choice of volume

B. The slider directly below allows the user to set up an automatic shut off time after the post-emptying phase has begun

c) Adjust the parameters as needed in “Volume and Rate Parameters”, “Stirring Speeds” and “Stirring Timing”

i. Values are preset, however may be changed

ii. Stomach volume calculated via the GIS I software as the experiment run progresses based on gastric emptying rate chosen

A. When the software calculates that the stomach is at final volume set, the experiment will stop.

B. Choosing a smaller final stomach volume will assure experiment completion in the event actual and computer generated stomach volumes are not the same.

iii. Pump rotation and timing parameters may also be changed although this is not advisable.

d) Saving experimental data (upper right corner)

i. Input desired data file name; a personal data file folder can be created

ii. Input user name

iii. Comments may be included; these will be retained in the output excel file after experiment is complete (this file also contains transfer rates, pHs of all probes„ calibration factors used, and initialized parameters)

e) VersaStar Current pH/temp and temperature configuration

i. This section shows configuration and current values for the pH meter. Under each channel, this section shows the current pH, temperature and whether a temperature probe is present

f) “Submit Parameters + Initialize Hardware”

i. Once all parameters have been set, click the oval S+I button

ii. Parameters will be submitted and saved in the end data file.

iii. Once this button is clicked, the green squares above tabs 2 and 3 will turn green, allowing user to proceed to “Prime/Purge” and/or “Calibration”

3. Screen Two: Purge or Prime Pump Lines: Pre and Post-Gastric Emptying

a) Pump prime/purge parameters

b) Default values have been chosen to assure adequate time for priming and purging, however speed and duration may be set for each individual pump.

c) The rpm values should be set as follows; time should be set to 600 seconds for all pumps to allow adequate tubing conditioning

i. Stomach – 45 rpm

ii. Transfer1 (S-D) –90 rpm

iii. Duodenum – 45 rpm

iv. Transfer2 (D-J) – 90 rpm

v. Jejunum-45 rpm

vi. Transfer3 (J-I)-90 rpm

d) Confirm rotation settings are correct

Tubing	Rotation
Stomach secretion	CCW
Stomach to duodenum transfer	CW
Duodenum secretion	CCW
Duodenum to jejunum transfer	CW
Jejunum secretion	CW
Jejunum to ileum transfer	CW

Table A.1: GIS2A Pump Rotation Directions

i.

Tubing	Rotation
Stomach secretion	CW
Stomach to duodenum transfer	CCW
Duodenum secretion	CW
Duodenum to jejunum transfer	CCW
Jejunum secretion	CCW
Jejunum to ileum transfer	CCW

Table A.2: GIS2B Pump Rotation Directions

ii.

e) Rotation of the pump (clockwise and counterclockwise) may be changed but do so with caution.
    i. Before purging/priming after changing flow direction, ensure tubing is set up to accommodate this direction change
f) Individual confirm buttons for each pump allow testing of one or more pumps.
g) Once speed and duration are set and confirm buttons chosen, start the prime/purge cycle by clicking the toggle switch.
h) Repeat as needed
i) Dynamic Status of pumps
    i. Slider bars show the status of prime/purge for each pump
j) E-Stop Pumps
    i. Click E-stop button on the upper right side of the screen if pumps must be stopped before prime/purge cycle is complete
k) Set up for prime/purge
    i. Fill beakers with deionized water and insert inlet tubing into water
    ii. Set up empty beakers at outlet tubing to collect water
    iii. Prime/purge the pumps as described
    iv. Once pumps are primed/purged move to “Calibrate Pumps” tab

4. Screen Three: Pump Calibration Factor Determination
    a) Pump calibration parameters
        i. Default values have been chosen to assure adequate time for calibration, however speed and duration may be set for each individual pump.
        ii. The rpm values should be set as follows; time is 180 seconds for all pumps
            A. Stomach – 10 rpm
            B. Transfer1 (S-D) – 50 rpm
            C. Duodenum – 10 rpm
            D. Transfer2 (D-J) – 50 rpm
            E. Jejunum-10 rpm
            F. Transfer3 (J-I) – 50 rpm
        iii. Rotation of the pumps may be changed but do so with caution
        iv. Individual confirm buttons for each pump allow testing of one or more pumps
        v. Once speed and duration are set and confirm buttons chosen, start the calibration cycle by clicking the "Start Calibration Cycle" toggle switch.
    b) Dynamic Status of pumps
        i. Slider bars show the status of calibration for each pump
    c) E-Stop Pumps
        i. Click E-stop button on the upper right side of the screen if pumps must be stopped before calibration cycle is complete
    d) Calibration factors determination
        i. Gather six plastic Erlenmeyer flasks which have been labelled and (empty) tare weight determined.

ii. Remove glass beakers from outlet tubing and replace with Erlenmeyer flasks.

iii. After the first calibration cycle is complete, enter the weight of the empty plastic volumetric flask for each respective pump under the left "Tare Weight" column

iv. Tab to the "Gross Weight" column

v. Enter the gross weight for each Erlenmeyer flask

vi. This table can be printed and should be used for recording gross and tare weights, calibration factors and percent difference for each run.

Item	Tare Weight (g)	Weight 1 (g)	Cal Factor	Tare Weight (g)	Weight 2 (g)	Cal Factor	% Diff	Tare Weight (g)	Weight 3 (g)	Cal Factor	% Diff
S Sec											
S->D											
D Sec											
D-> J											
J Sec											
J->I											

Table A.3: Table for recording pump calibration weights

vii. When the difference of Calibration Factors between runs is within 95 to 105 percent for an individual pump, the pump is considered calibrated and does not need to be re-calibrated with other pumps not within the acceptable range.

viii. Once the percent difference for all pumps is within the appropriate range, hit “Submit Cal factors” button and proceed to next tab.

5. Screen Four: Gastric Emptying Phase
    a) Warm up Stir On/Off-used to turn on stirrers prior to experiment
        i. To more quickly heat solutions in vessels
        ii. To assure nothing is impeding the rotation of the stirrers prior to the experiment
    b) Dose Drug
        i. Optional button which may be pressed prior to dosing drug
    c) Start Pumps
        i. Dose drug into the stomach beaker
        ii. Press “Start pumps” button to begin an experiment
            A. If desired, stirrers will run in cycles with intermittent high speed burst until user ends experiment or pauses
            B. Pumps will begin their programmed experimental cycles
    d) Pause On/Off & Stop Run early
        i. Pause – briefly stops the stirrers and pumps for a user defined amount of time. Stopwatch tracks the length of a pause
        ii. Stop Run Early – ends designated gastric emptying phase and offers user option to move onto post-emptying phase (Tab 5) or complete end of experiment and exit out of software
    e) Information Screens- screens on this page provide additional information
        i. Stirring speeds and cycles-show time to next stirring burst
        ii. pH and temperature-shows pH and temperature for each pH probe used

iii. Pump flow rates and speed" pH and temperatures-flow rates of each pump are shown. Next to this area is the computer calculated stomach volume

iv. Stomach, duodenum and jejunum Values

f) Procedure for Starting an Experimental Run

i. Remove calibration beakers and other non-essential materials and equipment.

ii. Assure all materials are prepared for sampling. Method of sampling and analysis will vary depending on the experiment.

iii. Insert pH probes and temperature sensors into their respective beakers. pH probes must be calibrated before each experiment.

iv. Confirm that pH of the solutions in each vessel are within the desired range. Adjust pH if needed.

v. Place tubing in appropriate containers. Stomach, duodenum and jejunum inlet tubing should be placed in the appropriate secretion bottles and transfer tubing should be set up in between vessels. Tubing should be placed above the hydrofoils.

vi. Press "Dose Drug" button and add dosage form (optional)

vii. Press Start Pump" to begin experimental run

g) Procedure for ending an experimental run

i. Click the red "Stop Run Early" button" if stopping before the end of the run. Button will turn green once it is pressed

ii. Wait for all cycles (stirrers and pumps) to stop and various text boxes to appear before proceeding.

iii. If maintain feature was chosen at initialization screen, press "Stop Run Early" button when stomach volume is at desired maintain volume (for example 50 mLs). GIS Software will pause briefly before moving on to tab 5 and "Post Emptying Data Phase" will begin.

6. Screen Five: Post Emptying Data Phase
    a) Post Emptying Phase
        i. Chosen post emptying phase is shown in upper left corner of screen
        ii. Maintain method will run until the end time specified on the first page (slider bar)
        iii. Run may be stopped early using “Stop Early” button (similar to screen 4: Gastric emptying phase) to end the run at a user specified time.
        iv. Information screens similar to that in the gastric emptying phase provide additional information
        v. Once run is ended, pop up information screens will inform user. Final pop up screen will allow user to return to prime/purge tab for tubing clean up.
        vi. Analysis of stomach, duodenum, jejunum, ileum solutions as well as tubing and dosage form container may be desired.
        vii. Vessel washes may be completed to determine where remaining undissolved drug is located
            A. Rinse the walls of the vessel with a solvent in which the drug is soluble (eg acetonitrile or methanol)
            B. Transfer the contents of the vessel into an appropriately sized volumetric flask based on initial dose, experience with the experiment, etc.
            C. Rinse any remaining particles from the vessel into the volumetric flask
            D. QS the volumetric flask with buffer or other fluid as needed
            E. Remaining particles could be excipients which may not completely dissolve
            F. Filter the final solution before analysis

G. Perform further dilutions if needed

viii. Tubing Washes

A. Place tubing outlet directly into a volumetric flask.

B. Add appropriate solvent to beaker and place tubing inlet into beaker.

C. Rinse tubing directly into volumetric flask (tubing flow may be reversed in order to more effectively remove particles)

D. QS with appropriate solvent.

ix. Filter wash

A. Using a syringe and appropriate solvent such as acetonitrile or methanol, flush filter five times into a 50 mL volumetric flask. QS with solvent

B. Additional dilutions may need to be performed (start with 1:10 dilution)

Screens

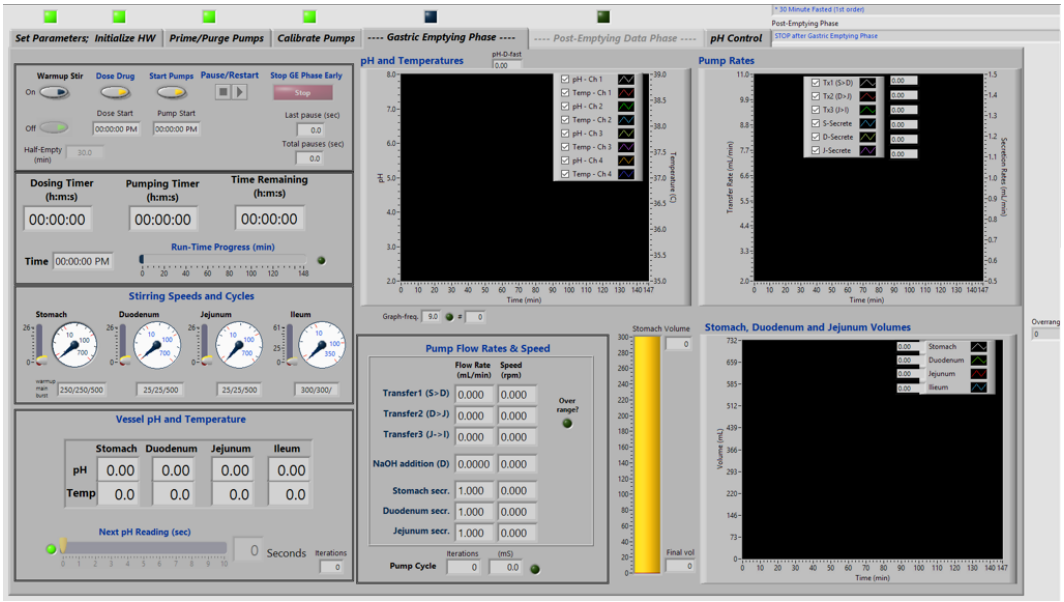

Figure A.1: Gastric Emptying Profile Tab in GIS-2 Software

Appendix B.

MatLAB Code for Duodenal pH and Titration Simulations

```
1
2  %%%%pH Time%%%
3
4  close all
5  %%%%Inputs%%%
6
7  % Stomach properties
8  Ka_HCl = 10^7; %dissociation constant of HCl
9  pKa_HCl = -log10(Ka_HCl);
10 Vol_HCl = 50E-3; %HCl volume (L)
11 Vol_w = 250E-3; %Water volume (L)
12 C_HCl = 0.01;%HCl (acid) concentration (0.01 N HCl = 0.01 M
       HCl)
13 Vol_aqs = Vol_w+Vol_HCl; %%Aqueous  volume (L)
14 Sec_Rate_S = 1/60*10^-3; %Secretion flow rate 2.5 mL/min
     --> L/s)
15 Sec_S_conc = 0.01; %(M)
16 Kw = 2.4825E-14;
```

```
17 Media_replace = 1.5*10^-3; %Media replacement volume (L)
18
19 %Timing
20 tstep = 0.5; %interval between points
21 tstop  = 120*60; %length of simulation
22 tspan = (tstop/tstep)+1; %number of data points during
      simulation
23
24 %Emptying Rate
25 zero_emp = 10E-3; %rate of emptying for zero order (L/min)
26 Emptying_rate = 15; %Emptying rate in (min)
27 k = log(2)/(Emptying_rate); %emptying rate for first order
      LEAVE AS POSITIVE
28 % beta = 0.81; %nu for Weibull --- 0.6 for median, 1.72 for
       Slow, 0.81 for mean, 0.31 for fast
29 % nu = 39.42;%gamma for Weibull 23.14 for median, 100.13
      for Slow, 39.42 for mean, 10.43 for fast
30 S_vol_stop = 75E-3; %Maintain Volume for Stomach (L)
31 beta = 0.6;
32 nu = 23.14;
33
34 % Duodenum Properties
35 Bulk_conc_D = 10*10^-3; %initial concentration of phosphate
       in duodenum (M)
36 Sec_Rate_D = 1/60*10^-3; %Secretion flow rate 1.0 mL/min
      --> L/s)
37 Sec_D_conc = 0.02; %(M)
38 pH_initial_D = 6.5; %initial pH
39 pH_sec_D = 6.5; %Secretion pH
40 Vol_D = 50E-3; %initial volume duodenum (L)
41 pka1 = 2.14; %pKa of H3PO4/H2PO4
```

```
pka2 = 6.8; %pKa of H2PO4/HPO4
ka1 = 10^(-pka1);
ka2 = 10^(-pka2);

% Titration Properties
Titrant_Conc = 0.1; %(M)
Titrant_pH = 7.0;
Titrant_pka = 6.8;
Titrant_ka = 10^(-Titrant_pka);
Setpoint_pH = 6.0; %pH to be titrated to
Threshold_pH = 5.5; %pH to be titrated from



Vol_emptying_rate = zeros(1,tspan);
Vol_xfer_S = zeros(1,tspan);
Vol_s_bulk = zeros(1,tspan);
mol_H_xfer = zeros(1,tspan);
pH_b_1 = zeros(1,tspan);

%%%Stomach Tracking%%%
%
    %%%%%%%%%%%%%%%%%%%%%%%%%%%%%%%%%%%%%%%%%%%%%%%%%%%%%%%%%%%%%%%%%%%%%%%%%%%%%%%%%%%%%%%

%Initialization of bulk Conc.
H_b_1(1,1) = (C_HCl*Vol_HCl/Vol_aqs); %Initial bulk
    concentration of H+ (M)
pH_b_1(1,1) = -log10(H_b_1(1,1));%Initial bulk PH
HA_b_1(1,1) = 0;%Initial bulk concentration of HA
A_b_1(1,1) = 0;%Initial bulk concentration of A-
HCl_b_1(1,1) = 0;%Initial bulk concentration of HCl
```

```
70
71 Vol_s_bulk(1,1) = Vol_aqs; %V0 for stomach (L)
72
73 for tindex = 2:tspan
74
75     t = (tindex - 1)*tstep;
76
77     %Emptying Regime Selection
78     if Vol_s_bulk(1,(tindex-1)) > S_vol_stop
79 %         Vol_emptying_rate(1,tindex) = zero_emp/60; %
    Zero order emptying rate (L/sec)
80         Vol_emptying_rate(1,tindex) = (Vol_aqs*k*exp(-k*(t
              /60)))/60; %first order emptying (L/sec)
81 %        Vol_emptying_rate(1,tindex) = ((Vol_aqs*beta/(t
    /60)*exp(-(((t/60)/nu)^beta))*(((t/60)^beta)/nu)))/60; %
    Weibull emptying rate (L/sec)
82     else
83         Vol_emptying_rate(1,tindex) = 0; %stops net
              emptying of Stomach at stop volume, similar to
              maintain function
84
85     end
86
87     %Xfer to Duodenum
88     Vol_xfer_S (1,tindex) = (Vol_emptying_rate(1,tindex)*
          tstep)+Sec_Rate_S*tstep; % Volume leaving Stomach at
           t (L)
89     mol_H_xfer (1,tindex) = (Vol_xfer_S(1,tindex))*H_b_1(1,
          tindex-1); %mol of H leaving Stomach at t (mol)
90
91     %Updates in Stomach
```

```
92      Vol_s_bulk(1,tindex) = Vol_s_bulk(1,(tindex-1)) -
            Vol_xfer_S(1,tindex) + Sec_Rate_S*tstep; %Current
            vol of Stomach(mL)
93      H_b_1(1,tindex) = (H_b_1(1,tindex-1)*Vol_s_bulk(1,(
            tindex-1)) + ((Sec_Rate_S*tstep)*Sec_S_conc) -
            mol_H_xfer(1,tindex))./Vol_s_bulk(1,(tindex)); %
            current proton concentration (M)
94      pH_b_1(1,tindex)= -log10(H_b_1(1,tindex));%current pH
            in stomach
95
96  %     %Media Replacement Check
97  %         if ismember(t
    ,[120,300,600,900,1800,2700,3600,4500,5400]) == 1
98  %             H_b_1(1,tindex) = (H_b_1(1,tindex)*Vol_s_bulk
    (1,tindex) - H_b_1(1,tindex)*Media_replace + Sec_S_conc*
    Media_replace)/Vol_s_bulk(1,tindex);
99  %         end
100 end
101
102
103 %%%%%%%%%%%%%%
104 %%%Duodenum Tracking%%%
105 %%%%%%%%%%%%%%
106
107 %%%%%%%%%%
108 %%%Initialization%%%
109 %%%%%%%%%%
110 H2B_D = zeros(1,tspan);
111 HB_D = zeros(1,tspan);
112 H_D = zeros(1,tspan);
113 x_d = zeros(1,tspan);
```

```
pH_D = zeros(1,tspan);
Vol_Xfer_D = zeros(1,tspan);
H2B_bb_D = zeros(1,tspan);
HB_bb_D = zeros(1,tspan);
HB_ab_D = zeros(1,tspan);
H2B_ab_D = zeros(1,tspan);
H3B_bb_D = zeros(1,tspan);
H3B_ab_D = zeros(1,tspan);
Total_B = zeros(1,tspan);
H2B_bb_D_2 = zeros(1,tspan);
HB_bb_D_2 = zeros(1,tspan);
H_D_preT = zeros(1,tspan);
H2B_D_preT = zeros(1,tspan);
Titrant_H = zeros(1,tspan);
Titrant_P = zeros(1,tspan);
Vol_Titrant = zeros(1,tspan);
Total_Vol_Titrant = zeros(1,tspan);

%%%
pH_D(1,1) = pH_initial_D; %Initial pH in D
H_D(1,1) = (10^-pH_initial_D); %Proton concentration (M)
HB_D(1,1) = Bulk_conc_D*ka2/(H_D(1,1)+ka2); %Concentration
    of HPO4 (2-) M
H2B_D(1,1) = Bulk_conc_D - HB_D(1,1); %concentration of
    H2PO4(-) M
H3B_D(1,1) = 0; % almost no chance there's any H3PO4 ever,
    but...
Vol_Xfer_D(1,1)=0; %no fluid transfer at t=0
Total_B (1,1) = HB_D(1,1) + H2B_D(1,1) + H3B_D(1,1); %total
    PO4 concentration in D

```

```
141 %%%secretion concentrations
142 H_D_Sec = (10^-pH_sec_D); %(M)
143 HB_D_Sec = Sec_D_conc*ka2/(H_D_Sec+ka2); %Concentration of
    HPO4 (2-) M
144 H2B_D_Sec = Sec_D_conc - HB_D_Sec; %concentration of H2PO4
    (-) M
145
146 %Titrant calculations
147
148 mEq_Titrant = Titrant_Conc*Titrant_ka/(10^-Titrant_pH+
    Titrant_ka) - Titrant_Conc*Titrant_ka/(10^-Setpoint_pH+
    Titrant_ka); %mEq that can be absorbed by 1 mL of buffer
     titrant to equilibrate at Setpoint
149 disp(mEq_Titrant);
150
151 for tindex = 2:tspan
152
153     t = (tindex - 1)*tstep;
154
155 %       if pH_D(1,(tindex-1)) > 3.5
156           W=@(Hdellp) -10^-pH_D(1,tindex-1)-10^-pH_b_1(1,
                tindex-1).*Vol_xfer_S(1,tindex-1)/Vol_D+10^-pH_D
                (1,tindex-1).*Vol_Xfer_D(1,tindex-1)/Vol_D-10^-
                pH_sec_D.*Sec_Rate_D*tstep/Vol_D+Hdellp+(Hdellp*
                HB_D(1,tindex-1)/(Hdellp+ka2))-((Kw/Hdellp)+(ka2
                *H2B_D(1,tindex-1)/(Hdellp+ka2)))+Kw/(10^-pH_D
                (1,tindex-1)-10^-pH_D(1,tindex-1).*Vol_Xfer_D(1,
                tindex-1)*tstep/Vol_D+10^-pH_b_1(1,tindex-1).*
                Vol_xfer_S(1,tindex-1)/Vol_D+10^-pH_sec_D.*
                Sec_Rate_D*tstep/Vol_D);
157 %       else
```

```
158 %           W=@(Hdellp) -10^-pH_D(1,tindex-1)-10^-pH_b_1(1,
    tindex-1).*Vol_xfer_S(1,tindex-1)/Vol_D+10^-pH_D(1,
    tindex-1).*Vol_Xfer_D(1,tindex-1)/Vol_D-10^-pH_sec_D.*
    Sec_Rate_D*tstep/Vol_D+Hdellp+(Hdellp*H2B_D(1,tindex-1)
    /(Hdellp+ka1))-((Kw/Hdellp)+(ka1*H3B_D(1,tindex-1)/(
    Hdellp+ka1)))+Kw/(10^-pH_D(1,tindex-1)-10^-pH_D(1,tindex
    -1).*Vol_Xfer_D(1,tindex-1)*tstep/Vol_D+10^-pH_b_1(1,
    tindex-1).*Vol_xfer_S(1,tindex-1)/Vol_D+10^-pH_sec_D.*
    Sec_Rate_D*tstep/Vol_D);
159 %       end
160
161     H_D(1,tindex)=fzero(W,[10^-0 10^-14]);
162     pH_D(1,tindex) = -log10(H_D(1,tindex));
163
164 %       if pH_D(1,tindex) > 3.5
165           H2B_bb_D(1,tindex) = H_D(1,tindex).*HB_D(1,tindex
                -1)./(H_D(1,tindex)+ka2);%Acid buffer derived
                from base
166           HB_bb_D(1,tindex) = ka2*H2B_bb_D(1,tindex)./H_D(1,
                tindex);%Base buffer derived from base
167           HB_ab_D(1,tindex) = ka2*H2B_D(1,tindex-1)./(H_D(1,
                tindex)+ka2);%Base buffer derived from acid
168           H2B_ab_D(1,tindex) = H_D(1,tindex).*HB_ab_D(1,
                tindex)/ka2;%Acid buffer derived from acid
169           H3B_ab_D(1,tindex) = 0;
170           H3B_bb_D(1,tindex) = 0;
171
172           H2B_D(1,tindex) = H2B_ab_D(1,tindex) + H2B_bb_D(1,
                tindex);
173           HB_D(1,tindex) = HB_ab_D(1,tindex) + HB_bb_D(1,
                tindex);
```

```
174             H3B_D(1,tindex) = H3B_ab_D(1,tindex) + H3B_bb_D(1,
                    tindex);
175 %       else
176 %           H2B_bb_D_2(1,tindex) = H_D(1,tindex).*HB_D(1,
    tindex-1)./(H_D(1,tindex)+ka2);%Acid buffer derived from
     base
177 %           HB_bb_D_2(1,tindex) = ka2*H2B_bb_D(1,tindex)./H_D
    (1,tindex);%Base buffer derived from base
178 %           H3B_bb_D(1,tindex) = H_D(1,tindex).*H2B_D(1,
    tindex-1)./(H_D(1,tindex)+ka1);%Acid buffer derived from
     base
179 %           H2B_bb_D(1,tindex) = ka1*H3B_bb_D(1,tindex)./H_D
    (1,tindex);%Base buffer derived from base
180 %           H2B_ab_D(1,tindex) = ka1*H3B_D(1,tindex-1)./(H_D
    (1,tindex)+ka1);%Base buffer derived from acid
181 %           H3B_ab_D(1,tindex) = H_D(1,tindex).*H2B_ab_D(1,
    tindex)/ka1;%Acid buffer derived from acid
182 %
183 %           HB_D(1,tindex) = HB_bb_D_2(1,tindex);
184 %           H2B_D(1,tindex) = H2B_bb_D_2(1,tindex) + H2B_ab_D
    (1,tindex) + H2B_bb_D(1,tindex);
185 %           H3B_D(1,tindex) = H3B_ab_D(1,tindex) + H3B_bb_D
    (1,tindex);
186 %
187 %       end
188
189
190
191           %update concentrations for inputs
192           H2B_D(1,tindex) = (H2B_D(1,tindex)*Vol_D +
                  Sec_Rate_D*tstep*H2B_D_Sec)/Vol_D; %Current +
```

```
            Input from Secretion
193         HB_D(1,tindex) = (HB_D(1,tindex)*Vol_D + Sec_Rate_D
                *tstep*HB_D_Sec)/Vol_D; %Current + input from
                Secretion
194         H_D(1,tindex) = H_D(1,tindex)+(mol_H_xfer(1,tindex)
                +(Sec_Rate_D*tstep*H_D_Sec)/Vol_D); %Current +
                input from Stomach + Input from Secretion
195
196         %Update for Exit
197         Vol_Xfer_D(1,tindex) = Vol_xfer_S(1,tindex) +
                Sec_Rate_D*tstep; %(mL) leaving Duodenum to
                maintian volume
198         H3B_D(1,tindex) = (H3B_D(1,tindex)*Vol_D - (
                Vol_Xfer_D(1,tindex))*H3B_D(1,tindex))/Vol_D; %
                Current Mol - Mol leaving over current vol
199         H2B_D(1,tindex) = (H2B_D(1,tindex)*Vol_D - (
                Vol_Xfer_D(1,tindex))*H2B_D(1,tindex))/Vol_D;
200         HB_D(1,tindex) = (HB_D(1,tindex)*Vol_D - (
                Vol_Xfer_D(1,tindex))*HB_D(1,tindex))/Vol_D;
201         H_D(1,tindex) = (H_D(1,tindex)*Vol_D - (Vol_Xfer_D
                (1,tindex))*H_D(1,tindex))/Vol_D;
202         Total_B(1,tindex) = HB_D(1,tindex) + H2B_D(1,tindex
                )+H3B_D(1,tindex); %Update current total PO4
                concentration in D
203
204 %           %Media Replacement Check
205 %           if ismember(t
    ,[120,300,600,900,1800,2700,3600,4500,5400]) == 1
206 %               H2B_D(1,tindex) = (H2B_D(1,tindex)*Vol_D -
    H2B_D(1,tindex)*Media_replace + H2B_D_Sec*Media_replace)
    /Vol_D;
```

```
207 %             HB_D(1,tindex) = (HB_D(1,tindex)*Vol_D - HB_D
    (1,tindex)*Media_replace + HB_D_Sec*Media_replace)/Vol_D
    ;
208 %             H_D(1,tindex) = (H_D(1,tindex)*Vol_D - H_D(1,
    tindex)*Media_replace + H_D_Sec*Media_replace)/Vol_D;
209 %         end
210
211         %Titration Check
212         if pH_D(1,tindex) < Threshold_pH
213             H_D_preT(1,tindex) = H_D(1,tindex);
214             H2B_D_preT(1,tindex) = H2B_D(1,tindex);
215             H_D(1,tindex) = 10^-Setpoint_pH;
216
217             %re-equilibrating buffer for new pH
218             %(assumes NaOH consumes all H+ to move pH from
                Threshold --> Setpoint)
219             HB_D(1,tindex) = Total_B(1,tindex)*ka2/(H_D(1,
                tindex)+ka2); %Concentration of HPO4 (2-) M
220             H2B_D(1,tindex) = Total_B(1,tindex) - HB_D(1,
                tindex); %concentration of H2PO4(-) M
221
222             %Calculate Volume based on [H+] in solution and
                 [H+}
223             %dissociated from H2B ->HB
224             Titrant_H(1,tindex) = H_D_preT(1,tindex)-H_D(1,
                tindex); %mEq required (effectively, though
                it's not corrected for volume until below
225             Titrant_P(1,tindex) = H2B_D_preT(1,tindex)-
                H2B_D(1,tindex); %mEq required (effectively)
226             Vol_Titrant(1,tindex) = (Titrant_H(1,tindex)+
                Titrant_P(1,tindex))*Vol_D/mEq_Titrant;  %(L
```

```
                )
227
228             %Recalculate concentrations to maintain volume
                    balance
229             Total_B(1,tindex) = ((1-Vol_Titrant(1,tindex))
                    *(Total_B(1,tindex)*Vol_D + Titrant_Conc*
                    Vol_Titrant(1,tindex)))/Vol_D;
230             HB_D(1,tindex) = Total_B(1,tindex)*ka2/(H_D(1,
                    tindex)+ka2); %Concentration of HPO4 (2-) M
231             H2B_D(1,tindex) = Total_B(1,tindex) - HB_D(1,
                    tindex); %concentration of H2PO4(-) M
232             H_D(1,tindex) = 10^-Setpoint_pH;
233
234             pH_D(1,tindex) = Setpoint_pH;
235         end
236         Total_Vol_Titrant(1,tindex) = Total_Vol_Titrant(1,(
                tindex-1)) + Vol_Titrant(1,tindex);
237 end
238
239 x = linspace(0,length(pH_b_1)/120,length(pH_b_1));
240 figure
241 plot(x,pH_b_1,x,pH_D)
242 title('Drug-less pH profile for GIS-2')
243 legend('Stomach','Duodenum','Location','best')
244 xlabel('Time (min)')
245 ylabel('pH')
246
247 figure
248 plot(x,Total_B)
249 title('Drug-less pH profile for GIS-2')
250 legend('Phosphate','Location','best')
```

```
xlabel('Time (min)')
ylabel('[Total PO4]')
%
% figure
% plot(x,H3B_D,x,H2B_D,x,HB_D)
% title('Drug-less pH profile for GIS-2')
% legend('H3PO4','H2PO4','HPO4','Location','best')
% xlabel('Time (min)')
% ylabel('[PO4] Species')

figure
plot(x,Total_Vol_Titrant*10^3)
title('Drug-less pH profile for GIS-2')
legend('Titrant','Location','best')
xlabel('Time (min)')
ylabel('vol (mL) Titrant')

figure
plot(x,Titrant_H*10^3,x,Titrant_P*10^3)

title('Drug-less pH profile for GIS-2')
legend('H','P','Location','best')
xlabel('Time (min)')
ylabel('vol (mL) Titrant')
```

Appendix C.

Example User-Defined Gastric Emptying Method for Testing User-Defined Profile Function

Time (min)	Emptying Profile
0-0.5	Held at 200
0.5-10 min	1st Order Emptying, 30 min half emptying time
10 - 15 min	7 mL/min
15 - 25 min	1st Order Emptying, 10 min half emptying time
25 - 35 min	2 mL/min

Table C.1: Summary of Emptying Profile Cycles for GIS-2 User Defined Test for Pump Validation

Appendix D.

Tables for Formulations

Experiment #	Solid Fraction	Micro-Crystalline Cellulose to Lactose Ratio	Croscarmellose Sodium	Dibasic Sodium Phosphate	Magnesium Stearate	Sodium Dodecyl Sulfate	Copovidone
1	+	+	+	-	+	-	-
2	-	+	+	+	-	+	-
3	-	-	+	+	+	-	+
4	+	-	-	+	+	+	-
5	-	+	-	-	+	+	+
6	+	-	+	-	-	+	+
7	+	+	-	+	-	-	+
8	-	-	-	-	-	-	-
9	-	+	-	-	+	+	+

Table D.1: Plackett-Burman Table for Formulations

Experiment #	Sequence #	Solid Fraction	Micro-Crystalline Cellulose	Lactose	Croscarmellose Sodium	Dibasic Sodium Phosphate	SDS	Copovidone	Ibuprofen	Magnesium Stearate
5	1	0.9	10828.13	3609.375	312.5	1250	1250	1250	6250	250
2	2	0.85	8859.375	2953.125	1250	4375	1250	0	6250	62.5
7	3	0.85	9328.125	3109.375	312.5	4375	312.5	1250	6250	62.5
3	4	0.9	2828.125	8484.375	1250	4375	312.5	1250	6250	250
9	5	0.85	10828.13	3609.375	312.5	1250	1250	1250	6250	250
1	6	0.9	11765.63	3921.875	1250	1250	312.5	0	6250	250
8	7	0.9	4203.125	12609.38	312.5	1250	312.5	0	6250	62.5
6	8	0.85	3421.875	10265.63	1250	1250	1250	1250	6250	62.5
4	9	0.85	3140.625	9421.875	312.5	4375	1250	0	6250	250

Table D.2: Formulation descriptions for each formulation. For excipients, masses listed are in mg.